University of California
Los Angeles

Energy Management in Microgrids: Algorithms and System

A dissertation submitted in partial satisfaction
of the requirements for the degree
Doctor of Philosophy in Mechanical Engineering

by

Wenbo Shi

2015

Abstract of the Dissertation

Energy Management in Microgrids: Algorithms and System

by

Wenbo Shi

Doctor of Philosophy in Mechanical Engineering

University of California, Los Angeles, 2015

Professor Rajit Gadh, Chair

Microgrids, as one of the key components to enable the future smart grid, refer to low-voltage power distribution systems integrated with distributed energy resources (DERs) and controllable loads, which can operate either with or without the grid (i.e., grid-connected or islanded mode). The integration of DERs and controllable loads brings tremendous opportunities to increase power system efficiency, sustainability, and reliability. However, the intermittency and variability of renewable DERs and limited supply especially when the microgrid is operating in islanded mode introduce significant challenges to maintain the fundamental supply-demand balance for system stability. Therefore, the goal of this dissertation is to solve the supply-demand balancing problem in microgrids using optimization-based energy management.

Most of the existing energy management algorithms in the literature consider the aggregate supply-demand balance as an abstract mathematical function while omitting the underlying power distribution network and the associated power flow and system operational constraints. Consequently, such approaches may result in control decisions that violate the real-world constraints. Therefore, in the first part of this dissertation, we study the supply-demand balancing problem in microgrids under more realistic conditions and propose algorithms for microgrid energy management that take into account the power flow and system operational constraints on a distribution network. By incorporating the distribution

network in the modeling, we present the relationship between the physical structure of a microgrid and the energy management on the network.

Another major challenge in microgrid energy management is to design a two-way communication system in order to implement the algorithms. A variety of heterogeneous devices in a microgrid need to be managed by such a system using the energy management algorithms. Unfortunately, most of those devices still use proprietary protocols and cannot interoperate with each other. Furthermore, many devices managed by the system reside on the customer side requiring autonomy and local intelligence. Therefore, in the second part of this dissertation, we focus on the design and implementation of a system architecture that enables interoperability and autonomy for microgrid energy management. We present the design of a unified communication interface that is protocol and technology agnostic for interoperability and a decentralized system architecture for autonomy on the customer side.

The dissertation of Wenbo Shi is approved.

Gregory P. Carman

Adrienne G. Lavine

Magali A. Delmas

Rajit Gadh, Committee Chair

University of California, Los Angeles

2015

To my dear family.

Table of Contents

1 Introduction **1**

1.1 Research Backgrounds 1

1.1.1 Smart Grid 1

1.1.2 Microgrid 2

1.1.3 Residential Demand Response 4

1.1.4 Distributed Energy Management 5

1.1.5 Real-Time Energy Management 7

1.1.6 Energy Management System 8

1.2 Structure and Contributions 9

2 Optimal Residential Demand Response in Distribution Networks **13**

2.1 Introduction 13

2.2 System Model 16

2.2.1 System Overview 16

2.2.2 Appliance Model 17

2.2.3 Customer Preference Model 19

2.2.4 Distribution Network Model 20

2.2.5 DR Model 22

2.3 Distributed DR Scheme 23

2.3.1 Introduction to PCPM 23

2.3.2 Convexification of OPF 25

2.3.3 Distributed Algorithm 26

2.4 Performance Evaluation 28

2.4.1 Simulation Setup 28
2.4.2 Case Study 32
2.4.3 Discussions 36
2.5 Summary 39

3 Distributed Optimal Energy Management in Microgrids 41
3.1 Introduction 41
3.2 System Model 44
3.2.1 System Overview 44
3.2.2 DG Model 45
3.2.3 DS Model 46
3.2.4 Load Model 47
3.2.5 Distribution Network Model 48
3.2.6 Energy Management 50
3.3 Distributed EMS 52
3.4 IEC 61850 Implementation 55
3.5 Performance Evaluation 56
3.5.1 Simulation Setup 57
3.5.2 Case Study 58
3.5.3 Discussions 60
3.6 Summary 64

4 Real-Time Energy Management in Microgrids 68
4.1 Introduction 68
4.2 System Model 72
4.2.1 System Overview 72

4.2.2 DG Model . . . 72
4.2.3 DS Model . . . 74
4.2.4 Load Model . . . 75
4.2.5 Distribution Network Model . . . 76
4.2.6 Real-Time Energy Management . . . 77
4.3 Online EMS . . . 79
4.3.1 Introduction to Lyapunov Optimization . . . 79
4.3.2 Virtual Queue Design . . . 81
4.3.3 Lyapunov Optimization . . . 82
4.3.4 Convexification of OPF . . . 84
4.3.5 Performance Gaps in the Optimizations . . . 85
4.4 Performance Evaluation . . . 86
4.4.1 Simulation Setup . . . 86
4.4.2 Benchmarks . . . 88
4.4.3 Case Study . . . 89
4.4.4 Discussions . . . 92
4.5 Summary . . . 97

5 Design and Implementation of a System Architecture for Microgrid Energy Management . . . 99

5.1 Introduction . . . 100
5.2 Design of a Microgrid EMS . . . 101
5.2.1 Functional Requirements . . . 102
5.2.2 Unified Communication Interface . . . 103
5.3 Implementation . . . 105

5.3.1 Decentralized System Architecture 105
5.3.2 Microgrid Testbeds 109
5.3.3 Microgrid Controls 113
5.4 Experiments 116
5.4.1 Energy Scheduling 116
5.4.2 DR 122
5.5 Summary 127

6 Conclusions 129

References 132

List of Figures

1.1 A smart grid. 2

1.2 A microgrid example. 3

1.3 An energy management strategy. 5

1.4 An energy management system. 8

2.1 An LSE's distribution network of H households. 17

2.2 HEM system in each household. 18

2.3 Modified IEEE standard distribution system. 29

2.4 Outside temperature of a day. 30

2.5 Load profile of the feeder $|s_0(t)|$ without and with DR. 32

2.6 Minimum bus voltage profile without and with DR. 33

2.7 Load profile of the appliances in one of the households without and with DR. 34

2.8 Dynamics of DR-household: the aggregate real power at bus 8. 35

2.9 Dynamics of DR-LSE: the real power injected to the system p_0. 36

2.10 Aggregate load profile of the households at each bus without DR. 37

2.11 Aggregate load profile of the households at each bus with DR. 38

2.12 Rebound effect of DR. 39

3.1 System architecture. 45

3.2 IEC 61850 implementation. 56

3.3 Topology of the microgrid. 57

3.4 Day-ahead price from CAISO. 59

3.5 Output schedules in islanded mode. 60

3.6 Output schedules in grid-connected mode. 61

3.7 Net power injected to the microgrid. 62
3.8 Dynamics of EMS-MGCC and EMS-LC. 63
3.9 Maximum and minimum bus voltage in the microgrid. 64
3.10 Demand reduction of the loads. 65
3.11 Load shifting. 66
3.12 Effect of r_g on the objective. 67

4.1 System architecture. 73
4.2 Problem formulation scheme. 80
4.3 Topology of the microgrid. 87
4.4 Renewable generation profiles, load profile, and real-time price. 88
4.5 Real-time cost. 90
4.6 Time accumulated cost comparison. Time average cost: \$15.34 (greedy), \$13.68 (online), \$11.37 (offline). 91
4.7 Battery charging/discharging profile with different β. 92
4.8 Time average cost with different β. 93
4.9 Load shedding percentage at bus 2 with different V. 94
4.10 Time average cost with different V. 95
4.11 Comparison of the maximum and minimum bus voltages without and with considering the network constraints (Red lines indicate the allowed tolerance). 96
4.12 Hourly shed demands at each load bus in day 3. 97

5.1 An illustration of a microgrid EMS. 102
5.2 A unified communication interface for devices. 104
5.3 An illustration of the overall EMS architecture. 106
5.4 An illustration of the decentralized system architecture. 107

5.5 A screenshot of the control center showing the market pricing information. . 109
5.6 Some of the devices in the UCLA SMERC testbed. 110
5.7 Some of the devices in the KIER testbed. 111
5.8 Day-ahead energy price for the UCLA SMERC testbed. 117
5.9 Forecast and day-ahead schedule for the UCLA SMERC testbed. 118
5.10 Time-of-use price for the KIER testbed. 119
5.11 Forecast for the KIER testbed. 120
5.12 Simulated day-ahead schedule for the KIER testbed. 121
5.13 Real-time hardware-in-the-loop result in the KIER testbed. 123
5.14 Result of the DR experiment in the UCLA SMERC testbed. 125
5.15 Result of the DR experiment in the KIER testbed when the price changes from range 2 to range 3. 127
5.16 Result of the DR experiment in the KIER testbed when the price changes from range 3 to range 2. 128

List of Tables

2.1 Notations 20

3.1 Cost comparison under different ξ 66

Acknowledgments

This dissertation could not be finished without the generous help and constant support from my professors, colleagues, collaborators, friends, and family members. I would like to express my deepest gratitude to all of them.

First of all, I would like to thank my advisor Dr. Rajit Gadh for his continuous guidance, support, and patience during my entire Ph.D. study. It has been a truly wonderful experience working with him at the UCLA Smart Grid Energy Research Center (SMERC). I could not ask for more from him. I would also like to thank Dr. Magali Delmas, Dr. Adrienne Lavine, and Dr. Gregory Carman for serving as my committee members and their advice and encouragement along the way.

I am thankful to my dear colleagues at UCLA SMERC working on the same project with me: Dr. Chi-Cheng Chu who manages the project, Dr. Eun-Kyu Lee, Dr. Daoyuan Yao, and Rui Huang, who contribute to the implementation of the proposed microgrid EMS. I am very grateful to the sponsor of the project - Korea Institute of Energy Research (KIER) and our collaborators from KIER: Dr. Yu-Jin Song and Yoon-Dong Sung for their support and hospitality during my three visits to KIER. Special thanks go to Dr. Na Li for discussions on optimization and continuous help and encouragement along my Ph.D. and Dr. Xiaorong Xie for discussions on power systems and providing the microgrid data used in my simulations. It is my great honor to work with all these brightest minds.

I would also like to thank other people from UCLA SMERC with whom I shared a lot of time: Yubo Wang, Bin Wang, Hamidreza Nazaripouya, Joshua Chynoweth, Dr. Ching-Yen Chung, Dr. Himanshu Pota, and Omar Sheikh. Special thanks to Eric Rios who helped draw some of the figures in this dissertation.

Last but not least, I am most indebted to my entire family including my parents, grandparents, uncles, aunts, and cousins, whose unconditional love and support throughout the years means everything to me.

Vita

2009 B.E. (Information and Communications Engineering), Xi'an Jiaotong University, Xi'an, Shaanxi, China.

2011 M.A.Sc. (Electrical Engineering), University of British Columbia, Vancouver, BC, Canada.

Publications

JOURNAL PAPERS

Rui Huang, **Wenbo Shi**, Daoyuan Yao, Chi-Cheng Chu, Rajit Gadh, Yu-Jin Song, and Yoon-Dong Sung, "Design and Implementation of Communication Architecture in A Distributed Energy Resource System using IEC 61850 Standard," *International Journal of Energy Research*, under review, 2015.

Wenbo Shi, Na Li, Chi-Cheng Chu, and Rajit Gadh, "Real-Time Energy Management in Microgrids," *IEEE Transactions on Smart Grid*, to be published.

Wenbo Shi, Xiaorong Xie, Chi-Cheng Chu, and Rajit Gadh, "Distributed Optimal Energy Management in Microgrids," *IEEE Transactions on Smart Grid*, vol.6, no.3, pp.1137-1146, May 2015.

Wenbo Shi, Na Li, Xiaorong Xie, Chi-Cheng Chu, and Rajit Gadh, "Optimal Residential Demand Response in Distribution Networks," *IEEE Journal on Selected Areas in Communications*, vol.32, no.7, pp.1441-1450, Jul. 2014.

CONFERENCE PAPERS

Rui Huang, Yubo Wang, **Wenbo Shi**, Daoyuan Yao, Boyang Hu, Chi-Cheng Chu, and Rajit Gadh, "Integration of IEC 61850 into a Vehicle-to-Grid System with Networked Electric Vehicles," in *Proc. of IEEE PES Conference on Innovative Smart Grid Technologies (ISGT)*, Washington, DC, Feb. 2015.

Wenbo Shi, Eun-Kyu Lee, Daoyuan Yao, Rui Huang, Chi-Cheng Chu, and Rajit Gadh, "Evaluating Microgrid Management and Control with an Implementable Energy Management System," in *Proc. of IEEE International Conference on Smart Grid Communications (SmartGridComm)*, Venice, Italy, Nov. 2014.

Wenbo Shi, Xiaorong Xie, Chi-Cheng Chu, and Rajit Gadh, "A Distributed Optimal Energy Management Strategy for Microgrids," in *Proc. of IEEE SmartGridComm*, Venice, Italy, Nov. 2014.

PATENT

Rajit Gadh, Chi-Cheng Chu, **Wenbo Shi**, and Daoyuan Yao, "A Decentralized Energy Management System for Microgrids," UCLA Case No. 2015-789, Apr. 2015.

CHAPTER 1

Introduction

In this chapter, we introduce the research backgrounds and summarize the contributions of this dissertation.

1.1 Research Backgrounds

This section introduces the backgrounds of the research in the dissertation including smart grid, microgrid, residential demand response (DR), distributed energy management, real-time energy management, and energy management system.

1.1.1 Smart Grid

A smart grid, as the next-generation power grid, is a combination of the legacy power system and the latest information and communications technologies to incorporate renewable energy sources, increase system efficiency and reliability, and allow for more customer participation [1]. New technologies are transforming the conventional power grid towards a smart, responsive, and user-friendly grid from every aspect - generation, transmission, distribution, and utilization as illustrated in Fig. 1.1.

On the generation side of a smart grid, more renewables such as solar and wind will be used in addition to the conventional bulk power generation. Grid-level energy storage can buffer the power flow, serving as generation when discharging and load when charging. On the transmission side, massive advanced phasor measurement units will be installed to monitor wide-area real-time system states for reliability. On the distribution side, microgrids which can be considered as a small-scale grid will play an important role for integrating

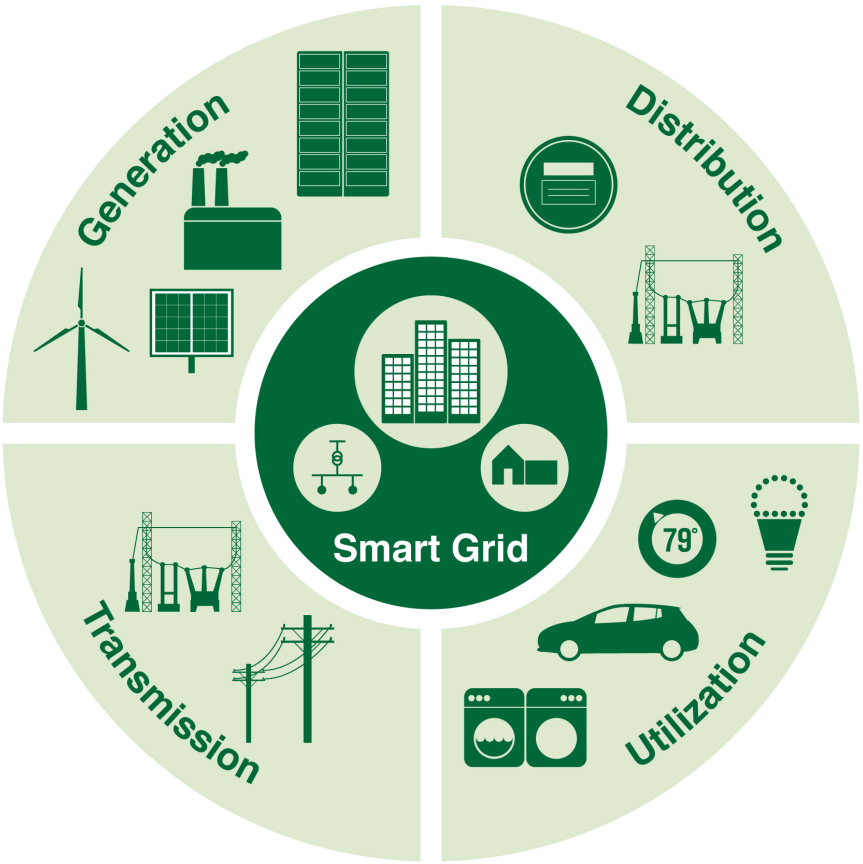

Figure 1.1: A smart grid.

distributed energy resources (DERs) and smart meters will be installed to establish two-way real-time communications between utilities and customers. Lastly, on the utilization side, smart appliances with the ability to be controlled over a network and emerging electrical vehicles (EVs) are expected to change the way how customers interact with the grid. Based on the infrastructure of a smart grid, various new applications and services such as the concepts of smart home, smart building, microgrid, and automated DR are emerging.

1.1.2 Microgrid

A microgrid refers to a power distribution system integrated with DERs and controllable loads, which can either operate with the main grid (i.e., grid-connected mode) or use the DERs to supply the loads without the main grid (i.e., islanded mode) [2]. It can be viewed

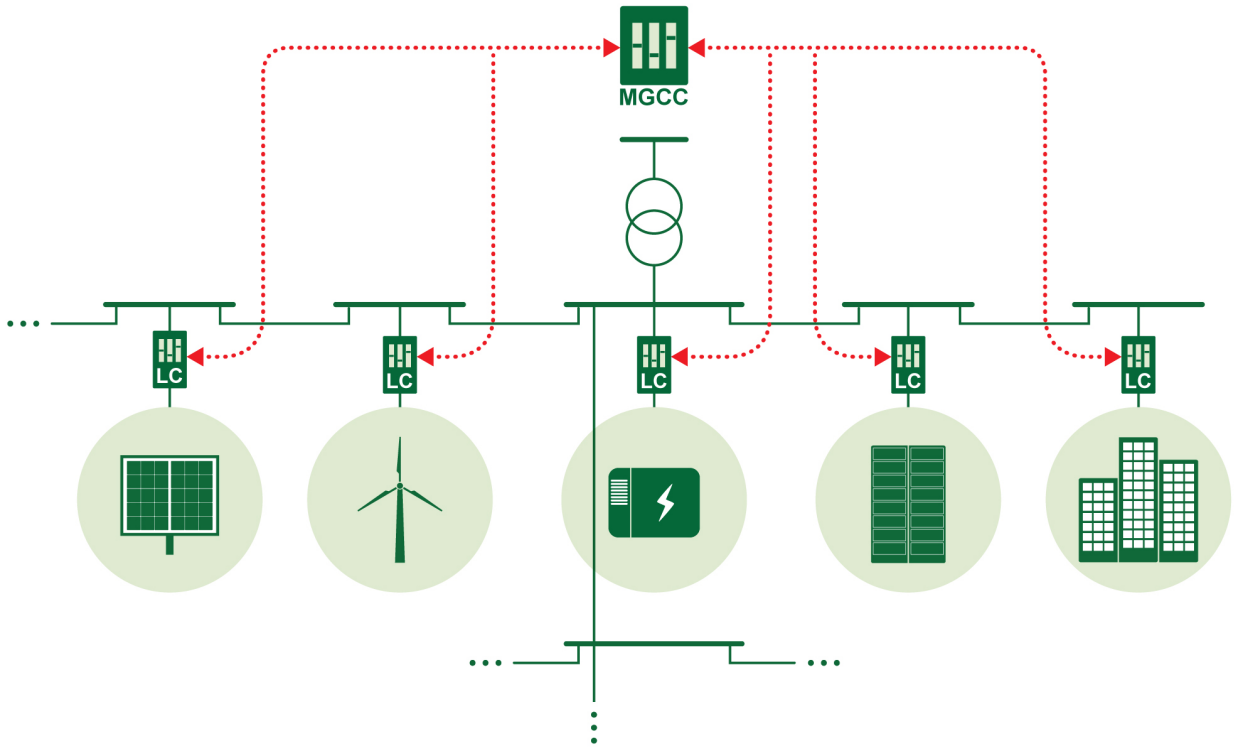

Figure 1.2: A microgrid example.

as small-scale grid and it is widely considered as one of the key components to integrate renewable DERs and save transmission losses for effiency [1].

In a conventional power system, the power flow is single directional from bulk generation, e.g., a power plant, to loads via a transmission and distribution system. As more DERs such as roof-top photovoltaics (PVs), small wind turbines (WTs), battery systems (e.g., Tesla Powerwall[1]) are becoming available on the distribution side, bi-directional power flow is now possible and it makes a conventional power distribution system into a microgrid which can use only the DERs as the power supply without the main grid (i.e., islanded mode) or even sell back its surplus power to the main grid. The size of a microgrid may vary depending on the application. For example, the concept of microgrid can be implemented as a smart home, a smart building, or a smart campus. Fig. 1.2 shows a microgrid example consisting of PVs, WTs, diesel generators, batteries, and loads. Two-way communications are available

[1]http://www.teslamotors.com/powerwall

between the local controllers (LCs) and the microgrid central controller (MGCC). There are a few on-going projects focusing on building the microgrid infrastructure such as the smart power infrastructure demonstration for energy reliability and security (SPIDERS) from Sandia National Labs [3] and the UCSD microgrid project [4].

In a microgrid, it is essential to maintain the power supply-demand balance for stability because the intermittent DERs such as PVs and WTs are hard to predict and their generation may fluctuate significantly depending on the availability of the primary sources (e.g., solar and wind). The supply-demand balancing problem becomes even more challenging when the microgrid is operating in islanded mode where only limited supply is available to balance the demand. To solve this problem, energy management is needed to manage the operations of the DERs and loads in order to maintain the supply-demand balance in a microgrid. In the following, we will introduce the backgrounds of three optimization-based energy management algorithms followed by microgrid energy management system (EMS) that provides the communication infrastructure required to implement the energy management algorithms.

1.1.3 Residential Demand Response

DR is a mechanism to enable customers to participate in the electricity market in order to improve power system efficiency and integrate renewable generation [5]. Most of the existing DR programs in the United States are for commercial and industrial customers and they have been well studied. Very few DR programs are in use for residential customers [6]. However, as smart grid technologies such as smart metering, smart appliances, and home area network technologies developed significantly over the past years, residential DR becomes increasingly attractive due to its great potential [7].

Residential DR requires the coordination of a large number of households in order to improve the overall power system efficiency and reliability. Such coordination is usually implemented via pricing signals, assuming that customers are price responsive. Extensive algorithms [7–12] have been proposed in the literature to determine the prices and customers' responses to the prices. Most of these studies consider the supply-demand matching in DR

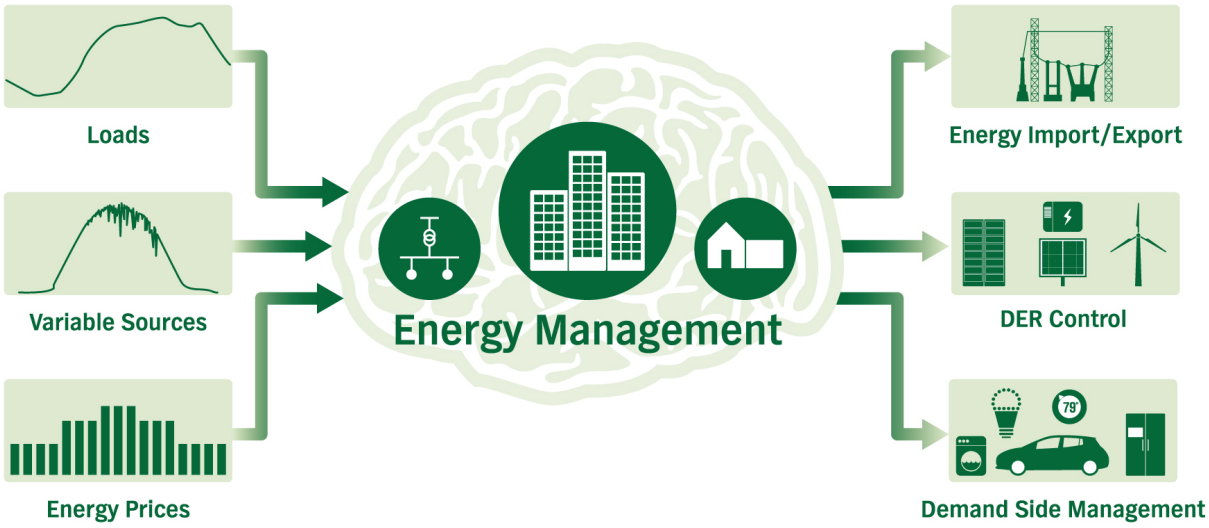

Figure 1.3: An energy management strategy.

in an abstract way where the aggregate demand is simply equal to the supply. However, households are not isolated with each other, but they are connected by a power distribution network with the associated power flow constraints (e.g. Kirchhoff's laws) and system operational constraints (e.g. voltage tolerances). As a result, the schemes proposed by previous studies may end up with electricity consumption/shedding decisions that violate those constraints and thus are not feasible. There are few studies which consider DR in direct current (DC) distribution networks [13]. However, they cannot be applied to the most widely-used alternating current (AC) distribution networks.

1.1.4 Distributed Energy Management

Sound operation of a microgrid requires an energy management strategy (EMS)[2] which controls the power flows in the microgrid by adjusting the power imported/exported from/to the main grid, the dispatchable DERs, and the controllable loads based on the present and forecasted information of the market, the generations, and the loads in order to meet certain

[2]In this dissertation, we use EMS interchangeably for energy management system or energy management strategy depending on the context.

operational objectives (e.g., minimizing costs) [2].

Energy management in microgrids is typically formulated as a non-linear optimization problem. Various centralized methods have been proposed to solve it in the literature, including mixed integer programming [14], sequential quadratic programming [15], particle swarm optimization [16], neural networks [17], etc. The centralized approaches [14–17] require high computational capabilities at the MGCC, which is neither efficient nor scalable. Moreover, a centralized EMS requires the MGCC to gather information of the DERs (e.g., production costs, constraints, etc.) and the loads (e.g., customer preferences, constraints, etc.) as the inputs for optimization. However, different DERs may belong to different entities and they may keep their information private [18]. Customers may also be unwilling to expose their information due to privacy [19].

Several distributed algorithms have been proposed for the operation of microgrids in the literature. In [18], a distributed algorithm based on the classical symmetrical assignment problem is proposed. Energy management is formulated as a resource allocation problem in [20] and distributed algorithms are proposed for distributed allocation. A convex problem formulation can be found in [21] and dual decomposition is used to develop a distributed EMS to maintain the supply-demand balance in microgrids. A privacy-preserving energy scheduling algorithm in microgrids is proposed in [19], where the privacy constraints are integrated with the linear programming model and distributed algorithms are developed. In [22], the additive-increase/multiplicative-decrease algorithm is adopted to optimize DER operations in a distributed fashion.

The problem with the existing distributed approaches [18–22] is that they consider the supply-demand matching in an abstract way where the aggregate demand is simply equal to the supply. They assume that all generations and loads are connected to one bus and ignore the underlying power distribution network and the associated power flow (e.g., Kirchhoff's law) and system operational constraints (e.g., voltage tolerances). Consequently, the schedules produced by those algorithms may violate those constraints and thus are not feasible in practice. It is worth noting that distribution networks have been taken into account in a few recent DR studies [23]. However, the idea of integrating distribution networks with

distributed energy management in microgrids, where both supply side and demand side management are considered, has not been explored.

1.1.5 Real-Time Energy Management

Energy management in microgrids is typically formulated as an offline optimization problem for day-ahead scheduling by previous studies [15, 24–27]. Most of these offline approaches assume perfect forecasting of the renewables, the demands, and the market, which is difficult to achieve in practice due to the intermittency and variability of renewables, the spatial and temporal uncertainty in controllable loads (e.g., EVs), and the randomness in real-time pricing. To tackle this problem, efforts have been made to capture the uncertainties in day-ahead scheduling through modeling different scenarios [21, 28–32]. These approaches typically use stochastic programming to formulate energy management as a deterministic problem based on the scenarios that are usually generated by Monte Carlo simulations. The number of these scenarios may be large and thus it can be computationally expensive to use these methods. Although these approaches consider the uncertainties, they still require certain forecasting and usually do not adapt to real-time changes in the environment. Other studies [16, 17] consider the energy management problem at each time independently and focus on how to efficiently solve the optimization problem in real time.

Recently, there have been attempts to develop online algorithms for real-time energy management in microgrids to optimize the long-term cost, which take into account the uncertainties of the renewables, the demands, and the market [33–35]. These approaches do not require any a priori statistical knowledge of the underlying stochastic processes and can adapt to the time-varying environment. However, these existing online approaches consider the aggregate supply-demand balance while omitting the underlying power distribution network, the associated power flow (e.g., Kirchhoffs laws), and system operational constraints (e.g., voltage tolerances). Consequently, such approaches may result in control decisions that violate the real-world constraints.

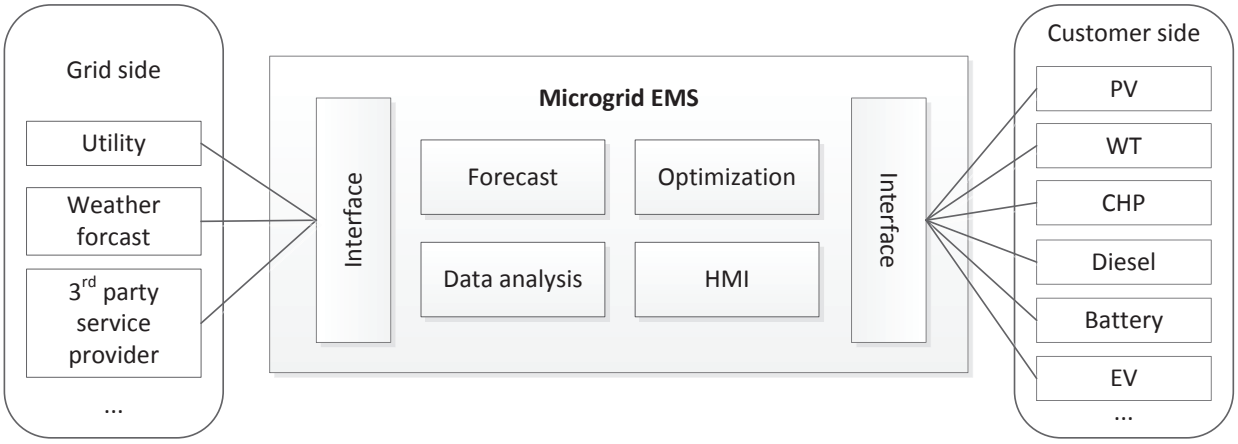

Figure 1.4: An energy management system.

1.1.6 Energy Management System

An EMS monitors, controls, and optimizes the operation of a microgrid to achieve certain operational objectives (e.g., minimize costs). It is essential to implement any energy management algorithms. Due to the integration of distributed generation (DG), distributed storage (DS), and controllable loads, the operation and management of a microgrid is more complicated than a conventional distribution system, which is implemented by an EMS. A microgrid EMS can be significantly different from the EMS used in conventional power systems due to these challenges [36].

To understand the challenges, Su and Wang [36] discussed the role of EMS in microgrid operations and listed four essential functionalities that a microgrid EMS must support: forecast, optimization, data analysis, and human-machine interface (HMI) as shown in Fig. 1.4. Due to the importance of EMS in power systems, many EMS frameworks [37–40] have been investigated in the literature. While these previous studies focused on different issues in EMS, they commonly suffer from engineering challenges that must be taken into account when designing an implementable microgrid EMS.

First of all, intermittency and variability of DERs (e.g., PVs and WTs) and spatiotemporal uncertainty in controllable loads complicate the microgrid management, which the EMS must be able to cope with. Next, a microgrid triggers a number of new applications

(e.g., DR, coordinated EV charging, vehicle-to-grid (V2G), etc.) and innovative control algorithms [1, 23, 41]. The EMS must be able to interface with them seamlessly. Moreover, since many devices managed by the EMS reside on the customer side, they require certain level of autonomy and local intelligence that the EMS must be able to provide. Last but not least, a microgrid instruments a number of energy components. But, most of them still use proprietary protocols and cannot interoperate with each other [37]. The EMS must handle the heterogeneity and achieve interoperation. A microgrid EMS can be implemented to perform efficient management and control only when overcoming the engineering challenges and satisfying aforementioned functional requirements. Unfortunately, few previous EMS studies have accomplished both of them.

1.2 Structure and Contributions

This section presents the structure of the dissertation and summarizes the contributions as below.

The goal of this dissertation is to solve the supply-demand balancing problem in microgrids using optimization-based energy management. We propose three energy management algorithms under different context in Chapters 2-4. We then propose a system architecture that enables interoperability and autonomy for microgrid energy management that can be used to implement those algorithms in Chapter 5.

Chapter 2 focuses on the design of a residential DR scheme that can coordinate a large number of household appliances to achieve DR. Most previous studies on DR consider the supply-demand matching in an abstract way without taking into account the underlying power distribution network and the associated power flow and system operational constraints. As a result, the schemes proposed by those studies may end up with electricity consumption/shedding decisions that violate those constraints and thus are not feasible in practice. In Chapter 2, we study residential DR with consideration of the power distribution network and the associated constraints and formulate it as an optimal power flow problem (OPF) and propose a distributed scheme where the load serving entity (LSE) and the households

interactively communicate to compute an optimal demand schedule. To complement our theoretical results, we also simulate an IEEE test distribution system. The simulation results demonstrate two interesting effects of DR. One is the location effect, meaning that the households far away from the feeder tend to reduce more demands in DR. The other is the rebound effect, meaning that DR may create a new peak after the DR event ends if the DR parameters are not chosen carefully. The two effects suggest certain rules we should follow when designing a DR program. Chapter 2 is based on the work published in [23].

Chapter 3 focuses on the design of a distributed EMS for the optimal operation of microgrids. Energy management in microgrids is typically formulated as a non-linear optimization problem. Solving it in a centralized manner does not only require high computational capabilities at the MGCC but may also infringe customer privacy. Existing distributed approaches, on the other hand, assume that all generations and loads are connected to one bus and ignore the underlying power distribution network and the associated power flow and system operational constraints. Consequently, the schedules produced by those algorithms may violate those constraints and thus are not feasible in practice. Therefore, in Chapter 3, we develop a distributed EMS for the optimal operation of microgrids with consideration of the distribution network and the associated constraints. Specifically, we formulate microgrid energy management as an OPF and propose a distributed EMS where the MGCC and the local controllers jointly compute an optimal schedule. We also provide an implementation of the proposed distributed EMS based on the IEC 61850 standard [42]. As one demonstration, we apply the proposed distributed EMS to a real microgrid in Guangdong Province, China, consisting of PVs, WTs, diesel generators, and a battery energy storage system (BESS). The simulation results demonstrate the effectiveness and fast convergence of the proposed distributed EMS. Chapter 3 is based on the work published in [27].

Chapter 4 focuses on developing an online EMS for real-time operation of microgrids to deal with the uncertainties in the energy management problem. Energy management in microgrids is typically formulated as an offline optimization problem for day-ahead scheduling by previous studies. Most of these offline approaches assume perfect forecasting of the renewables, the demands, and the market, which is difficult to achieve in practice. Existing

online algorithms, on the other hand, oversimplify the microgrid model by only considering the aggregate supply-demand balance while omitting the underlying power distribution network and the associated power flow and system operational constraints. Consequently, such approaches may result in control decisions that violate the real-world constraints. Therefore, in Chapter 4, we develop an online EMS for real-time operation of microgrids that takes into account the power flow and system operational constraints on a distribution network. We model the online energy management as a stochastic optimal power flow (SOPF) problem and propose an online EMS based on Lyapunov optimization. The proposed online EMS is subsequently applied to a real microgrid system. The simulation results demonstrate that the performance of the proposed EMS exceeds a greedy algorithm and is close to an optimal offline algorithm. Lastly, the effect of the underlying network structure on the energy management is observed and analyzed. Chapter 4 is based on the work to be published in [43].

Chapter 5 focuses on the design and implementation of a system architecture that enables interoperability and autonomy on the customer side for microgrid energy management. In a microgrid, there are a variety of heterogeneous DERs and loads that need to be managed by an EMS. Unfortunately, most of those devices still use proprietary protocols and cannot interoperate with each other. Furthermore, many devices managed by the system reside on the customer side requiring autonomy and local intelligence. Therefore, in Chapter 5, we design a system architecture for microgrid energy management that enables interoperability and autonomy on the customer side. We design a unified communication interface that is protocol and technology agnostic for the system to interoperate with heterogeneous devices in a microgrid. We then propose a decentralized system architecture, in which the system components are highly decoupled and independent to enable autonomy on the customer side. Moreover, we deploy a prototype of the proposed system architecture and conduct experiments to evaluate microgrid management and control in real-world settings in two microgrid testbeds. Our experimental results demonstrate that the system is able to manage various DERs and loads in the testbeds using different industrial standards and protocols, interact with external systems, and perform efficient energy management using different

algorithms. A part of Chapter 5 is based on the work published in [44].

The conclusions and future work are given in Chapter 6.

CHAPTER 2

Optimal Residential Demand Response in Distribution Networks

DR enables customers to adjust their electricity usage to balance supply and demand. Most previous studies on DR consider the supply-demand matching in an abstract way without taking into account the underlying power distribution network and the associated power flow and system operational constraints. As a result, the schemes proposed by those studies may end up with electricity consumption/shedding decisions that violate those constraints and thus are not feasible in practice. In this chapter, we study residential DR with consideration of the power distribution network and the associated constraints. We formulate residential DR as an OPF problem and propose a distributed scheme where the LSE and the households interactively communicate to compute an optimal demand schedule. To complement our theoretical results, we also simulate an IEEE test distribution system. The simulation results demonstrate two interesting effects of DR. One is the location effect, meaning that the households far away from the feeder tend to reduce more demands in DR. The other is the rebound effect, meaning that DR may create a new peak after the DR event ends if the DR parameters are not chosen carefully. The two effects suggest certain rules we should follow when designing a DR program.

2.1 Introduction

DR is a mechanism to enable customers to participate in the electricity market in order to improve power system efficiency and integrate renewable generation [5]. Most of the existing DR programs in the United States are for commercial and industrial customers and they have

been well studied. Very few DR programs are in use for residential customers [6]. However, as smart grid technologies such as smart metering, smart appliances, and home area network technologies developed significantly over the past years, residential DR becomes increasingly attractive due to its great potential [7].

Residential DR requires the coordination of a large number of households in order to improve the overall power system efficiency and reliability. Such coordination is usually implemented via pricing signals, assuming that customers are price responsive. Extensive algorithms [7–12] have been proposed in the literature to determine the prices and customers' responses to the prices. Most of those studies consider the supply-demand matching in DR in an abstract way where the aggregate demand is simply equal to the supply. However, households are not isolated with each other, but they are connected by a power distribution network with the associated power flow constraints (e.g., Kirchhoff's laws) and system operational constraints (e.g., voltage tolerances). As a result, the schemes proposed by previous studies may end up with electricity consumption/shedding decisions that violate those constraints and thus are not feasible. There are few studies which consider DR in DC distribution networks [13]. However, they cannot be applied to the most widely-used AC distribution networks.

This chapter focuses on the design of a DR scheme for a large number of residential households with consideration of the AC power distribution network and the associated constraints in a smart grid where two-way communications between the LSE and the households are available. More specifically, we consider a direct residential DR program where customers who participate in it sign a contract with the LSE in advance to let the LSE control some of their appliances for a certain period of time. The HEMs in the participating households can receive DR control signals from the LSE to coordinate their appliance operations in order to meet the DR objective in a DR event. The objective of the DR is to manage the appliances for each household such that (i) the social welfare (i.e., the customer utilities minus the power losses) is maximized, (ii) the system demand is below a certain limit during peak hours, and (iii) the appliance operational constraints, the power flow constraints, and the system operational constraints are satisfied.

Specifically, we formulate residential DR as an OPF using a branch flow model [45]. The OPF problem is non-convex due to the power flow constraints and thus is difficult to solve. We relax the problem to be a convex problem. The convex relaxation is not exact in general (i.e., the solution to the relaxed problem is not the same as the solution to the original problem). Recent studies [46–48] have derived sufficient conditions under which the relaxation is exact for radial networks. Roughly speaking, if the bus voltage is kept around the nominal value and the power injection at each bus is not too large, then the relaxation is exact. For detailed conditions, please refer to [46]. More sufficient conditions can be found in [47,48]. Those conditions can be checked a priori and hold for a variety of IEEE standard distribution networks and real-world networks. Therefore, we focus on solving the relaxed OPF problem (OPF-r) in this chapter. The OPF-r problem is a centralized optimization problem. To solve it in a distributed manner, we propose a DR scheme where the LSE and the HEMs in the households jointly compute an optimal demand schedule. In our proposed DR scheme, the HEM in each household keeps the private information locally (i.e., utility functions and appliance operational constraints) and the LSE has the system information (i.e., network topology, line impedances, power losses, etc.). Therefore, customer privacy (i.e., detailed appliance-level information) is protected in the DR process.

To complement our theoretical model, we apply the proposed DR scheme to an IEEE test radial distribution system [49]. The simulation results demonstrate the effectiveness of our proposed DR scheme and show two interesting effects of DR. One is the location effect meaning that the households far away from the feeder tend to reduce more demands in DR. The other is the rebound effect meaning that DR may create a new peak after the DR event ends if the DR parameters are not chosen carefully. The two effects suggest certain rules we should follow when designing a DR program.

The rest of this chapter is organized as follows. We introduce the system model in Section 2.2 and propose the DR scheme in Section 2.3. The simulation results and discussions on the location effect and the rebound effect are provided in Section 2.4. The summary is given in Section 2.5.

2.2 System Model

This section describes the system model of the proposed distributed residential DR scheme. We give an overview of the system followed by the appliance model, the customer preference model, the distribution network model, and the DR model. Those models will be used for designing the DR scheme in the following section.

2.2.1 System Overview

We consider a residential DR over a distribution network, which is operated by one LSE. In the network, each load bus is connected with a set of households and there are a total of H households $\mathcal{H} := \{h_1, h_2, \ldots, h_H\}$ in the system. In each household $h \in \mathcal{H}$, there is a HEM system managing a set of appliances $\mathcal{A}_h := \{a_{h,1}, a_{h,2}, \ldots, a_{h,A}\}$ such as air conditioners (ACs), electric vehicles (EVs), dryers, etc. The HEM is also connected with the LSE's communications network via a smart meter so that there is a two-way communication link between the LSE and the household [50]. Since most distribution networks are radial, we focus on only radial distribution networks in this chapter. The overall system architecture is shown in Fig. 2.1 and 2.2.

We use a discrete-time model with a finite horizon in this chapter. We consider a time period or namely a scheduling horizon which is divided into T equal intervals Δt, denoted by $\mathcal{T}$. For each appliance $a \in \mathcal{A}_h$, let $p_{h,a}(t)$ and $q_{h,a}(t)$ be the real power and reactive power it draws at time $t \in \mathcal{T}$. The complex power of the appliance can be denoted by $s_{h,a}(t) := p_{h,a}(t) + \mathbf{i} q_{h,a}(t)$. The HEM system in each household is able to gather the power consumption information of the appliances $\{s_{h,a}(t)\}_{a \in \mathcal{A}_h}$ and adjust the electricity usage to achieve certain energy efficiency for the customer. If the customer is enrolled in a DR program, the HEM system can receive DR events issued by the LSE. A DR event would request the participants to shed or reschedule their demands in exchange for some incentives. Although it is possible that customers can change their demands manually, a fully-automated system which can respond to DR events automatically is more favorable for residential customers [51]. To implement such an auto DR system, an intelligent control algorithm is needed for the HEM

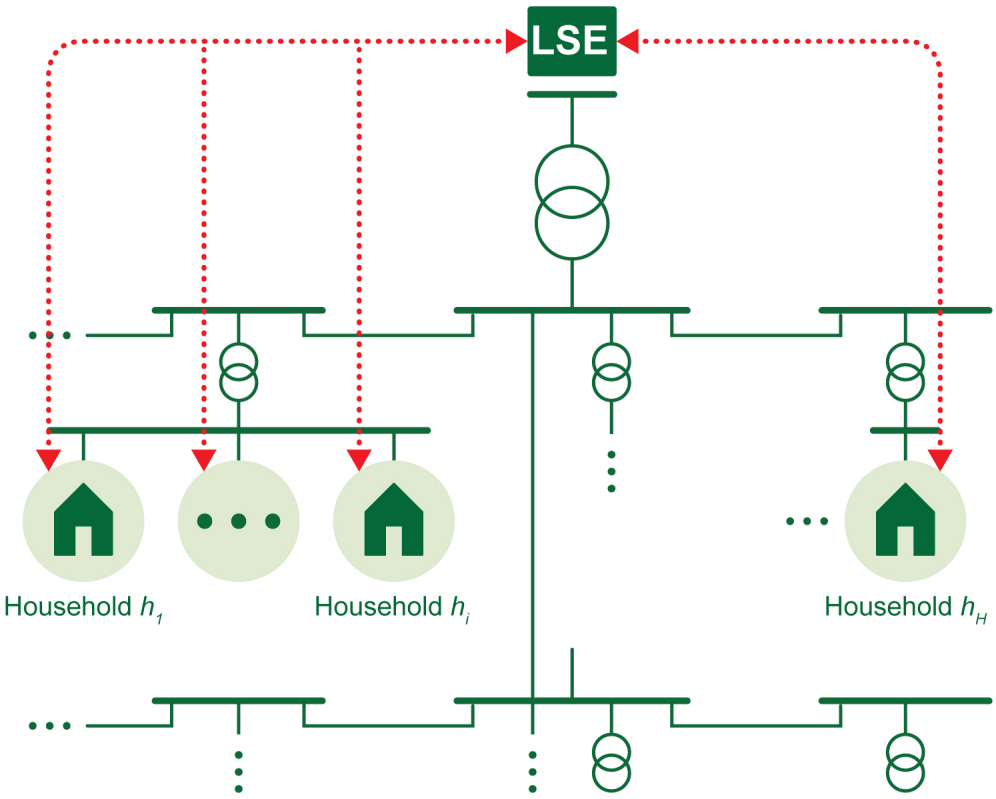

Figure 2.1: An LSE's distribution network of H households.

to manage the operations of the appliances in order to meet the DR objective.

2.2.2 Appliance Model

Household appliances can be classified into three types in the context of DR: critical, interruptible, and deferrable loads [10]. Critical loads such as refrigerators, cooking, and critical lighting should not be shifted or shed at any time. Interruptible loads such as ACs and optional lighting can be shed during DR. Deferrable loads such as washers, dryers, and EVs can be shifted during DR but they are required to consume a certain minimum energy before deadlines to finish their tasks. Since critical loads cannot participate in DR, we do not consider them here.

For a given appliance $a \in \mathcal{A}_h$, the relationship between the real power and the reactive

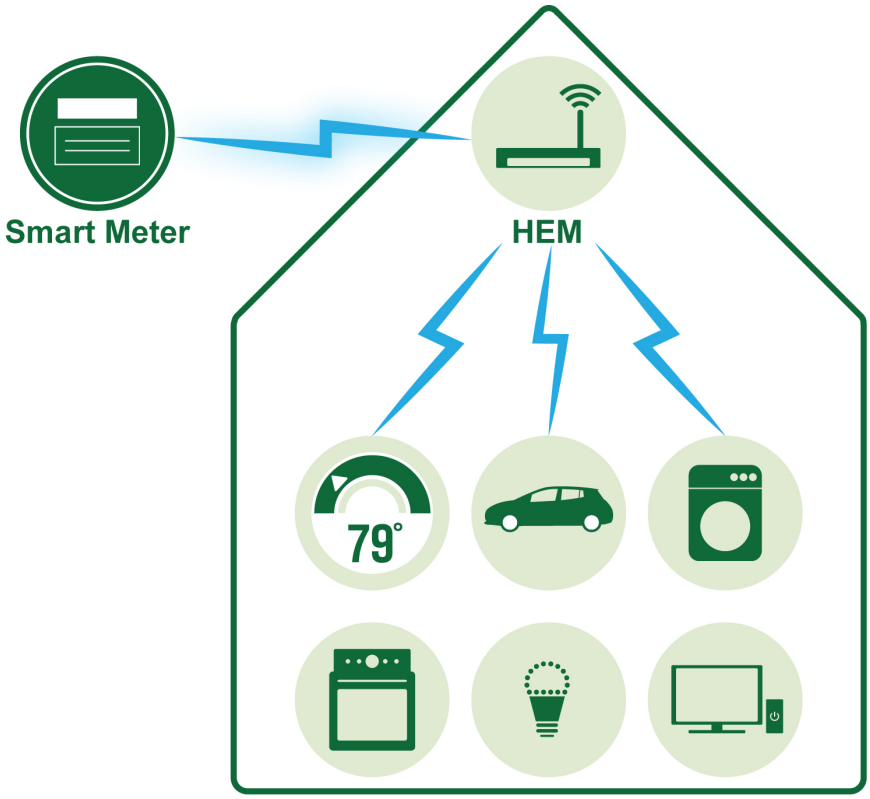

Figure 2.2: HEM system in each household.

power is given by the power factor $\eta_{h,a}(t)$:

$$\eta_{h,a}(t) = \frac{p_{h,a}(t)}{|s_{h,a}(t)|}, \forall t \in \mathcal{T}. \tag{2.1}$$

And we characterize an appliance by a set of constraints on its demand vector $\mathbf{p}_{h,a} := (p_{h,a}(t), t \in \mathcal{T})$.

Now we introduce the appliance operational constraints [11].

- For each appliance, the demand is constrained by a minimum and a maximum power denoted by $p^{\min}_{h,a}(t)$ and $p^{\max}_{h,a}(t)$, respectively:

$$p^{\min}_{h,a}(t) \leq p_{h,a}(t) \leq p^{\max}_{h,a}(t), \forall t \in \mathcal{T}. \tag{2.2}$$

  Note that $p^{\min}_{h,a}(t)$ and $p^{\max}_{h,a}(t)$ can be also used to set the available working time for the appliance. For example, if the appliance cannot run at time t, then we set $p^{\max}_{h,a}(t) = p^{\min}_{h,a}(t) = 0$.

- For thermostatically controlled appliances such as ACs and heaters, the constraint (2.2) alone is not enough. To model this kind of appliances, we need to find the relationship between the indoor temperature $T_h^{\text{in}}(t)$ and the demand vector $\mathbf{p}_{h,a}$ (refer to [11] or Section 2.4 for details). We assume that the customer sets a most comfortable temperature $T_h^{\text{comf}}(t)$ and there is a range of temperature that the customer can bear, denoted by $[T_h^{\text{comf,min}}, T_h^{\text{comf,max}}]$. In addition to (2.2), a thermostatically controlled appliance can be modeled as:

$$T_h^{\text{comf,min}} \leq T_h^{\text{in}}(t) \leq T_h^{\text{comf,max}}, \forall t \in \mathcal{T}. \tag{2.3}$$

- For deferrable loads, the cumulative energy consumption of the appliances must exceed a certain threshold in order to finish their tasks before deadlines. Let $E_{h,a}^{\min}$ and $E_{h,a}^{\max}$ denote the minimum and maximum total energy that the appliance is required to consume, respectively. The constraint on the total energy consumed by a deferrable load is given by:

$$E_{h,a}^{\min} \leq \sum_{t \in \mathcal{T}} p_{h,a}(t) \Delta t \leq E_{h,a}^{\max}. \tag{2.4}$$

2.2.3 Customer Preference Model

We model customer preference in the DR using the concept of utility function from economics. The utility function $U_{h,a}(\mathbf{p}_{h,a})$ quantifies a customer's benefit or comfort obtained by running an appliance $a \in \mathcal{A}_h$ using its demand vector $\mathbf{p}_{h,a}$. Depending on the type of the appliance, the utility function may take different forms [11].

- For interruptible loads, the utility is dependent on the power it draws at time t and may be time variant if the operation is time sensitive. For example, the utility function for interruptible loads can be defined as:

$$U_{h,a}(\mathbf{p}_{h,a}) := \sum_{t \in \mathcal{T}} U_{h,a}\left(p_{h,a}(t), t\right). \tag{2.5}$$

- For thermostatically controlled appliances, the utility is related to the temperature $T_h^{\text{in}}(t)$ and the most comfort temperature $T_h^{\text{comf}}(t)$. Therefore, the utility function can

Table 2.1: Notations

$V_i(t)$, $v_i(t)$	complex voltage on bus i with $v_i(t) = \|V_i(t)\|^2$
$s_i(t) = p_i(t) + \mathbf{i}q_i(t)$	complex load on bus i
$I_{ij}(t)$, $\ell_{ij(t)}$	complex current from buses i to j with $\ell_{ij}(t) = \|I_{ij}(t)\|^2$
$S_{ij}(t) = P_{ij}(t) + \mathbf{i}Q_{ij}(t)$	complex power from buses i to j
$z_{ij} = r_{ij} + \mathbf{i}x_{ij}$	impedance on line (i, j)

be defined in the form of:

$$U_{h,a}(\mathbf{p}_{h,a}) := \sum_{t\in\mathcal{T}} U_{h,a}\left(T_h^{\text{in}}(t), T_h^{\text{comf}}(t)\right). \tag{2.6}$$

- For deferrable loads, since a customer mainly concerns if the task can be finished before deadline, we define the utility as a function of the total energy consumption:

$$U_{h,a}(\mathbf{p}_{h,a}) := U_{h,a}\left(\sum_{t\in\mathcal{T}} p_{h,a}(t)\Delta t\right). \tag{2.7}$$

For the rest of this chapter, we assume that the utility function $U_{h,a}(\mathbf{p}_{h,a})$ is a continuously differentiable concave function for all $h \in \mathcal{H}, a \in \mathcal{A}_h$.

2.2.4 Distribution Network Model

A power distribution network can be modeled as a connected graph $\mathcal{G} = (\mathcal{N}, \mathcal{E})$, where each node $i \in \mathcal{N}$ represents a bus and each link in $\mathcal{E}$ represents a branch (line or transformer). The graph $\mathcal{G}$ is a tree for radial distribution networks. We denote a branch by $(i, j) \in \mathcal{E}$. We index the buses in $\mathcal{N}$ by $i = 0, 1, \ldots, n$, and bus 0 denotes the feeder which has a fixed voltage and flexible power injection. Table 2.1 summarizes the key notations used in modeling distribution networks for the ease of reference.

For each branch $(i, j) \in \mathcal{E}$, let $z_{ij} := r_{ij} + \mathbf{i}x_{i,j}$ denote the complex impedance of the branch, $I_{ij}(t)$ denote the complex current from buses i to j, and $S_{ij}(t) := P_{ij}(t) + \mathbf{i}Q_{ij}(t)$ denote the complex power flowing from buses i to j.

For each bus $i \in \mathcal{N}$, let $V_i(t)$ denote the complex voltage at bus i and $s_i(t) := p_i(t)+\mathbf{i}q_i(t)$ denote the complex bus load. Specifically, the feeder voltage V_0 is fixed and given. $s_0(t)$ is the power injected to the distribution system. Each load bus $i \in \mathcal{N} \setminus \{0\}$ supplies a set of households which are connected to the bus denoted by $\mathcal{H}_i \subset \mathcal{H}$. The aggregate load at each bus satisfies:

$$s_i(t) = \sum_{h \in \mathcal{H}_i} \sum_{a \in \mathcal{A}_h} s_{h,a}(t), \forall i \in \mathcal{N} \setminus \{0\}, \forall t \in \mathcal{T}. \tag{2.8}$$

Given the radial distribution network, the feeder voltage, and the impedances, then the other variables including the power flows, the voltages, the currents, and the bus loads satisfy the following physical laws for all branches $(i,j) \in \mathcal{E}$ and all $t \in \mathcal{T}$.

- Ohm's law:

$$V_i(t) - V_j(t) = z_{ij} I_{ij}(t); \tag{2.9}$$

- Power flow definition:

$$S_{ij}(t) = V_i(t) I_{ij}^*(t); \tag{2.10}$$

- Power balance:

$$S_{ij}(t) - z_{ij}|I_{ij}(t)|^2 - \sum_{k:(j,k)\in\mathcal{E}} S_{jk}(t) = s_j(t). \tag{2.11}$$

Using equations (2.9)–(2.11) and in terms of real variables, we have [52]: $\forall (i,j) \in \mathcal{E}, \forall t \in \mathcal{T}$,

$$\begin{aligned}
p_j(t) &= P_{ij}(t) - r_{ij}\ell_{ij}(t) - \sum_{k:(j,k)\in\mathcal{E}} P_{jk}(t), && (2.12)\\
q_j(t) &= Q_{ij}(t) - x_{ij}\ell_{ij}(t) - \sum_{k:(j,k)\in\mathcal{E}} Q_{jk}(t), && (2.13)\\
v_j(t) &= v_i(t) - 2\left(r_{ij}P_{ij}(t) + x_{ij}Q_{ij}(t)\right) + (r_{ij}^2 + x_{ij}^2)\ell_{ij}(t), && (2.14)\\
\ell_{ij}(t) &= \frac{P_{ij}(t)^2 + Q_{ij}(t)^2}{v_i(t)}, && (2.15)
\end{aligned}$$

where $\ell_{ij}(t) := |I_{ij}(t)|^2$ and $v_i(t) := |V_i(t)|^2$.

Equations (2.12)–(2.15) define a system of equations in the variables $(\mathbf{P}(t), \mathbf{Q}(t), \mathbf{v}(t), \mathbf{l}(t), \mathbf{s}(t))$, where $\mathbf{P}(t) := (P_{ij}(t), (i,j) \in \mathcal{E})$, $\mathbf{Q}(t) := (Q_{ij}(t), (i,j) \in \mathcal{E})$, $\mathbf{v}(t) := (v_i(t), i \in$

$\mathcal{N} \setminus \{0\})$, $\mathbf{l}(t) := (\ell_{ij}(t), (i,j) \in \mathcal{E})$, and $\mathbf{s}(t) := (s_i(t), i \in \mathcal{N} \setminus \{0\})$. The phase angles of the voltages and the currents are not included. But they can be uniquely determined for radial distribution networks [45].

2.2.5 DR Model

The objective of the LSE is to deliver reliable and high-quality power to the customers through the distribution network. However, during peak hours, the system demand may exceed the capacity or the LSE may need to use expensive generations to guarantee reliability. The voltages may also deviate significantly from their nominal values, which reduces power quality. Thus, in this chapter, we study DR aiming at keeping the system demand under a certain limit while meeting the voltage tolerance constraints during peak hours.

A DR event can be defined by a schedule and a demand limit $(\mathcal{T}_d, s_{\max})$, where $\mathcal{T}_d \subseteq \mathcal{T}$ is the schedule which specifies the start time and the end time of the DR event and $s_{\max}$ is the demand limit imposed by either the system capacity or the LSE according to the supply.

Given the DR event, the system demand constraint can be modeled as:

$$|s_0(t)| \leq s_{\max}, \forall t \in \mathcal{T}_d, \tag{2.16}$$

where $s_0(t)$ is the total complex power injected to the distribution system and it is given by:

$$s_0(t) = \sum_{j:(0,j)\in\mathcal{E}} S_{0j}(t), \forall t \in \mathcal{T}. \tag{2.17}$$

We also consider the voltage tolerance constraints in the distribution network which keep the magnitudes of the voltage at each load bus within a certain range during a DR event:

$$V_i^{\min} \leq |V_i(t)| \leq V_i^{\max}, \ \forall i \in \mathcal{N} \setminus \{0\}, \forall t \in \mathcal{T}_d. \tag{2.18}$$

The allowed voltage range for different distribution systems can be found in the standard [53].

The objective of the proposed DR scheme is to find a set of optimal demand vectors to maximize the aggregate utilities of the appliances in the households and minimize the power losses in the distribution network subject to the appliance operational constraints, the power

flow constraints, the system demand constraint, and the system operational constraints (voltage tolerances).

We define $\mathbf{P} := (\mathbf{P}(t), t \in \mathcal{T})$, $\mathbf{Q} := (\mathbf{Q}(t), t \in \mathcal{T})$, $\mathbf{v} := (\mathbf{v}(t), t \in \mathcal{T})$, $\mathbf{l} := (\mathbf{l}(t), t \in \mathcal{T})$, $\mathbf{s}_{h,a} := (s_{h,a}(t), t \in \mathcal{T})$, and $\mathbf{s} := (\mathbf{s}_{h,a}, h \in \mathcal{H}, a \in \mathcal{A}_h)$. The residential DR can be formulated as an OPF problem.

OPF

$$\begin{aligned} \max_{\mathbf{P},\mathbf{Q},\mathbf{v},\mathbf{l},\mathbf{s}} \quad & \sum_{h\in\mathcal{H}} \sum_{a\in\mathcal{A}_h} U_{h,a}(\mathbf{p}_{h,a}) - \kappa \sum_{t\in\mathcal{T}} \sum_{(i,j)\in\mathcal{E}} r_{ij}\ell_{ij}(t) \\ \text{s.t.} \quad & (2.1) - (2.4), (2.8), (2.12) - (2.18), \end{aligned}$$

where $U_{h,a}(\mathbf{p}_{h,a})$ is defined by (2.5)–(2.7); (2.1)–(2.4) are the appliance operational constraints; (2.8), (2.12)–(2.15) are the power flow constraints; (2.16) and (2.17) are the system demand constraints; (2.18) is the voltage tolerance constraint; and κ is a parameter to trade off between customer utility maximization and power loss minimization. A large κ means that the LSE is more self-interested in minimizing the power losses rather than maximizing the customer utilities.

2.3 Distributed DR Scheme

In this chapter, we focus on developing a scalable distributed DR scheme rather than a centralized scheme due to the large number of appliances that need to be managed by the scheme. Moreover, the proposed DR scheme also needs to protect the privacy for the residential customers. To design such a distributed DR scheme, we relax the previous OPF problem to be a convex problem and propose a distributed algorithm to solve it. The convexity of the relaxed OPF problem guarantees the convergence of the distributed algorithm.

2.3.1 Introduction to PCPM

In this chapter, we develop a distributed DR scheme using the predictor corrector proximal multiplier (PCPM) algorithm [54]. PCPM is a decomposition method for solving convex

optimization problem. At each iteration, it computes two proximal steps in the dual variables and one proximal step in the primal variables. We give a very brief description of the PCPM algorithm below.

Consider a convex optimization problem with separable structure of the form:

$$\min_{\mathbf{x}\in\mathcal{X},\mathbf{y}\in\mathcal{Y}} \quad f(\mathbf{x}) + g(\mathbf{y}) \tag{2.19}$$

$$\text{s.t.} \quad A\mathbf{x} + B\mathbf{y} = \mathbf{c}. \tag{2.20}$$

Let $\mathbf{z}$ be the Lagrangian variable for the constraint (2.20).

The steps of the PCPM algorithm to solve the problem are given as follows:

1. Initially set $k \leftarrow 0$ and choose the initial $(\mathbf{x}^0, \mathbf{y}^0, \mathbf{z}^0)$ randomly.

2. For each $k \geq 0$, update a virtual variable $\hat{\mathbf{z}}^k := \mathbf{z}^k + \gamma(A\mathbf{x}^k + B\mathbf{y}^k - \mathbf{c})$ where $\gamma > 0$ is a constant step size.

3. Solve

$$\begin{aligned}
\mathbf{x}^{k+1} &= \arg\min_{\mathbf{x}\in\mathcal{X}}\{f(\mathbf{x}) + (\hat{\mathbf{z}}^k)^T A\mathbf{x} + \frac{1}{2\gamma}||\mathbf{x} - \mathbf{x}^k||^2\}, \\
\mathbf{y}^{k+1} &= \arg\min_{\mathbf{y}\in\mathcal{Y}}\{g(\mathbf{y}) + (\hat{\mathbf{z}}^k)^T B\mathbf{y} + \frac{1}{2\gamma}||\mathbf{y} - \mathbf{y}^k||^2\}.
\end{aligned}$$

4. Update $\mathbf{z}^{k+1} := \mathbf{z}^k + \gamma(A\mathbf{x}^{k+1} + B\mathbf{y}^{k+1} - \mathbf{c})$.

5. $k \leftarrow k + 1$, and go to step 2 until convergence.

Steps 2 and 4 can be seen as a predictor step and a corrector step to the Lagrange multiplier, respectively. It has been shown in [54] that the above algorithm will converge to a primal-dual optimal solution $(\mathbf{x}^*, \mathbf{y}^*, \mathbf{z}^*)$ for a sufficient small positive step size γ as long as strong duality holds for the convex problem (2.19).

2.3.2 Convexification of OPF

The previous OPF problem is non-convex due to the quadratic equality constraint in (2.15) and thus is difficult to solve. Moreover, most decentralized algorithms require convexity to ensure convergence [55]. We therefore relax them to inequalities:

$$\ell_{ij}(t) \geq \frac{P_{ij}(t)^2 + Q_{ij}(t)^2}{v_i(t)}, \ \forall (i,j) \in \mathcal{E}, \forall t \in \mathcal{T}. \tag{2.21}$$

Now we consider the following convex relaxation of OPF.

OPF-r

$$\begin{aligned} \max_{\mathbf{P},\mathbf{Q},\mathbf{v},\mathbf{l},\mathbf{s}} \quad & \sum_{h\in\mathcal{H}} \sum_{a\in\mathcal{A}_h} U_{h,a}(\mathbf{p}_{h,a}) - \kappa \sum_{t\in\mathcal{T}} \sum_{(i,j)\in\mathcal{E}} r_{ij}\ell_{ij}(t) \\ \text{s.t.} \quad & (2.1)-(2.4), (2.8), (2.12)-(2.14), (2.16)-(2.21). \end{aligned}$$

OPF-r provides an upper bound to OPF. For an optimal solution of OPF-r, if the equality in (2.21) is attained at the solution, then it is also an optimal solution of OPF. We call OPF-r an exact relaxation of OPF if every solution to OPF-r is also a solution of OPF, and vice versa.

The sufficient conditions under which OPF-r is an exact relaxation of OPF for radial distribution networks have been derived in previous studies [46–48]. Roughly speaking, if the bus voltage is kept around the nominal value and the power injection at each bus is not too large, then the relaxation is exact. For detailed conditions, please refer to [46]. More sufficient conditions can be found in [47, 48]. Those conditions are verified to hold for many IEEE standard distribution networks and real-world networks. When OPF-r is an exact relaxation of OPF, we can focus on solving the convex optimization problem OPF-r. In this chapter, we assume that the conditions for exact relaxation of OPF to OPF-r specified in [46–48] hold for the radial distribution network and therefore OPF-r is an exact relaxation of OPF and strong duality holds for OPF-r.

2.3.3 Distributed Algorithm

To solve OPF-r in a centralized way, it requires not only the distribution network information but also the private information of the appliances (i.e., utility functions and schedules). In order to protect customer privacy and make the DR scalable, we propose a distributed DR scheme to solve the OPF-r problem using the PCPM algorithm (refer to [54] or Section 2.3.1 for details).

Initially set $k \leftarrow 0$. The HEM in each household $h \in \mathcal{H}$ sets the initial demand schedule $\mathbf{s}_{h,a}^k$ for each appliance $a \in \mathcal{A}_h$ according to its preferable demand schedule. The HEM then communicates its aggregate demand schedule $\mathbf{s}_h^k := \sum_{a\in\mathcal{A}_h} \mathbf{s}_{h,a}^k$ to the LSE. In the meantime, the LSE randomly chooses the initial $s_i^k(t) := p_i^k(t) + \mathbf{i}q_i^k(t)$ and two virtual control signals $\{\mu_i^k(t)\}_{t\in\mathcal{T}}$, $\{\lambda_i^k(t)\}_{t\in\mathcal{T}}$ for each bus $i \in \mathcal{N} \setminus \{0\}$.

At the beginning of the k-th step, the LSE sends two DR control signals $\hat{\mu}_i^k(t) := \mu_i^k(t) + \gamma(\sum_{h\in\mathcal{H}_i} p_h^k(t) - p_i^k(t))$ and $\hat{\lambda}_i^k(t) := \lambda_i^k(t) + \gamma(\sum_{h\in\mathcal{H}_i} q_h^k(t) - q_i^k(t))$ to the HEMs in households $h \in \mathcal{H}_i$ for all $t \in \mathcal{T}$, where γ is a positive constant. Then,

- The HEM in each household $h \in \mathcal{H}_i$ solves the following problem for each appliance $a \in \mathcal{A}_h$.

  DR-household

$$\begin{aligned} \max_{\mathbf{s}_{h,a}} \quad & U_{h,a}(\mathbf{p}_{h,a}) - (\hat{\boldsymbol{\mu}}_i^k)^T \mathbf{p}_{h,a} - (\hat{\boldsymbol{\lambda}}_i^k)^T \mathbf{q}_{h,a} - \frac{1}{2\gamma}||\mathbf{p}_{h,a} - \mathbf{p}_{h,a}^k||^2 \\ & - \frac{1}{2\gamma}||\mathbf{q}_{h,a} - \mathbf{q}_{h,a}^k||^2 \\ \text{s.t.} \quad & (2.1) - (2.4), \end{aligned}$$

  where $\hat{\boldsymbol{\mu}}_i^k := (\hat{\mu}_i^k(t), t \in \mathcal{T})$ and $\hat{\boldsymbol{\lambda}}_i^k := (\hat{\lambda}_i^k(t), t \in \mathcal{T})$. The optimal $\mathbf{s}_{h,a}^*$ is set as $\mathbf{s}_{h,a}^{k+1}$.

- The LSE solves the following problem for each time $t \in \mathcal{T}$.

Algorithm 1 - The Proposed Distributed DR Scheme.

1: **initialization** $k \leftarrow 0$. The HEM sets the initial $\mathbf{s}_{h,a}^k$ and returns the aggregate demand schedule $\mathbf{s}_h^k$ to the LSE. The LSE sets the initial $\mu_i^k(t)$, $\lambda_i^k(t)$ and the initial $s_i^k(t)$ randomly.

2: **repeat**

3: The LSE updates $\hat{\mu}_i^k(t)$ and $\hat{\lambda}_i^k(t)$ and sends the DR control signals $\hat{\boldsymbol{\mu}}_i^k$ and $\hat{\boldsymbol{\lambda}}_i^k$ to the HEMs in the households $h \in \mathcal{H}_i$.

4: The HEM in each household calculates a new demand schedule $\mathbf{s}_{h,a}^{k+1}$ for each appliance $a \in \mathcal{A}_h$ by solving the DR-household problem.

5: The LSE computes a new $\mathbf{s}^{k+1}(t)$ for each time $t \in \mathcal{T}$ by solving the DR-LSE problem.

6: The HEM communicates the aggregate demand schedule $\mathbf{s}_h^{k+1}$ to the LSE.

7: The LSE updates $\mu_i^{k+1}(t)$ and $\lambda_i^{k+1}(t)$.

8: $k \leftarrow k+1$.

9: **until** convergence

DR-LSE

$$\begin{aligned} \max_{\substack{\mathbf{P}(t),\mathbf{Q}(t),\\ \mathbf{v}(t),\mathbf{l}(t),\mathbf{s}(t)}} \quad & (\hat{\boldsymbol{\mu}}^k(t))^T\mathbf{p}(t) + (\hat{\boldsymbol{\lambda}}^k(t))^T\mathbf{q}(t) - \kappa \sum_{(i,j)\in\mathcal{E}} r_{ij}\ell_{ij}(t) \\ & -\frac{1}{2\gamma}||\mathbf{p}(t) - \mathbf{p}^k(t)||^2 - \frac{1}{2\gamma}||\mathbf{q}(t) - \mathbf{q}^k(t)||^2 \\ \text{s.t.} \quad & (2.12) - (2.14), (2.16) - (2.21), \end{aligned}$$

where $\hat{\boldsymbol{\mu}}^k(t) := (\hat{\mu}_i^k(t), i \in \mathcal{N} \setminus \{0\})$ and $\hat{\boldsymbol{\lambda}}^k(t) := (\hat{\lambda}_i^k(t), i \in \mathcal{N} \setminus \{0\})$. The optimal $\mathbf{s}^*(t)$ is set as $\mathbf{s}^{k+1}(t)$.

At the end of the k-th step, the HEM in household h communicates its aggregate demand schedule $\mathbf{s}_h^{k+1} := \sum_{a\in\mathcal{A}_h} \mathbf{s}_{h,a}^{k+1}$ to the LSE and the LSE updates $\mu_i^{k+1}(t) := \mu_i^k(t) + \gamma(\sum_{h\in\mathcal{H}_i} p_h^{k+1}(t) - p_i^{k+1}(t))$ and $\lambda_i^{k+1}(t) := \lambda_i^k(t) + \gamma(\sum_{h\in\mathcal{H}_i} q_h^{k+1}(t) - q_i^{k+1}(t))$ for all $i \in \mathcal{N}\setminus\{0\}$ and all $t \in \mathcal{T}$. Set $k \leftarrow k+1$, and repeat the process until convergence.

A complete description of the proposed DR scheme can be found in Algorithm 1. When γ is small enough, the above algorithm will converge to the optimal solution of OPF-r which is also the optimal solution of OPF if the relaxation is exact, and $(\sum_{h\in\mathcal{H}_i} p_h^k(t) - p_i^k(t))$ and $(\sum_{h\in\mathcal{H}_i} q_h^k(t) - q_i^k(t))$ will converge to zero [54]. As we can see, the LSE and the HEMs in the

households interactively communicate to compute the optimal demand schedule. Therefore, the two-way communications network in the distribution system is crucial to implement the proposed DR scheme. Notice that after the LSE and the customers jointly compute the optimal demand schedule over $t \in \mathcal{T}$, the LSE only controls the demands during the DR period according to the optimal schedule over $t \in \mathcal{T}_d$. The customers may or may not follow the optimal demand schedule exactly for the rest of the time $\mathcal{T} \setminus \mathcal{T}_d$.

In the proposed DR scheme, the private information of the customer including the utility functions $U_{h,a}(\mathbf{p}_{h,a})$ and the appliance operational constraints (2.1)–(2.4) appears only in the DR-household problem which is solved by the HEM owned by the customer. The LSE solves the DR-LSE problem using the system information including the power flow constraints (2.12)–(2.14) and (2.21), the system demand constraints (2.16) and (2.17), the voltage tolerance constraints (2.18), and the power losses $\sum_{(i,j)\in\mathcal{E}} r_{ij}\ell_{ij}(t)$. Therefore, there is no appliance-level information gathered by the LSE and customer privacy can be protected in the DR process.

2.4 Performance Evaluation

In this section, we demonstrate the proposed DR scheme by applying it to an IEEE standard distribution system. We first describe the distribution system used in the simulation and give the parameters of the scheme. Then we present the simulation results of the proposed DR scheme and discuss the interesting effects that we observe from the simulation.

2.4.1 Simulation Setup

We use the IEEE 13-node test feeder [49] as the power distribution system which is shown in Fig. 2.3.[1] We assume that there are 10 households connected to each load bus. In the

[1]In order to exemplify the effect of DR on both the households and the distribution network, we made several changes to the standard IEEE 13-node test feeder: the inline transformer between node 633 and node 634 is omitted, the switch between node 671 and node 692 is closed, and the line lengths are increased by 5 times. The feeder has a nominal voltage of 4.16kV. Since our focus is on residential customers, we assume that there is a secondary distribution transformer at each load bus which scales the voltage down to 120/240V to serve multiple households.

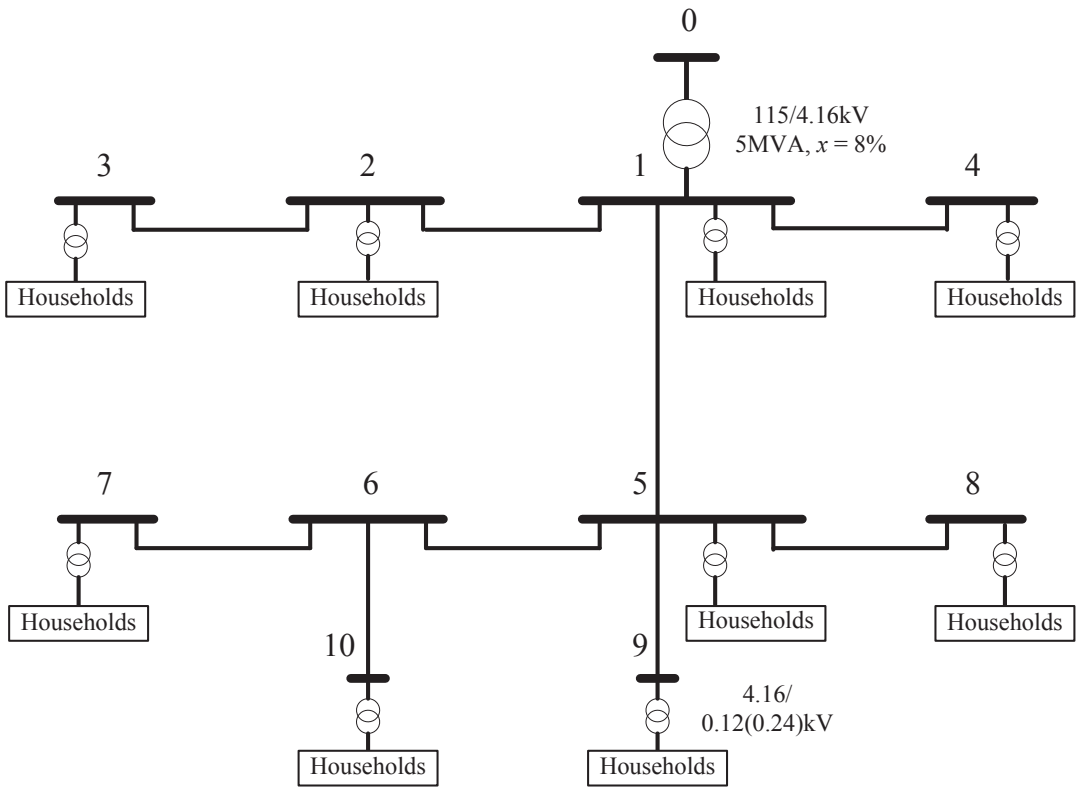

Figure 2.3: Modified IEEE standard distribution system.

simulation, a day starts from 8 am. The time interval Δt in the model is one hour and we denote a day by $\mathcal{T}_D := \{8, 9, \ldots, 24, 1, \ldots, 7\}$ where each $t \in \mathcal{T}_D$ denotes the hour of $[t, t+1]$. The scheduling horizon $\mathcal{T}$ used by the LSE to calculate the optimal DR strategy is chosen to be $\mathcal{T} := \{t_s, t_s + 1, \ldots, 7\} \subseteq \mathcal{T}_D$, where t_s is the time that the DR event starts.

A total of 6 different appliances including ACs, EVs, washers, dryers, lighting, and plug loads are considered in the simulation. The power factor of each appliance $\eta_{h,a}(t)$ is assumed to be constant and its value is selected randomly from $[0.8, 0.9]$. We further assume that there is a preferable demand schedule (i.e., the baseline power consumption without any DR incentives) for each appliance denoted by $\mathbf{p}_{h,a}^{\text{pref}} := (p_{h,a}^{\text{pref}}(t), t \in \mathcal{T})$. Detailed descriptions for the appliances are given as follows.

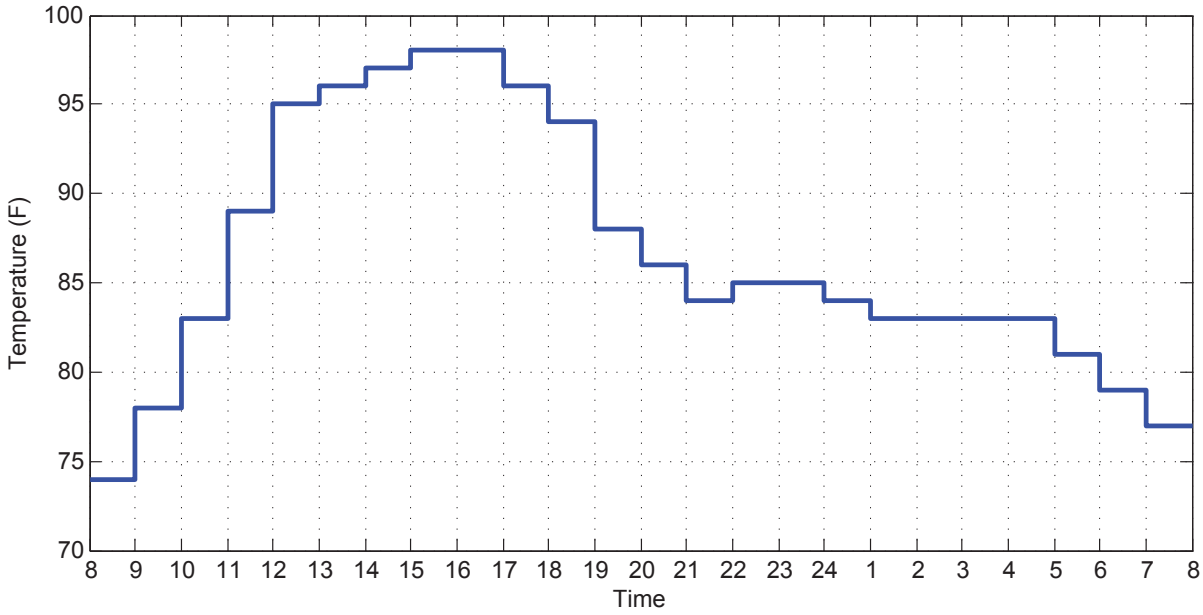

Figure 2.4: Outside temperature of a day.

2.4.1.1 ACs

An AC is a thermostatically controlled appliance. Let $T_h^{\text{out}}(t)$ denote the outside temperature. We assume that the indoor temperature evolves according to [11]:

$$T_h^{\text{in}}(t) = T_h^{\text{in}}(t-1) + \alpha \left(T_h^{\text{out}}(t) - T_h^{\text{in}}(t-1)\right) + \beta p_{h,a}(t), \tag{2.22}$$

where α and β are the thermal parameters of the environment and the appliance, respectively. α is a positive constant and β is positive if the AC is running in the heating mode or negative in the cooling mode. Using (2.22), we define the utility of an AC as $U_{h,a}\left(T_h^{\text{in}}(t), T_h^{\text{comf}}(t)\right) := c_{h,a} - b_{h,a}\left(T_h^{\text{in}}(t) - T_h^{\text{comf}}(t)\right)^2$, where $b_{h,a}$ and $c_{h,a}$ are positive constants.

In the simulation, we choose the thermal parameters as $\alpha = 0.9$ and β is chosen randomly from $[-0.008, -0.005]$. The outside temperature of the day is given in Fig. 2.4 which is a typical summer day in Southern California. For each household, we assume the comfortable temperature range to be $[70\text{F}, 79\text{F}]$ and the most comfortable temperature $T_h^{\text{comf}}(t)$ is chosen randomly from $[73\text{F}, 76\text{F}]$. The maximum and minimum power are $p_{h,a}^{\max} = 4\text{kW}$ and $p_{h,a}^{\min} = 0\text{kW}$, respectively.

2.4.1.2 EVs

An EV is a deferrable load. We assume that the EV arriving time $t_{h,e}$ is randomly chosen from $[17, 19]$. It starts charging immediately after arriving and must finish charging before $t = 6$. The maximum and minimum charging rates are $p_{h,a}^{\max} = 3\text{kW}$ and $p_{h,a}^{\min} = 0\text{kW}$, respectively. The maximum charging requirement $E_{h,a}^{\max}$ is chosen randomly from $[20\text{kWh}, 24\text{kWh}]$ and $E_{h,a}^{\min}$ is chosen randomly from $[15\text{kWh}, 18\text{kWh}]$. The utility function is in the form of $U_{h,a}(\mathbf{p}_{h,a}) := b_{h,a}\left(\sum_{t\in\mathcal{T}} p_{h,a}(t)\right) - \sum_{t\in\mathcal{T}} t|p_{h,a}(t) - p_{h,a}^{\text{pref}}(t)| + c_{h,a}$.

2.4.1.3 Washers

A washer is a deferrable load. Its starting time $t_{h,w}$ is chosen randomly from $[t_{h,e}, 20]$. It must finish its job within 2 hours. The maximum and minimum power are $p_{h,a}^{\max} = 700\text{W}$ and $p_{h,a}^{\min} = 0\text{W}$, respectively. The maximum energy requirement $E_{h,a}^{\max}$ is chosen randomly from $[900\text{Wh}, 1200\text{Wh}]$ and $E_{h,a}^{\min}$ is chosen randomly from $[600\text{Wh}, 800\text{Wh}]$. The utility function takes the same form as that of an EV.

2.4.1.4 Dryers

A dryer is a deferrable load. It starts working at $t_{h,w} + 2$ and must finish before $t = 1$. The maximum and minimum power are $p_{h,a}^{\max} = 5\text{kW}$ and $p_{h,a}^{\min} = 0\text{kW}$, respectively. The maximum energy requirement $E_{h,a}^{\max}$ is chosen randomly from $[7.5\text{kWh}, 10\text{kWh}]$ and $E_{h,a}^{\min}$ is chosen randomly from $[4\text{kWh}, 5\text{kWh}]$. The utility function takes the same form as that of an EV.

2.4.1.5 Lighting

Lighting is an interruptible load. Its working time is $[19, 24] \cup [1, 7]$. The maximum and minimum power are $p_{h,a}^{\max} = 1.0\text{kW}$ and $p_{h,a}^{\min} = 0.5\text{kW}$, respectively. The utility function takes the form of $U_{h,a}\left(p_{h,a}(t), t\right) := c_{h,a} - b_{h,a}(p_{h,a}(t) - p_{h,a}^{\text{pref}}(t))^2$.

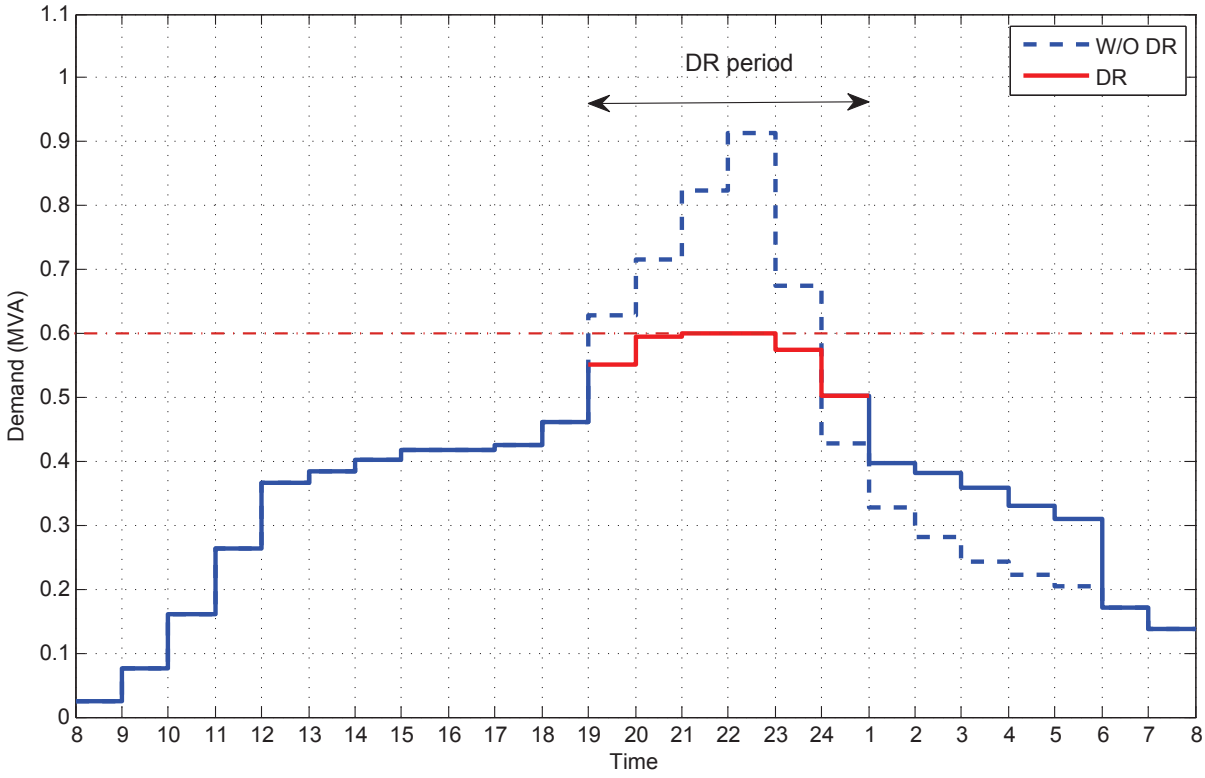

Figure 2.5: Load profile of the feeder $|s_0(t)|$ without and with DR.

2.4.1.6 Plug Loads

Plug loads include other common household appliances such as TVs, home theaters, PCs, etc. They belong to interruptible loads. The maximum and minimum power are $p_{h,a}^{\max} = 500\text{W}$ and $p_{h,a}^{\min} = 0\text{W}$, respectively. The utility function takes the same form as that of lighting.

2.4.2 Case Study

We simulate our proposed DR scheme in the modified IEEE standard distribution system. The voltage at the feeder V_0 is assumed to be fixed at 4.16kV and there are no voltage regulators or capacitors on the distribution lines. The minimum allowed voltage at each load bus $V_i^{\min}$ is set to be 4.05kV [53]. The parameters in our proposed DR scheme are chosen as $\kappa := 0.01$ and $\gamma := 0.25$.

We use the preferable schedules of the appliances as the baseline in the simulation. More

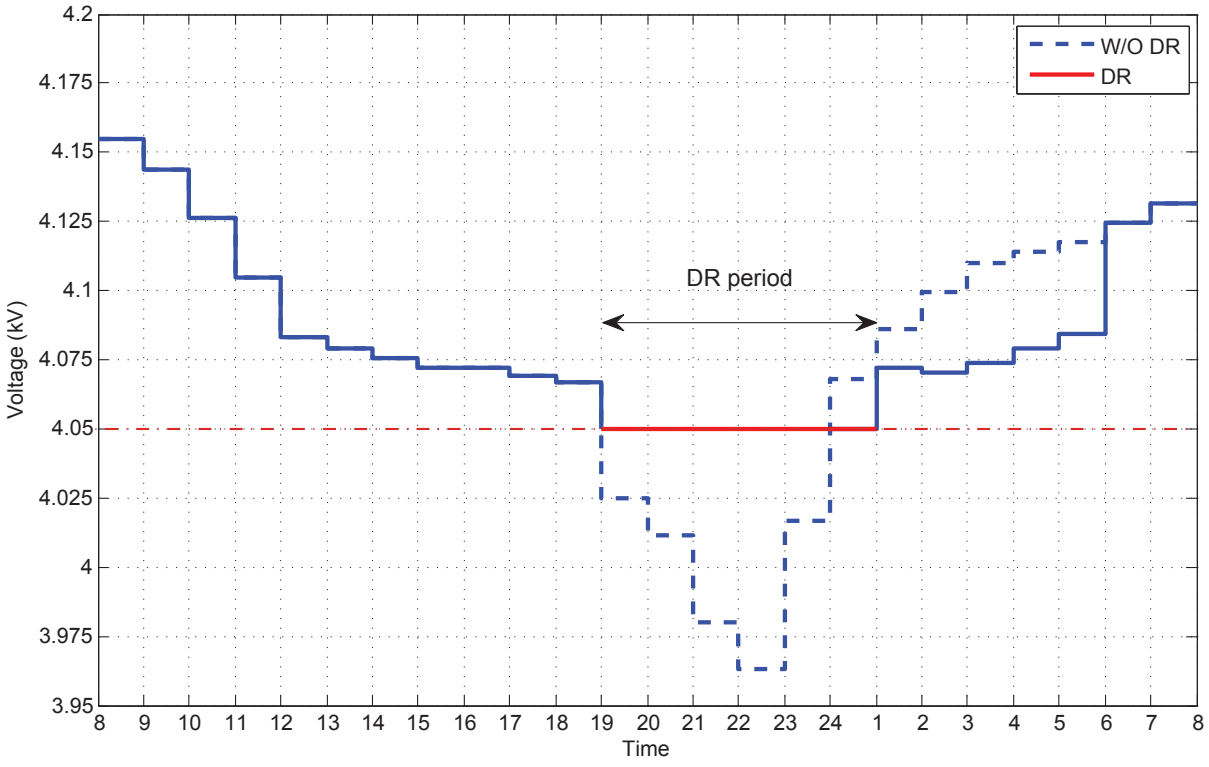

Figure 2.6: Minimum bus voltage profile without and with DR.

specifically, the AC keeps the indoor temperature to the most comfortable temperature $T_h^{\text{comf}}(t)$ all day. The EV, the washer, and the dryer run at their maximum power $p_{h,a}^{\max}(t)$ until the maximum energy requirement $E_{h,a}^{\max}$ is met. Lighting and the plug loads use the power as they request.

The load profile of the feeder $|s_0(t)|$ without DR is shown by the dashed line in Fig. 2.5. It can be seen that the system demand is low for most of the day. The peak starts at $t = 19$ and lasts until $t = 23$. The dashed line in Fig. 2.6 shows the minimum bus voltage in the distribution network over time. It can be seen that the minimum bus voltage is below the voltage rating during the peak hours. By comparing Fig. 2.5 with Fig. 2.6, we can find that there is a significant correlation between the load level and the voltage drop. The higher the demand is, the more significant the voltage drop is.

To simulate a DR event, we need to choose the DR parameters including the demand limit $s_{\max}$ and the schedule $\mathcal{T}_d$. In our simulation, we assume that the LSE imposes a demand

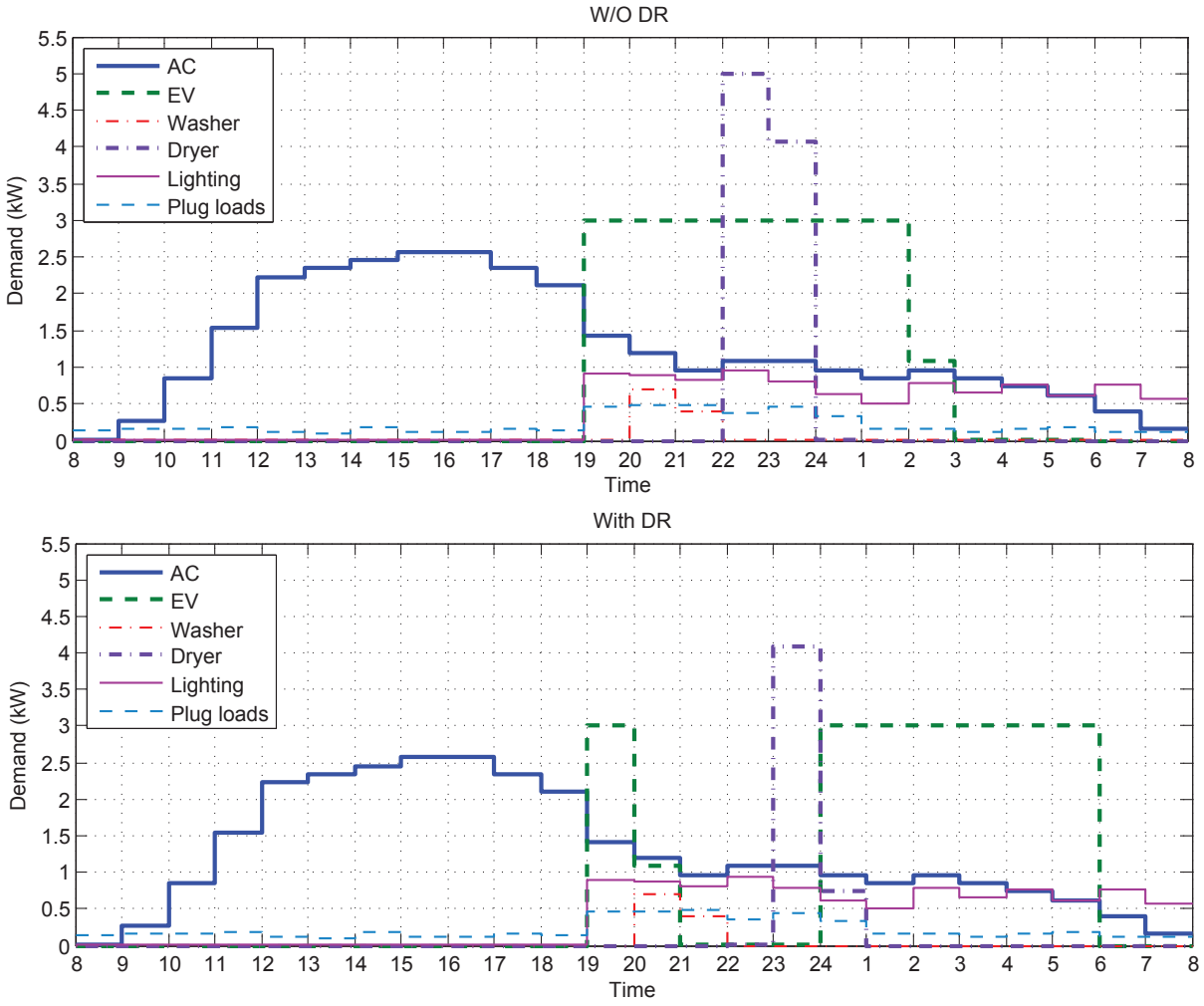

Figure 2.7: Load profile of the appliances in one of the households without and with DR.

limit of $s_{\max} = 0.6$MVA during the time period $[19, 24]$. The DR period is chosen in a way to prevent the rebound effect which will be discussed later.

The simulated load profile of the feeder $|s_0(t)|$ with DR is shown by the solid line in Fig. 2.5. Note that the LSE only controls the demands during the peak hours (shown by red). The load profile after the DR ends is based on the optimal demand schedules produced by our proposed DR scheme. The customers may or may not follow the optimal demand schedules. From Fig. 2.5, it can be seen that our proposed DR scheme can effectively manage the appliances of the households in the distribution network to keep the system demand under the demand limit during the DR event. The solid line in Fig. 2.6 shows the minimum bus

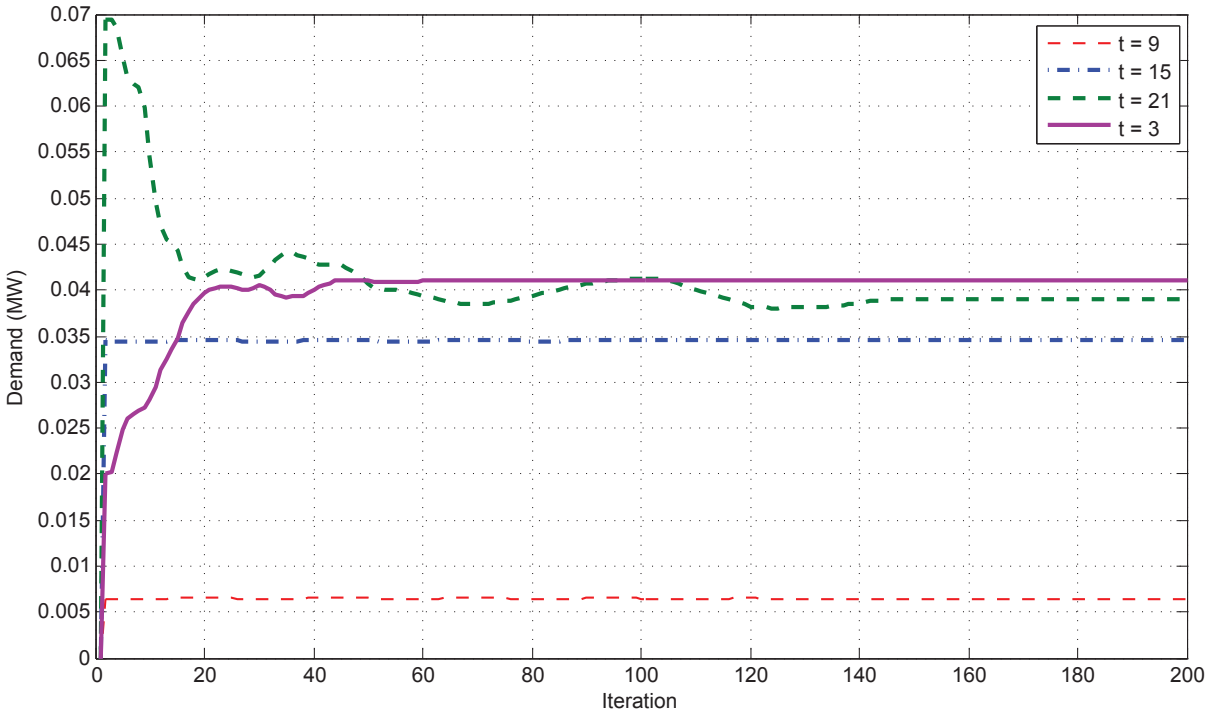

Figure 2.8: Dynamics of DR-household: the aggregate real power at bus 8.

voltage profile with DR. We can see that in addition to keep the system demand below the limit, our proposed DR scheme is also able to maintain the bus voltage levels within the allowed range during the DR event.

Fig. 2.7 shows the load profile of the appliances in one of the households without and with DR. Both load shifting and load shedding can be found in the figure: the deferrable loads (the EV and the dryer) are shifted and the total energy that the dryer consumes is reduced. If we compare the daily system demand without and with DR, we can find a demand reduction of 0.05MVA which is about 3% of the daily system demand.

Fig. 2.8 and Fig. 2.9 show the dynamics of the proposed distributed DR scheme. As we can see from the figures, both DR-household and DR-LSE converge fast in the simulation. For all the simulations, we also verify that the solution to the centralized OPF-r problem is the same as the solution to the distributed algorithm using the CVX package [56]. We further verify that the equality in (2.21) is attained in the optimal solution to OPF-r, i.e., OPF-r is an exact relaxation of OPF.

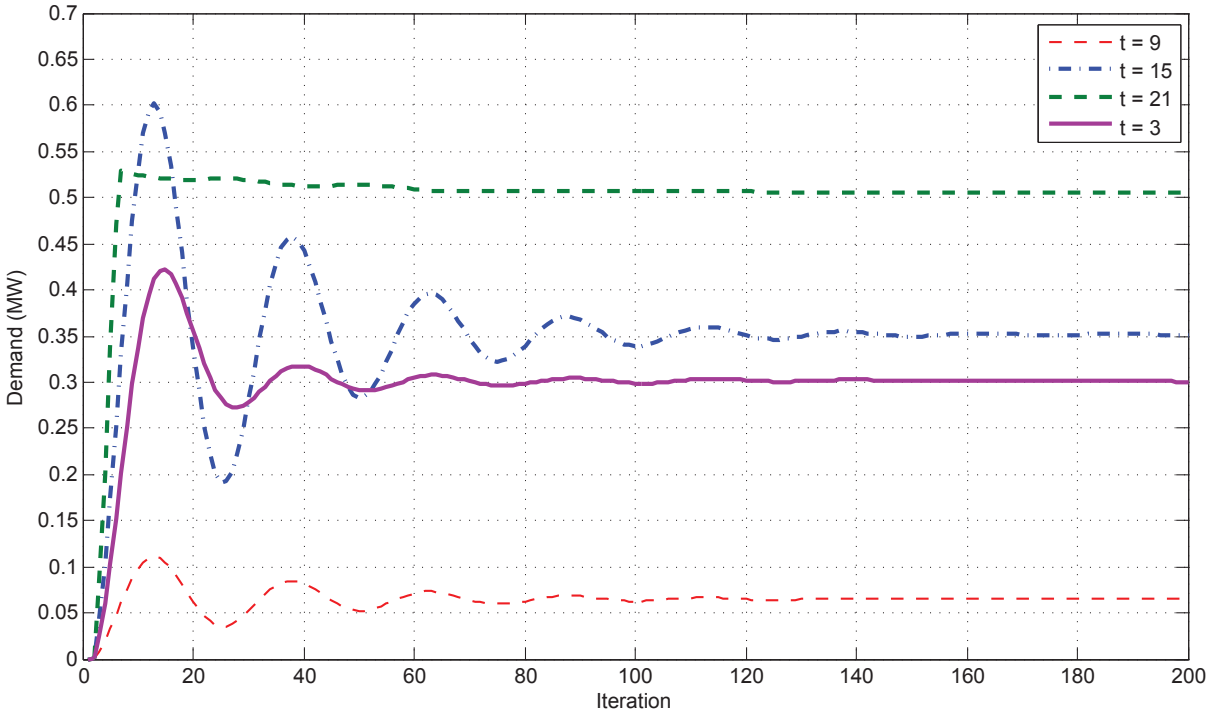

Figure 2.9: Dynamics of DR-LSE: the real power injected to the system p_0.

2.4.3 Discussions

2.4.3.1 Location Effect

Fig. 2.10 and Fig. 2.11 show the aggregate load profile of the households at each load bus $|s_i(t)|$ without and with DR, respectively. By comparing the two figures, it can be found that the loads at the buses far away from the feeder (buses 5–10) contribute more than the loads at the buses close to the feeder (buses 1–4) to the demand reduction in the DR event. The shifted demands from on-peak hours to off-peak hours are largely from the buses far away from the feeder.

The reason for this location effect is due to both the power loss minimization and the voltage regulation in DR. The power loss and voltage drop along the distribution line are related to not only the load level but also the length of the line. As the length of the distribution line increases, the impedance of the line increases, leading to a higher power loss and voltage drop. Therefore, in order to decrease the total power injection into the

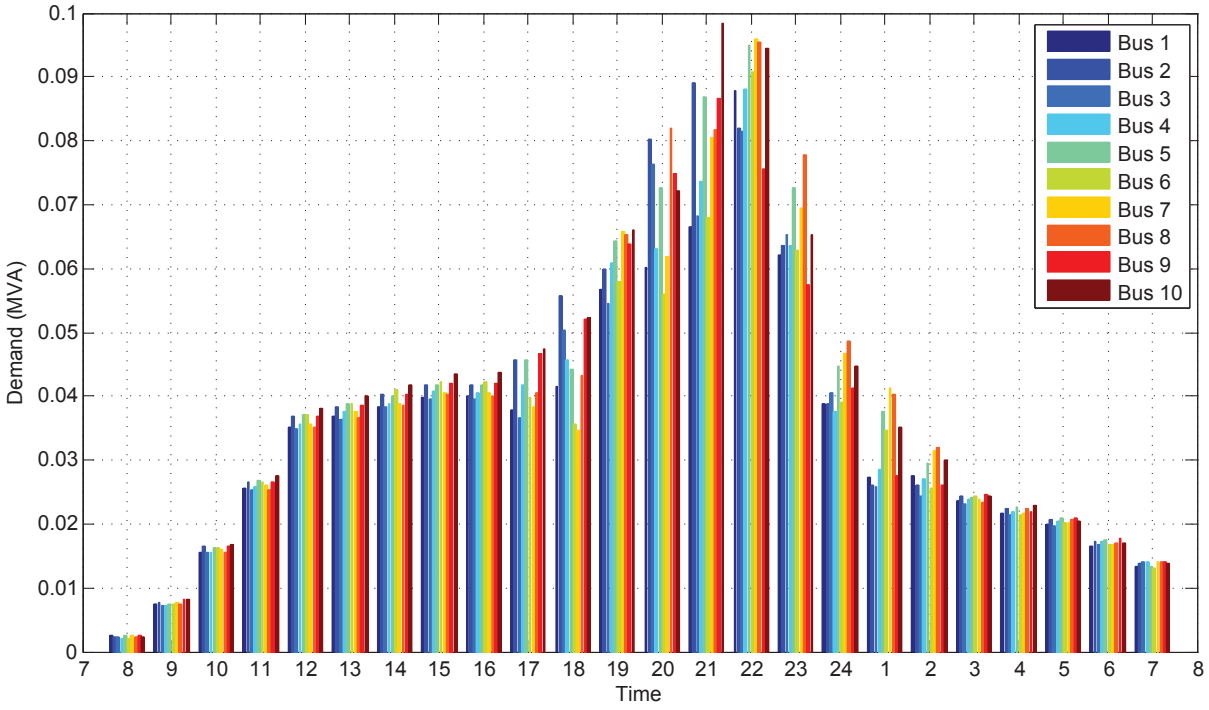

Figure 2.10: Aggregate load profile of the households at each bus without DR.

distribution system, which includes both the total power consumption and the power losses, and also to meet the voltage tolerance constraints, the households at the buses far away from the feeder must shed or shift more demands than the households at the buses close to the feeder. This location effect implies a potential fairness issue in DR since the impacts of DR on the households are not the same. The LSE may need to set the DR incentives given to the households differently based on their locations in the network. Mechanisms to compensate such location discrimination can be developed in the future.

2.4.3.2 Rebound Effect

In the previous simulation, we use the DR schedule $[19, 24]$. An interesting rebound effect of DR can be observed if we reduce the DR period by one hour. The simulation result using the new schedule $[19, 23]$ is shown in Fig. 2.12. It can be seen from the figure that although our proposed DR scheme is effective to keep the system demand below the demand limit during the DR period $[19, 23]$, it creates a rebound peak about 0.8MVA at $t = 24$ right after

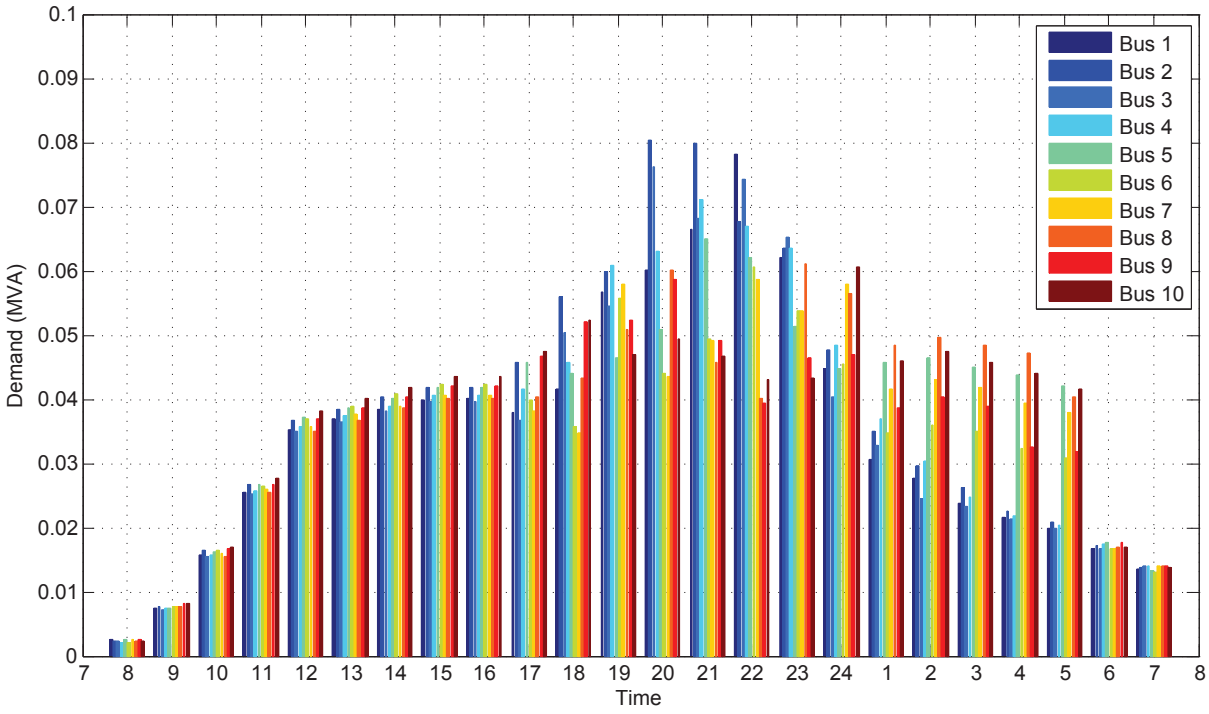

Figure 2.11: Aggregate load profile of the households at each bus with DR.

the DR event ends. The rebound effect is not desirable because the new peak brings the same problems to the system as the old peak.

The reason for this rebound effect is that when the DR shifts the peak demands to off-peak periods, it may create another peak. The rebound effect shown in our simulation suggests that the LSE should choose the DR parameters (i.e., the demand limit and the DR schedule) carefully when designing a DR event. Since the demand limit is usually determined by the system capacity and the power supply, the freedom of the design lies mainly in the DR schedule. Both the load profile and the voltage profile need to be considered when determining the DR schedule because the time needed for the demand reduction and the voltage regulation may not be the same. A protection time period may also be needed in the DR schedule to prevent the rebound effect. In our pervious simulation, the protection period is one hour. Heuristic methods can be developed for the LSE to set the length of the protection period in the future.

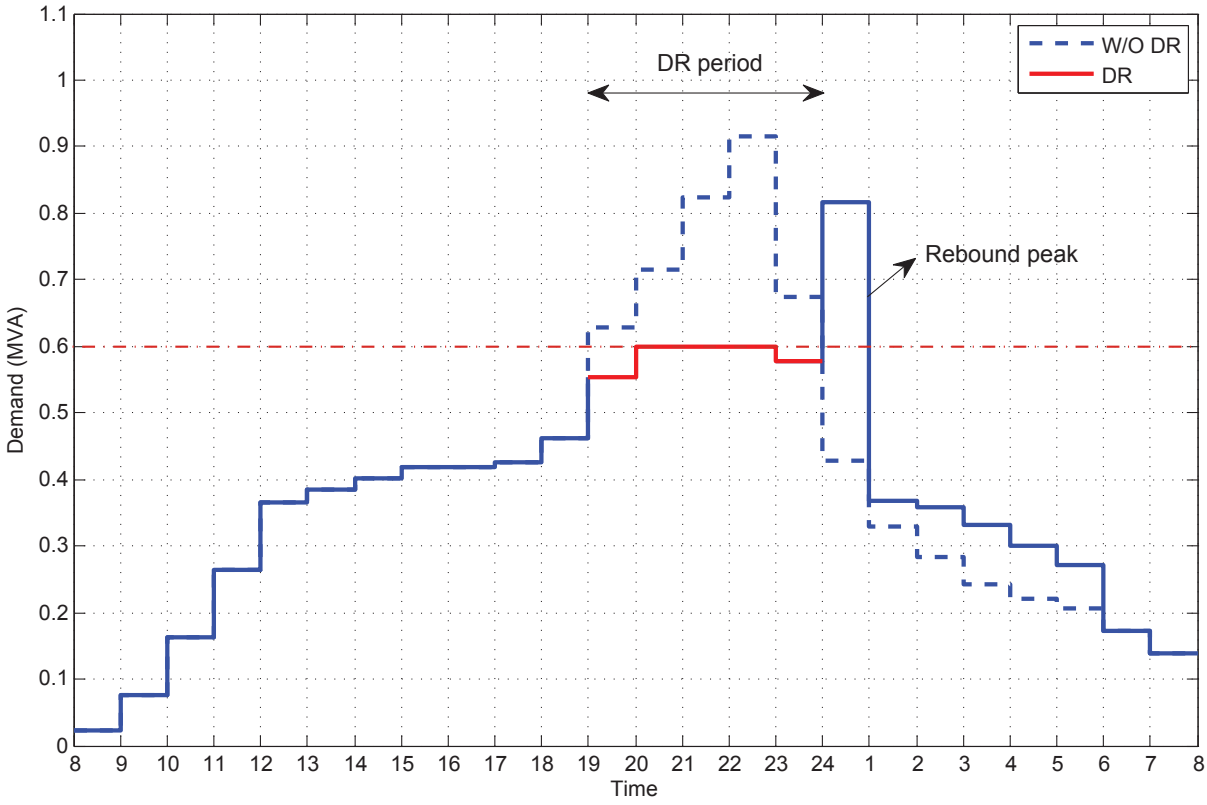

Figure 2.12: Rebound effect of DR.

2.5 Summary

In this chapter, we study residential DR with consideration of the underlying AC power distribution network and the associated power flow and system operational constraints. This residential DR is modeled as an OPF problem. We then relax the non-convex OPF problem to be a convex problem and propose a distributed DR scheme for the LSE and the households to jointly compute an optimal demand schedule. Using an IEEE test distribution system as an illustrative example, we demonstrate two interesting effects of DR. One is the location effect, meaning that the households far away from the feeder tend to reduce more demands in DR. The other is the rebound effect, meaning that DR may create a new peak after the DR event ends if the DR parameters are not chosen carefully. The two effects suggest certain rules we should follow when designing a DR program. Future work includes designing compensation mechanisms for the location discrimination and heuristic methods to deal with

the rebound effect.

CHAPTER 3

Distributed Optimal Energy Management in Microgrids

Energy management in microgrids is typically formulated as a non-linear optimization problem. Solving it in a centralized manner does not only require high computational capabilities at the MGCC but may also infringe customer privacy. Existing distributed approaches, on the other hand, assume that all generations and loads are connected to one bus and ignore the underlying power distribution network and the associated power flow and system operational constraints. Consequently, the schedules produced by those algorithms may violate those constraints and thus are not feasible in practice. Therefore, the focus of this chapter is on the design of a distributed EMS for the optimal operation of microgrids with consideration of the distribution network and the associated constraints. Specifically, we formulate microgrid energy management as an OPF problem and propose a distributed EMS where the MGCC and the LCs jointly compute an optimal schedule. We also provide an implementation of the proposed distributed EMS based on IEC 61850. As one demonstration, we apply the proposed distributed EMS to a real microgrid in Guangdong Province, China, consisting of PVs, WTs, diesel generators, and a BESS. The simulation results demonstrate the effectiveness and fast convergence of the proposed distributed EMS.

3.1 Introduction

Microgrids are low-voltage distribution systems consisting of DERs and controllable loads, which can operate in either islanded or grid-connected mode [2]. DERs include a variety of DG units such as PVs and WTs and DS units such as batteries. Sound operation of a

microgrid requires an EMS which controls the power flows in the microgrid by adjusting the power imported/exported from/to the main grid, the dispatchable DERs, and the controllable loads based on the present and forecasted information of the market, the generations, and the loads in order to meet certain operational objectives (e.g., minimizing costs) [2].

Energy management in microgrids is typically formulated as a non-linear optimization problem. Various centralized methods have been proposed to solve it in the literature, including mixed integer programming [14], sequential quadratic programming [15], particle swarm optimization [16], neural networks [17], etc. The centralized approaches [14–17] require high computational capabilities at the MGCC, which is neither efficient nor scalable. Moreover, a centralized EMS requires the MGCC to gather information of the DERs (e.g., production costs, constraints, etc.) and the loads (e.g., customer preferences, constraints, etc.) as the inputs for optimization. However, different DERs may belong to different entities and they may keep their information private [18]. Customers may also be unwilling to expose their information due to privacy [19]. Therefore, in this chapter, we are interested in developing a distributed EMS which is efficient, scalable, and privacy preserving.

Several distributed algorithms have been proposed for the operation of microgrids in the literature. In [18], a distributed algorithm based on the classical symmetrical assignment problem is proposed. Energy management is formulated as a resource allocation problem in [20] and distributed algorithms are proposed for distributed allocation. A convex problem formulation can be found in [21] and dual decomposition is used to develop a distributed EMS to maintain the supply-demand balance in microgrids. A privacy-preserving energy scheduling algorithm in microgrids is proposed in [19], where the privacy constraints are integrated with the linear programming model and distributed algorithms are developed. In [22], the additive-increase/multiplicative-decrease algorithm is adopted to optimize DER operations in a distributed fashion.

The problem with the existing distributed approaches [18–22] is that they consider the supply-demand matching in an abstract way where the aggregate demand is simply equal to the supply. They assume that all generations and loads are connected to one bus and ignore the underlying power distribution network and the associated power flow (e.g., Kirchhoff's

law) and system operational constraints (e.g., voltage tolerances). Consequently, the schedules produced by those algorithms may violate those constraints and thus are not feasible in practice. It is worth noting that distribution networks have been taken into account in a few recent DR studies [23]. However, the idea of integrating distribution networks with distributed energy management in microgrids, where both supply-side and demand-side management are considered, has not been explored.

The focus of this chapter is on the design of a distributed EMS for the optimal operation of microgrids with consideration of the underlying power distribution network and the associated constraints. More specifically, we consider a microgrid consisting of multiple DERs and controllable loads. The objective of the EMS is to control the power flows in the microgrid in order to i) minimize the cost of generation, the cost of energy storage, and the cost of energy purchase from the main grid, ii) minimize the dissatisfactions of customers in the demand side management, and iii) minimize the power losses subject to the DER constraints, the load constraints, the power flow constraints, and the system operational constraints.

Specifically, we formulate energy management in microgrids as an OPF problem. The OPF problem is difficult to solve due to the non-convex power flow constraints. We convexify the OPF problem by relaxing the power flow constraints (See [57,58] for a tutorial on convex relaxation of OPF). Sufficient conditions for the exactness of the relaxation have been derived in recent works [46–48,59], which hold for a variety of IEEE test systems and real distribution systems. Therefore, we focus on solving the OPF-r in this chapter. Note that most of the convex relaxations of OPF [46–48, 59] assume a single-phase or balanced three-phase distribution network. See [60] for convex relaxation of OPF in multi-phase networks. The OPF-r problem is a centralized convex optimization problem. To solve it in a distributed manner, we propose a distributed EMS where the MGCC and the LCs jointly compute an optimal schedule.

In order to illustrate the feasibility of the proposed EMS in real systems, we provide an implementation based on the IEC 61850 standard which provides standardized communication and control interfaces for all DER devices. As one demonstration, we apply the proposed EMS to a real microgrid in Guangdong Province, China, consisting of PVs, WTs,

diesel generators, and a BESS. The simulation results demonstrate the effectiveness and fast convergence of the proposed EMS. We show that the proposed EMS is able to manage the operations in the microgrid to achieve the objective while maintaining the bus voltages within the allowed range. Furthermore, we discuss the location effect, the load shedding/shifting, the ramping constraint, and the trade-offs in the objective.

The rest of this chapter is organized as follows. We introduce the system model in Section 3.2 and propose the EMS in Section 3.3. The simulation results are provided in Section 3.5. The summary is given in Section 3.6.

3.2 System Model

In this section, we describe the system model for developing the proposed distributed EMS. We first give an overview of the system followed by the DG model, the DS model, and the load model. We then model the power distribution network using a branch flow model and formulate microgrid energy management as an OPF problem.

3.2.1 System Overview

A low-voltage power distribution network generally has a radial structure [23]. Thus, we consider a radial microgrid consisting of a set of DG units denoted by $\mathcal{G} \triangleq \{g_1, g_2, \ldots, g_G\}$, DS units denoted by $\mathcal{B} \triangleq \{b_1, b_2, \ldots, b_B\}$, and controllable loads denoted by $\mathcal{L} \triangleq \{l_1, l_2, \ldots, l_L\}$. In the microgrid, there is a MGCC which coordinates the operations of the DERs and the controllable loads. At each DER and load, there is a LC which is able to coordinate with the MGCC to compute its schedule locally via a two-way communication infrastructure. Fig. 3.1 shows the system architecture.

In this chapter, we use a discrete-time model with a finite horizon. We consider a time period or namely a scheduling horizon which is divided into T equal intervals Δt, denoted by $\mathcal{T} \triangleq \{0, 1, \ldots, T-1\}$.

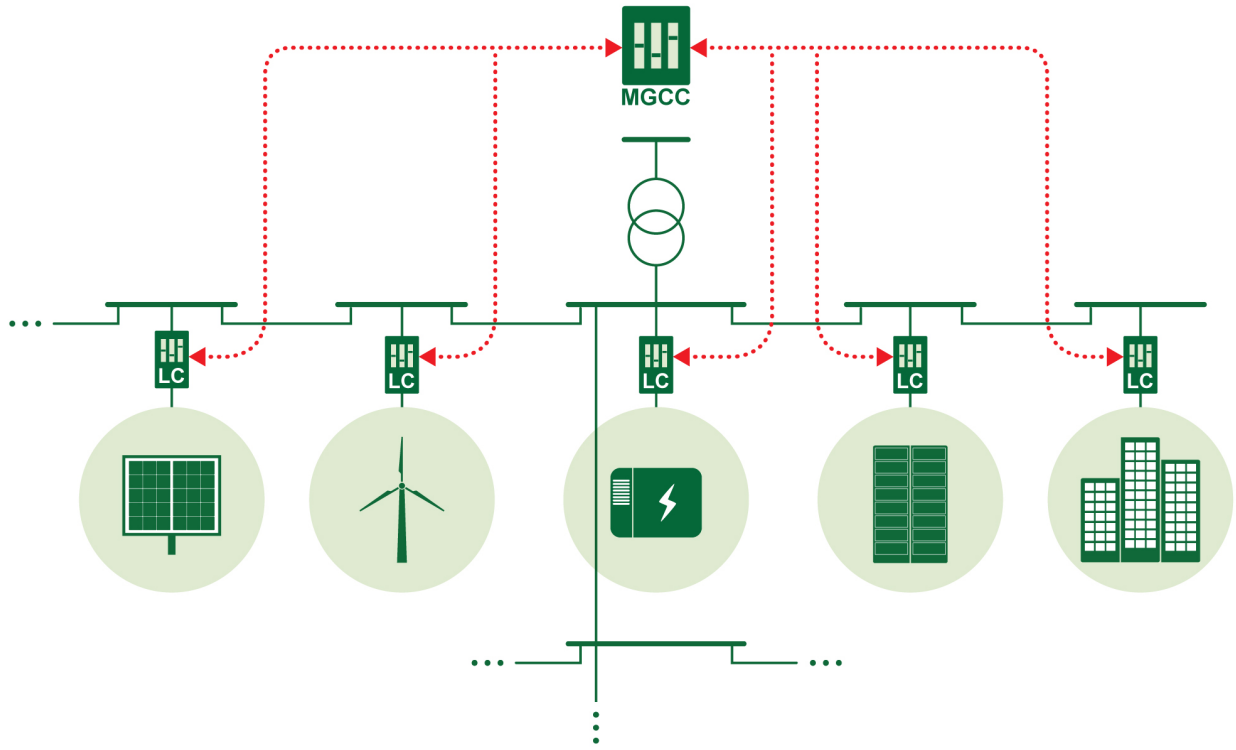

Figure 3.1: System architecture.

3.2.2 DG Model

We consider both renewable and conventional DGs in the microgrid. Renewable DGs such as PVs and WTs are non-dispatchable and conventional DGs such as diesel are dispatchable. For each DG $g \in \mathcal{G}$, we denote its complex output power by $s_g(t) \triangleq p_g(t) + \mathbf{i}q_g(t)$, where $p_g(t)$ is the active power and $q_g(t)$ is the reactive power.

3.2.2.1 Renewable DG

A renewable DG unit such as PV or WT is not dispatchable and its output power is dependent on the availability of the primary sources (i.e., sun irradiance or wind). Therefore, forecast is required in order to consider them in the energy management optimization. Methods for PV forecasting [61] and WT forecasting [62] can be utilized. In our model, we assume that the complex power of a renewable DG unit over the scheduling horizon is given and there is

no generation cost for renewable DGs.

3.2.2.2 Conventional DG

A conventional DG unit such as diesel is a dispatchable source, its output power is a variable with the following constraints:

$$0 \leq p_g(t) \leq \bar{p}_g, \ \forall t \in \mathcal{T}, \tag{3.1}$$

$$|p_g(t) - p_g(t-1)| \leq r_g \bar{p}_g, \ \forall t \in \mathcal{T}, \tag{3.2}$$

where $\bar{p}_g$ is the maximum output power and $r_g \in (0, 1]$ is the ramping parameter.

For a given conventional DG unit, its reactive power generated at the inverter is bounded by:

$$p_g(t)^2 + q_g(t)^2 \leq s_g^2, \ \forall t \in \mathcal{T}, \tag{3.3}$$

where s_g is the capacity of the inverter.

We model the conventional DG generation cost at each time $t \in \mathcal{T}$ using a quadratic model [21]:

$$C_g(p_g(t)) \triangleq \alpha_g \left(p_g(t)\Delta t\right)^2 + \beta_g p_g(t)\Delta t + c_g, \tag{3.4}$$

where α_g, β_g, and c_g are constants.

3.2.3 DS Model

We consider batteries as the DS units in the microgrid. For a given battery $b \in \mathcal{B}$, we denote its complex power by $s_b(t) \triangleq p_b(t) + \mathbf{i}q_b(t)$, where $p_b(t)$ is the active power (positive when charging and negative when discharging) and $q_b(t)$ is the reactive power. Let $E_b(t)$ denote the energy stored in the battery at time t. A given battery can be modeled by the following

constraints:

$$\underline{p}_b \leq p_b(t) \leq \bar{p}_b, \ \forall t \in \mathcal{T}, \tag{3.5}$$

$$p_b(t)^2 + q_b(t)^2 \leq s_b^2, \ \forall t \in \mathcal{T}, \tag{3.6}$$

$$E_b(t+1) = \eta_b E_b(t) + p_b(t)\Delta t, \ \forall t \in \mathcal{T}, \tag{3.7}$$

$$\underline{E}_b \leq E_b(t) \leq \bar{E}_b, \ \forall t \in \mathcal{T}, \tag{3.8}$$

$$E_b(T) \geq E_b^e, \tag{3.9}$$

where $\bar{p}_b$ is the maximum charging rate, $-\underline{p}_b$ is the maximum discharging rate, s_b is the capacity of the inverter, $\eta_b \in (0, 1]$ captures the battery efficiency, $\underline{E}_b$ and $\bar{E}_b$ are the minimum and maximum allowed energy stored in the battery, respectively, and E_b^e is the minimum energy that the battery should maintain at the end of the scheduling horizon.

We use a cost function to capture the damages to the battery by the charging and discharging operations. Three types of damages are considered: fast charging, frequent switches between charging and discharging, and deep discharging. We model the battery cost as [11]:

$$C_b(\mathbf{p}_b) \triangleq \ \alpha_b \sum_{t\in\mathcal{T}} p_b(t)^2 - \beta_b \sum_{t=0}^{T-2} p_b(t+1)p_b(t) + \gamma_b \sum_{t\in\mathcal{T}} \left(\min(E_b(t) - \delta_b \bar{E}_b, 0)\right)^2, \tag{3.10}$$

where $\mathbf{p}_b \triangleq (p_b(t), t \in \mathcal{T})$ is the charging/discharging vector, α_b, β_b, γ_b, and δ_b are positive constants. α_b, β_b, and γ_b trade off among fast charging, switches between charging and discharging, and deep discharging. The above function is convex when $\alpha_b > \beta_b$. We choose $\delta_b = 0.2$, meaning that the cost function penalizes deep charging when the energy stored in the battery $E_b(t)$ is less than 20% of the battery capacity $\bar{E}_b$.

3.2.4 Load Model

We consider two types of controllable loads in the microgrid: interruptible and deferrable loads. An interruptible load can be shed and a deferrable load can be shifted in time but need to consume a certain amount of energy before a deadline.

For each load $l \in \mathcal{L}$, we denote its complex power by $s_l(t) \triangleq p_l(t) + \mathbf{i}q_l(t)$ and it is

bounded by:

$$\underline{p}_l(t) \leq p_l(t) \leq \bar{p}_l(t),\ \forall t \in \mathcal{T}, \tag{3.11}$$

$$\underline{q}_l(t) \leq q_l(t) \leq \bar{q}_l(t),\ \forall t \in \mathcal{T}, \tag{3.12}$$

where $\underline{p}_l(t)$ and $\bar{p}_l(t)$ are the minimum and maximum active power, respectively, and $\underline{q}_l(t)$ and $\bar{q}_l(t)$ are the minimum and maximum reactive power, respectively.

For a deferrable load, we assume that its consumed energy is bounded by:

$$\underline{E}_l \leq \sum_{t \in \mathcal{T}} p_l(t)\Delta t \leq \bar{E}_l, \tag{3.13}$$

where $\underline{E}_l$ and $\bar{E}_l$ are the energy lower and upper bound, respectively.

For each load, we define a demand vector denoted by $\mathbf{p}_l \triangleq (p_l(t), t \in \mathcal{T})$ and a cost function $C_l(\mathbf{p}_l)$ which measures the dissatisfaction of the customer using the demand schedule $\mathbf{p}_l$.

The cost function of an interruptible load is dependent on the shed load and can be defined as:

$$C_l(\mathbf{p}_l) \triangleq \sum_{t \in \mathcal{T}} \alpha_l(\min(p_l(t) - p_l^f(t), 0))^2, \tag{3.14}$$

where $p_l^f(t)$ is the forecasted load and α_l is a positive constant. The above cost function is non-zero only when there is load shedding, i.e., $p_l(t) < p_l^f(t)$.

The cost function of a deferrable load is dependent on the unfulfilled energy and can be defined as:

$$C_l(\mathbf{p}_l) \triangleq \alpha_l(\bar{E}_l - \sum_{t \in \mathcal{T}} p_l(t)\Delta t), \tag{3.15}$$

where α_l is a positive constant.

3.2.5 Distribution Network Model

A distribution network can be modeled as a connected graph $(\mathcal{N}, \mathcal{E})$, where each node $i \in \mathcal{N}$ represents a bus and each link in $\mathcal{E}$ represents a branch (line or transformer). We denote a link by $(i, j) \in \mathcal{E}$. Power distribution networks are typically radial and the graph becomes a

tree for radial distribution systems. We index the buses in $\mathcal{N}$ by $i = 0, 1, \ldots, n$, and bus 0 denotes the feeder which has a fixed voltage and flexible power injection.

For each link $(i, j) \in \mathcal{E}$, let $z_{ij} \triangleq r_{ij} + \mathbf{i}x_{i,j}$ be the complex impedance of the branch, $I_{ij}(t)$ be the complex current from buses i to j, and $S_{ij}(t) \triangleq P_{ij}(t) + \mathbf{i}Q_{ij}(t)$ be the complex power flowing from buses i to j.

For each bus $i \in \mathcal{N}$, let $V_i(t)$ be the complex voltage at bus i and $s_i(t) \triangleq p_i(t) + \mathbf{i}q_i(t)$ be the net load which is the load minus the generation at bus i. Each bus $i \in \mathcal{N} \setminus \{0\}$ is connected to a subset of DG units $\mathcal{G}_i$, DS units $\mathcal{B}_i$, and loads $\mathcal{L}_i$. The net load at each bus i satisfies:

$$s_i(t) = s_{li}(t) + s_{bi}(t) - s_{gi}(t), \ \forall i \in \mathcal{N} \setminus \{0\}, \forall t \in \mathcal{T}, \tag{3.16}$$

where $s_{li}(t) \triangleq \sum_{l \in \mathcal{L}_i} s_l(t)$, $s_{bi}(t) \triangleq \sum_{b \in \mathcal{B}_i} s_b(t)$, and $s_{gi} \triangleq \sum_{g \in \mathcal{G}_i} s_g(t)$.

Given the radial distribution network $(\mathcal{N}, \mathcal{E})$, the feeder voltage V_0, and the impedances $\{z_{ij}\}_{(i,j)\in\mathcal{E}}$, then the other variables including the power flows, the voltages, the currents, and the bus loads satisfy the following physical laws for all branches $(i, j) \in \mathcal{E}$ and all $t \in \mathcal{T}$.

- Ohm's law:

$$V_i(t) - V_j(t) = z_{ij} I_{ij}(t); \tag{3.17}$$

- Power flow definition:

$$S_{ij}(t) = V_i(t) I_{ij}^*(t); \tag{3.18}$$

- Power balance:

$$S_{ij}(t) - z_{ij}|I_{ij}(t)|^2 - \sum_{k:(j,k)\in\mathcal{E}} S_{jk}(t) = s_j(t). \tag{3.19}$$

Using equations (3.17)–(3.19) and in terms of real variables, we can model the steady-

state power flows in a given distribution network $\mathcal{G}$ as [57]: $\forall (i,j) \in \mathcal{E}, \forall t \in \mathcal{T}$,

$$p_j(t) = P_{ij}(t) - r_{ij}\ell_{ij}(t) - \sum_{k:(j,k)\in\mathcal{E}} P_{jk}(t), \tag{3.20}$$

$$q_j(t) = Q_{ij}(t) - x_{ij}\ell_{ij}(t) - \sum_{k:(j,k)\in\mathcal{E}} Q_{jk}(t), \tag{3.21}$$

$$v_j(t) = v_i(t) - 2\left(r_{ij}P_{ij}(t) + x_{ij}Q_{ij}(t)\right) + (r_{ij}^2 + x_{ij}^2)\ell_{ij}(t), \tag{3.22}$$

$$\ell_{ij}(t) = \frac{P_{ij}(t)^2 + Q_{ij}(t)^2}{v_i(t)}, \tag{3.23}$$

where $\ell_{ij}(t) \triangleq |I_{ij}(t)|^2$ and $v_i(t) \triangleq |V_i(t)|^2$.

Equations (3.20)–(3.23) define a system of equations in the variables $(\mathbf{P}(t), \mathbf{Q}(t), \mathbf{v}(t), \mathbf{l}(t), \mathbf{s}(t))$, where $\mathbf{P}(t) \triangleq (P_{ij}(t), (i,j) \in \mathcal{E})$, $\mathbf{Q}(t) \triangleq (Q_{ij}(t), (i,j) \in \mathcal{E})$, $\mathbf{v}(t) \triangleq (v_i(t), i \in \mathcal{N} \setminus \{0\})$, $\mathbf{l}(t) \triangleq (\ell_{ij}(t), (i,j) \in \mathcal{E})$, and $\mathbf{s}(t) \triangleq (s_i(t), i \in \mathcal{N} \setminus \{0\})$. The phase angles of the voltages and the currents are not included. But they can be uniquely determined for radial systems [58].

3.2.6 Energy Management

The objective of the microgrid operator is to minimize its operational cost, while delivering reliable and high-quality power to the loads. However, the introduction of DERs makes it challenging to balance the supply and demand in a microgrid, especially in islanded mode where only DERs are used as the supply. The integration of DERs may also increase the voltage significantly, which reduces the quality of the voltage received by other users in the distribution network. Thus in this chapter, we study microgrid energy management aiming at achieving the operational objective of the microgrid operator, while meeting the supply-demand balance and the voltage tolerance constraints.

We consider the following voltage tolerance constraints in the microgrid:

$$\underline{V}_i \le |V_i(t)| \le \bar{V}_i, \ \forall i \in \mathcal{N} \setminus \{0\}, \forall t \in \mathcal{T}, \tag{3.24}$$

where $\underline{V}_i$ and $\bar{V}_i$ correspond to the minimum and maximum allowed voltage according to the specification, respectively.

The net power injected to the microgrid from the main grid is given by:

$$s_0(t) = \sum_{j:(0,j)\in\mathcal{E}} s_{0j}(t),\ \forall t \in \mathcal{T}. \tag{3.25}$$

If the microgrid is operated in islanded mode, then $s_0(t) = 0$. If the microgrid is operated in grid-connected mode, then $s_0(t)$ is is the net complex power traded between the microgrid and the main grid.

We model the cost of energy purchase from the main grid at each time $t \in \mathcal{T}$ as:

$$C_0(t, p_0(t)) \triangleq \rho(t) p_0(t) \Delta t, \tag{3.26}$$

where $\rho(t)$ is the market energy price. Note that $p_0(t)$ can be negative, meaning that the microgrid can sell its surplus power to the main grid.

The objective of the energy management in the microgrid is to (i) minimize the cost of generation, the cost of energy storage, and the cost of energy purchase from the main grid, and (ii) minimize the dissatisfactions of customers in the demand side management, and (iii) minimize the power losses subject to the DER constraints, the load constraints, the power flow constraints, and the system operational constraints (voltage tolerances).

We define $\mathbf{P} \triangleq (\mathbf{P}(t), t \in \mathcal{T})$, $\mathbf{Q} \triangleq (\mathbf{Q}(t), t \in \mathcal{T})$, $\mathbf{v} \triangleq (\mathbf{v}(t), t \in \mathcal{T})$, $\mathbf{l} \triangleq (\mathbf{l}(t), t \in \mathcal{T})$, $\mathbf{s}_g \triangleq (s_g(t), t \in \mathcal{T})$, $\mathbf{s}_b \triangleq (s_b(t), t \in \mathcal{T})$, $\mathbf{s}_l \triangleq (s_l(t), t \in \mathcal{T})$, $\mathbf{s} \triangleq (\mathbf{s}_g, \mathbf{s}_b, \mathbf{s}_l, g \in \mathcal{G}, b \in \mathcal{B}, l \in \mathcal{L})$, and $C_g(\mathbf{p}_g) \triangleq \sum_{t\in\mathcal{T}} C_g(p_g(t))$. Microgrid energy management can be formulated as an OPF problem:

OPF

$$\begin{aligned}
\min_{\mathbf{P},\mathbf{Q},\mathbf{v},\mathbf{l},\mathbf{s}} \quad & \xi_g \sum_{g\in\mathcal{G}} C_g(\mathbf{p}_g) + \xi_b \sum_{b\in\mathcal{B}} C_b(\mathbf{p}_b) + \xi_l \sum_{l\in\mathcal{L}} C_l(\mathbf{p}_l) + \xi_0 \sum_{t\in\mathcal{T}} C_0(t, p_0(t)) \\
& + \xi_p \sum_{t\in\mathcal{T}} \sum_{(i,j)\in\mathcal{E}} r_{ij} \ell_{ij}(t) \\
\text{s.t.} \quad & (3.1) - (3.3), (3.5) - (3.9), (3.11) - (3.13), (3.16), \\
& (3.20) - (3.25),
\end{aligned}$$

where ξ_g, ξ_b, ξ_l, ξ_0, and ξ_p are the parameters to trade off among the cost minimizations and the power loss minimization.

3.3 Distributed EMS

The previous OPF problem is non-convex due to the quadratic equality constraint in (3.23) and is NP-hard to solve in general [57]. We therefore relax them to inequalities:

$$\ell_{ij}(t) \geq \frac{P_{ij}(t)^2 + Q_{ij}(t)^2}{v_i(t)}, \ \forall (i,j) \in \mathcal{E}, \forall t \in \mathcal{T}. \tag{3.27}$$

We then consider the following convex relaxation of OPF:

OPF-r

$$\begin{aligned}
\min_{\mathbf{P},\mathbf{Q},\mathbf{v},\mathbf{l},\mathbf{s}} \quad & \xi_g \sum_{g\in\mathcal{G}} C_g(\mathbf{p}_g) + \xi_b \sum_{b\in\mathcal{B}} C_b(\mathbf{p}_b) + \xi_l \sum_{l\in\mathcal{L}} C_l(\mathbf{p}_l) + \xi_0 \sum_{t\in\mathcal{T}} C_0(t, p_0(t)) \\
& + \xi_p \sum_{t\in\mathcal{T}} \sum_{(i,j)\in\mathcal{E}} r_{ij}\ell_{ij}(t) \\
\text{s.t.} \quad & (3.1)-(3.3), (3.5)-(3.9), (3.11)-(3.13), (3.16), \\
& (3.20)-(3.22), (3.24), (3.25), (3.27).
\end{aligned}$$

If the equality in (3.27) is attained in the solution to OPF-r, then it is also an optimal solution to OPF. The sufficient conditions under which the relaxation is exact have been exploited in previous works [46–48, 59]. Roughly speaking, if the bus voltage is kept around the nominal value and the power injection at each bus is not too large, then the relaxation is exact. Detailed conditions when the voltage upper bound is not important can be found in [46, 47]. See [48, 59] on how to deal with the voltage upper bound. In this chapter, we assume that the sufficient conditions specified in [59] hold for the microgrid and thus we focus on solving the OPF-r problem.

The above OPF-r problem is a centralized optimization problem. In order to design an efficient, scalable, and privacy-preserving EMS, we propose a distributed algorithm to solve the OPF-r problem using the PCPM algorithm (refer to [54] or Section 2.3.1 for details). Note that we use PCPM to develop the proposed distributed algorithm here. Other distributed algorithms such as the alternating direction method of multipliers (ADMM) algorithm [63] may also apply to solve the OPF-r problem in a distributed manner.

Initially set $k \leftarrow 0$. The LCs of the DERs and the loads set their initial schedules randomly and communicate them to the MGCC. In the meantime, the MGCC randomly

chooses the initial $s_i^k(t) \triangleq p_i^k(t)+\mathbf{i}q_i^k(t)$ and two virtual control signals $\{\mu_i^k(t)\}_{t\in\mathcal{T}}$, $\{\lambda_i^k(t)\}_{t\in\mathcal{T}}$ for each bus $i \in \mathcal{N}\setminus\{0\}$. $\mu_i(t)$ and $\lambda_i(t)$ are the Lagrangian multipliers associated with the active and reactive power at bus i, respectively.

At the beginning of the k-th step, the MGCC sends two control signals $\hat{\mu}_i^k(t) \triangleq \mu_i^k(t) + \gamma(p_{li}^k(t) + p_{bi}^k(t) - p_{gi}^k(t) - p_i^k(t))$ and $\hat{\lambda}_i^k(t) \triangleq \lambda_i^k(t) + \gamma(q_{li}^k(t) + q_{bi}^k(t) - q_{gi}^k(t) - q_i^k(t))$ to the LCs of the DERs and the loads connected to bus i, where γ is a positive constant. Then,

- The LC of each conventional DG unit solves the following problem:

  EMS-LC(DG)

$$\begin{aligned} \min_{\mathbf{s}_g} \quad & \xi_g C_g(\mathbf{p}_g) - (\hat{\boldsymbol{\mu}}_i^k)^T\mathbf{p}_g - (\hat{\boldsymbol{\lambda}}_i^k)^T\mathbf{q}_g + \frac{1}{2\gamma}||\mathbf{p}_g - \mathbf{p}_g^k||^2 + \frac{1}{2\gamma}||\mathbf{q}_g - \mathbf{q}_g^k||^2 \\ \text{s.t.} \quad & (3.1) - (3.3), \end{aligned}$$

  where $\hat{\boldsymbol{\mu}}_i^k \triangleq (\hat{\mu}_i^k(t), t \in \mathcal{T})$ and $\hat{\boldsymbol{\lambda}}_i^k \triangleq (\hat{\lambda}_i^k(t), t \in \mathcal{T})$. The optimal $\mathbf{s}_g^*$ is set as $\mathbf{s}_g^{k+1}$.

- The LC of each DS unit solves the following problem:

  EMS-LC(DS)

$$\begin{aligned} \min_{\mathbf{s}_b} \quad & \xi_b C_b(\mathbf{p}_b) + (\hat{\boldsymbol{\mu}}_i^k)^T\mathbf{p}_b + (\hat{\boldsymbol{\lambda}}_i^k)^T\mathbf{q}_b + \frac{1}{2\gamma}||\mathbf{p}_b - \mathbf{p}_b^k||^2 + \frac{1}{2\gamma}||\mathbf{q}_b - \mathbf{q}_b^k||^2 \\ \text{s.t.} \quad & (3.5) - (3.9). \end{aligned}$$

  The optimal $\mathbf{s}_b^*$ is set as $\mathbf{s}_b^{k+1}$.

- The LC of each load solves the following problem:

  EMS-LC(Load)

$$\begin{aligned} \min_{\mathbf{s}_l} \quad & \xi_l C_l(\mathbf{p}_l) + (\hat{\boldsymbol{\mu}}_i^k)^T\mathbf{p}_l + (\hat{\boldsymbol{\lambda}}_i^k)^T\mathbf{q}_l + \frac{1}{2\gamma}||\mathbf{p}_l - \mathbf{p}_l^k||^2 + \frac{1}{2\gamma}||\mathbf{q}_l - \mathbf{q}_l^k||^2 \\ \text{s.t.} \quad & (3.11) - (3.13). \end{aligned}$$

  The optimal $\mathbf{s}_l^*$ is set as $\mathbf{s}_l^{k+1}$.

- The MGCC solves the following problem for each time $t \in \mathcal{T}$:

Algorithm 2 - The Proposed Distributed EMS.

1: **initialization** $k \leftarrow 0$. The LCs set the initial schedules randomly and return them to the MGCC. The MGCC sets the initial $\mu_i^k(t)$, $\lambda_i^k(t)$ and the initial $s_i^k(t)$ randomly.

2: **repeat**

3: The MGCC updates $\hat{\mu}_i^k(t)$ and $\hat{\lambda}_i^k(t)$ and sends two control signals $\hat{\boldsymbol{\mu}}_i^k$ and $\hat{\boldsymbol{\lambda}}_i^k$ to the LCs connected to bus i.

4: The LC at each DER and each load calculates a new schedule by solving the corresponding EMS-LC problem.

5: The MGCC computes a new $\mathbf{s}^{k+1}(t)$ for each time $t \in \mathcal{T}$ by solving the EMS-MGCC problem.

6: The LC communicates the new schedule to the MGCC.

7: The MGCC updates $\mu_i^{k+1}(t)$ and $\lambda_i^{k+1}(t)$.

8: $k \leftarrow k+1$.

9: **until** convergence

EMS-MGCC

$$\min_{\substack{\mathbf{P}(t),\mathbf{Q}(t),\\ \mathbf{v}(t),\mathbf{l}(t),\mathbf{s}(t)}} \xi_0 C_0(t,p_0(t)) + \xi_p \sum_{(i,j)\in\mathcal{E}} r_{ij}\ell_{ij}(t) - (\hat{\boldsymbol{\mu}}^k(t))^T\mathbf{p}(t) - (\hat{\boldsymbol{\lambda}}^k(t))^T\mathbf{q}(t)$$
$$+\frac{1}{2\gamma}||\mathbf{p}(t)-\mathbf{p}^k(t)||^2 + \frac{1}{2\gamma}||\mathbf{q}(t)-\mathbf{q}^k(t)||^2$$
$$\text{s.t.} \quad (3.20)-(3.22),(3.24),(3.25),(3.27),$$

where $\hat{\boldsymbol{\mu}}^k(t) \triangleq (\hat{\mu}_i^k(t), i \in \mathcal{N}\setminus\{0\})$ and $\hat{\boldsymbol{\lambda}}^k(t) \triangleq (\hat{\lambda}_i^k(t), i \in \mathcal{N}\setminus\{0\})$. The optimal $\mathbf{s}^*(t)$ is set as $\mathbf{s}^{k+1}(t)$.

At the end of the k-th step, the LCs communicate their new schedules $\mathbf{s}_l^{k+1}$, $\mathbf{s}_g^{k+1}$, and $\mathbf{s}_b^{k+1}$ to the MGCC and the MGCC updates $\mu_i^{k+1}(t) \triangleq \mu_i^k(t)+\gamma(p_{li}^{k+1}(t)+p_{bi}^{k+1}(t)-p_{gi}^{k+1}(t)-p_i^{k+1}(t))$ and $\lambda_i^{k+1}(t) \triangleq \lambda_i^k(t)+\gamma(q_{li}^{k+1}(t)+q_{bi}^{k+1}(t)-q_{gi}^{k+1}(t)-q_i^{k+1}(t))$ for all $i \in \mathcal{N}\setminus\{0\}$ and all $t \in \mathcal{T}$. Set $k \leftarrow k+1$, and repeat the process until convergence.

A complete description of the proposed distributed EMS can be found in Algorithm 2. When γ is small enough, the above algorithm will converge to the optimal solution to OPF-r which is also the optimal solution to OPF if the relaxation is exact and $(p_{li}^k(t)+p_{bi}^k(t)-p_{gi}^k(t)-p_i^k(t))$ and $(q_{li}^k(t)+q_{bi}^k(t)-q_{gi}^k(t)-q_i^k(t))$ will converge to zero [54]. As we can see,

the MGCC and the LCs jointly compute the optimal schedule.

In the proposed distributed EMS, the private information of the DERs and the loads is stored at the LC where the EMS-LC problem is solved locally. The MGCC solves the EMS-MGCC problem using the system information, including the topology, the power losses, the market energy price, etc. The information exchanged between the MGCC and the LCs include only the control signals and the schedules. Therefore, the privacy of the DERs (i.e., production costs and constraints) and the loads (i.e., customer preferences and constraints) are both preserved by the proposed EMS.

3.4 IEC 61850 Implementation

IEC 61850 is a set of international standards designed originally for communications within substation automation systems [64]. More recently, IEC 61850 draws attention to researchers in the area of microgrids as it provides standardized communication and control interfaces for all DER devices to achieve interoperability in microgrids. Due to its essential role in microgrid systems, it is important that the microgrid EMS is compatible with IEC 61850. To this end, we provide an implementation of the proposed distributed EMS based on the IEC 61850 standard.

In IEC 61850, each DER unit is modelled as a logical device (LD). The LD is composed of the relevant logical nodes (LNs) which are pre-defined groupings of data objects that serve specific functions. Refer to [42] for detailed definitions of LNs for DER devices. The LN named DER energy and ancillary services schedule (DSCH) can be used to implement the proposed EMS. In a DSCH LN, an array of the timestamps and values can be read or written using the IEC 61850 ACSI services (e.g., GetDataValues and SetDataValues) and multiple schedules can be defined in parallel.

In order to implement the proposed EMS, we use four DSCH LNs: active power, reactive power, price for active power, and price for reactive power. The active power and reactive schedules are the results from solving the EMS-LC problem. The control signals sent by the MGCC $\hat{\boldsymbol{\mu}}_i^k$ and $\hat{\boldsymbol{\lambda}}_i^k$ can be viewed as the price for active power and reactive power,

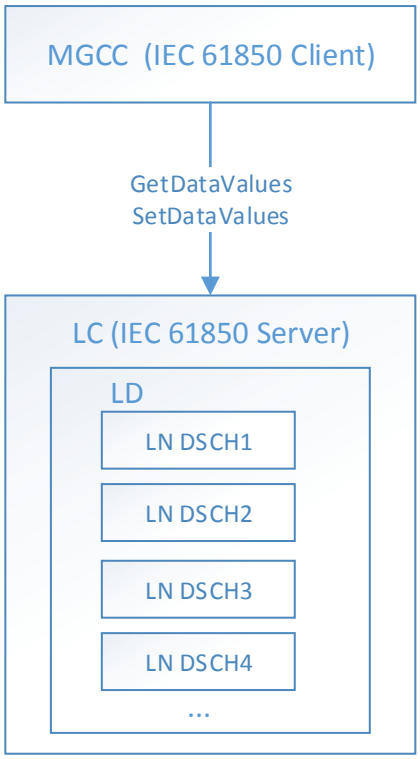

Figure 3.2: IEC 61850 implementation.

respectively. Fig. 3.2 illustrates the proposed IEC 61850 implementation.

Algorithm 2 needs a few updates to support the proposed IEC 61850 implementation. In step 3, the MGCC sends the control signals by writing to the DSCH LNs of the price for active and reactive power. In step 4, after the LC solves the EMS-LC problem using the control signals read from the DSCH LNs of the prices, the new schedules are written to the corresponding DSCH LNs. In step 6, the LC sends the new schedules to the MGCC using the IEC 61850 report control block (RCB) mechanism. At convergence, the optimal schedules will be stored in the DSCH LNs and used to control the DER device.

3.5 Performance Evaluation

In this section, we demonstrate the proposed distributed EMS by applying it to a real microgrid. We first describe the microgrid system and the simulation setup. We then present

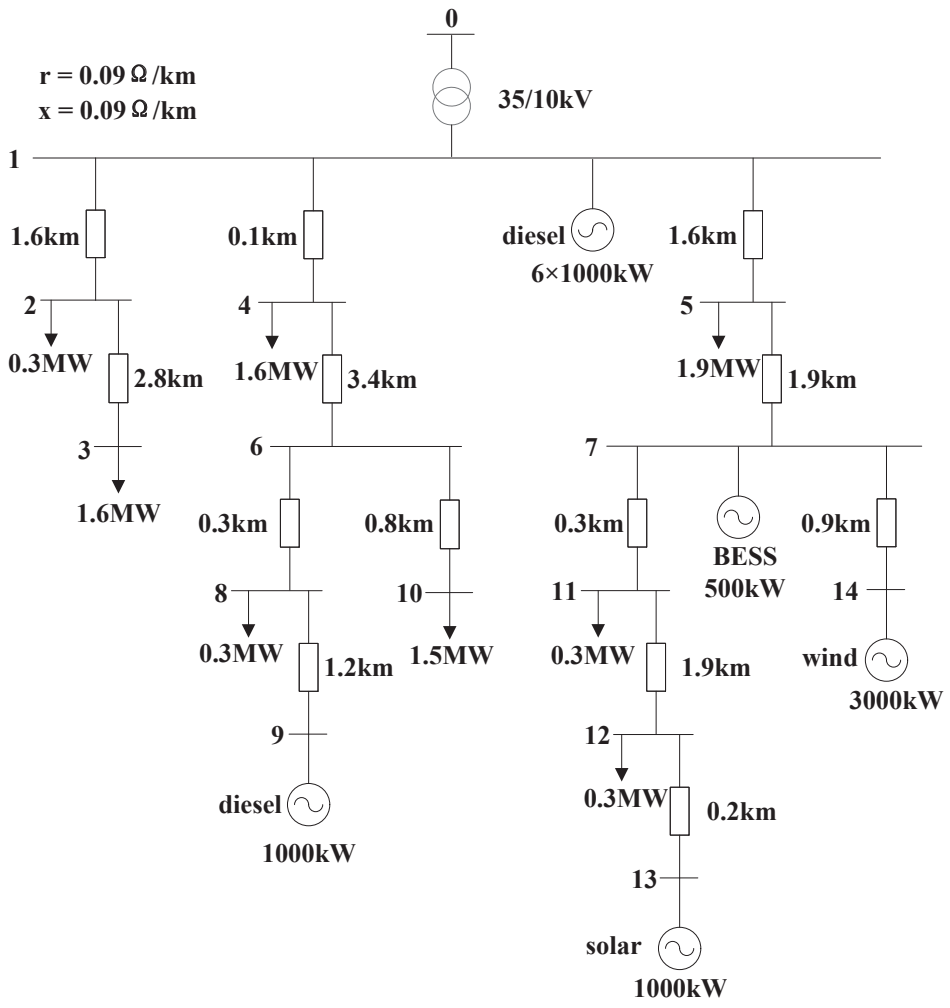

Figure 3.3: Topology of the microgrid.

the simulation results in islanded and grid-connected mode followed by the discussions on the location effect, the load shedding/shifting, the ramping constraint, and the trade-offs in the objective.

3.5.1 Simulation Setup

Fig. 3.3 shows the configuration of a real microgrid in Guangdong Province, China. The numbers under the DERs and the loads in the figure correspond to the maximum power. We use this microgrid to demonstrate the proposed distributed EMS. In the simulation, a day starts from 12 am. The time interval Δt in the model is one hour and we denote a day

by $\mathcal{T} \triangleq \{0, 1, \ldots, 23\}$, where each $t \in \mathcal{T}$ denotes the hour of $[t, t+1]$.

We set the cost function of diesel generation as $C_g(p_g(t)) \triangleq 10(p_g(t)\Delta t)^2 + 70(p_g(t)\Delta t)$. The generation ramping parameter r_g is chosen to be 0.3. The capacity of the BESS $\bar{E}_b$ is 3 MWh and $\underline{E}_b$ is chosen to be 0.1 MWh. We set $E_b(0) = 1.5$ MWh, $E_b^e = 1.0$ MWh, and $\eta_b = 0.95$. The parameters in the cost function of the battery are chosen as $\alpha_b = 1$, $\beta_b = 0.75$, and $\gamma_b = 0.5$. We choose $\alpha_l = 10^3$ and $\alpha_l = 10^2$ in the cost function of the interruptible and deferrable loads, respectively. We assume that bus 5 is a deferrable load and the rest of the loads are all interruptible. For the interruptible loads, the maximum load shedding percentage is chosen randomly from the range $[20\%, 50\%]$. For the deferable load, the start time is chosen randomly from $[10, 13]$ and the deadline is chosen randomly from $[20, 23]$. The minimum energy requirement $\underline{E}_l$ is chosen randomly from $[3\bar{p}_l, 5\bar{p}_l]$ and the energy upper bound is set to be $\bar{E}_l = \underline{E}_l + 2\bar{p}_l$, where $\bar{p}_l$ is the maximum power of load l. Perfect forecasting of the PV, the WT, and the loads is assumed. For the forecasting of the deferrable load, we assume that the load consumes power at the maximum rate from the start time until the consumed energy reaches the energy upper bound. We use the real day-ahead energy price from CAISO in the simulation as shown in Fig. 3.4.

3.5.2 Case Study

We apply the proposed EMS to the microgrid using the setup described above. The voltage tolerances are set to be [0.95 p.u., 1.05 p.u.]. The parameters in the algorithm are chosen as $\xi_g = 1$, $\xi_b = 1$, $\xi_l = 1$, $\xi_0 = 1$, $\xi_p = 1$, and $\gamma = 0.75$.

The day-ahead schedules produced by the proposed EMS in islanded mode is shown in Fig. 3.5. In islanded mode, the microgrid can utilize only the DERs to serve the loads. Since the non-dispatchable renewable generations (i.e., PV and WT) in the microgrid only serve for a small proportion of the loads, diesel is the main power source. From the figure, we can see that the total diesel generation changes in the same trend as the total load. We can also observe the charging/discharging cycles of the battery from the figure. The battery is charged when the renewable generation is high and discharged when it is low, serving as

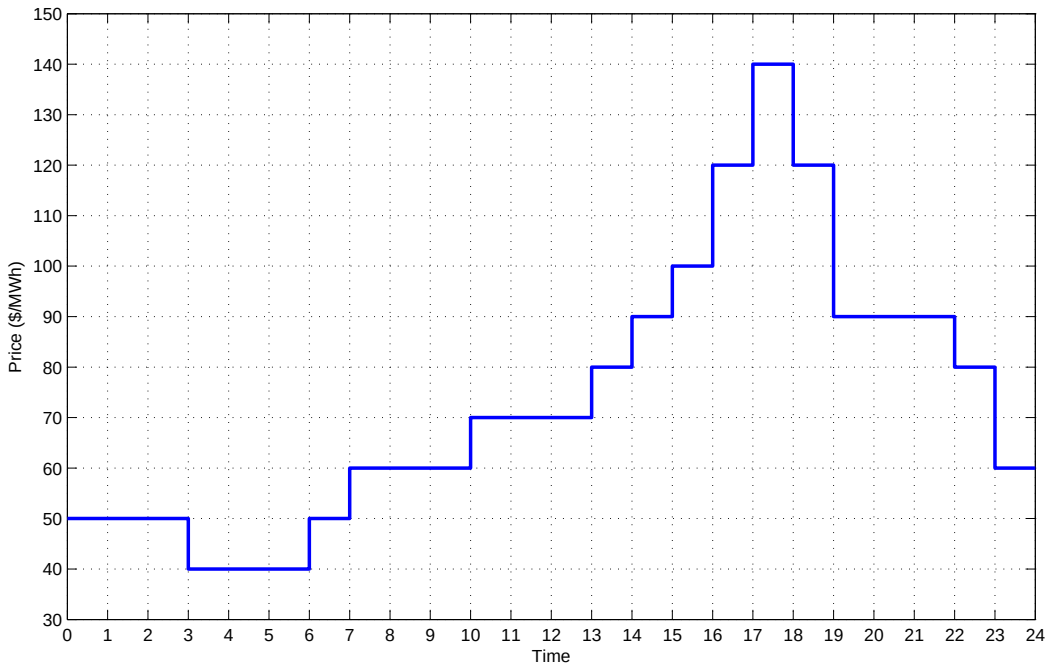

Figure 3.4: Day-ahead price from CAISO.

the storage for the renewables in the microgrid.

Fig. 3.6 shows the results in grid-connected mode. Compared with Fig. 3.5, the total diesel generation is decreased significantly in grid-connected mode. Diesel generation is no longer the main power source in grid-connected mode as the microgrid is able to import power from the main grid. The battery in grid-connected mode is the storage for not only the renewables but also the cheap power from the main grid. It is also charged when the energy price is low and discharged when the energy price is high, making profits for the microgrid.

The net power injected to the microgrid in grid-connected mode is shown in Fig. 3.7. It can be seen from the figure that the microgrid imports power when the energy price is low and exports power when the price is high ($t \in [16, 18]$). If we compare the total operational cost of the microgrid (i.e., the value of the objective function) in the two modes, we can find that grid-connected mode decreases the operational cost by $\frac{\$6491-\$5484}{\$6491} = 15.5\%$.

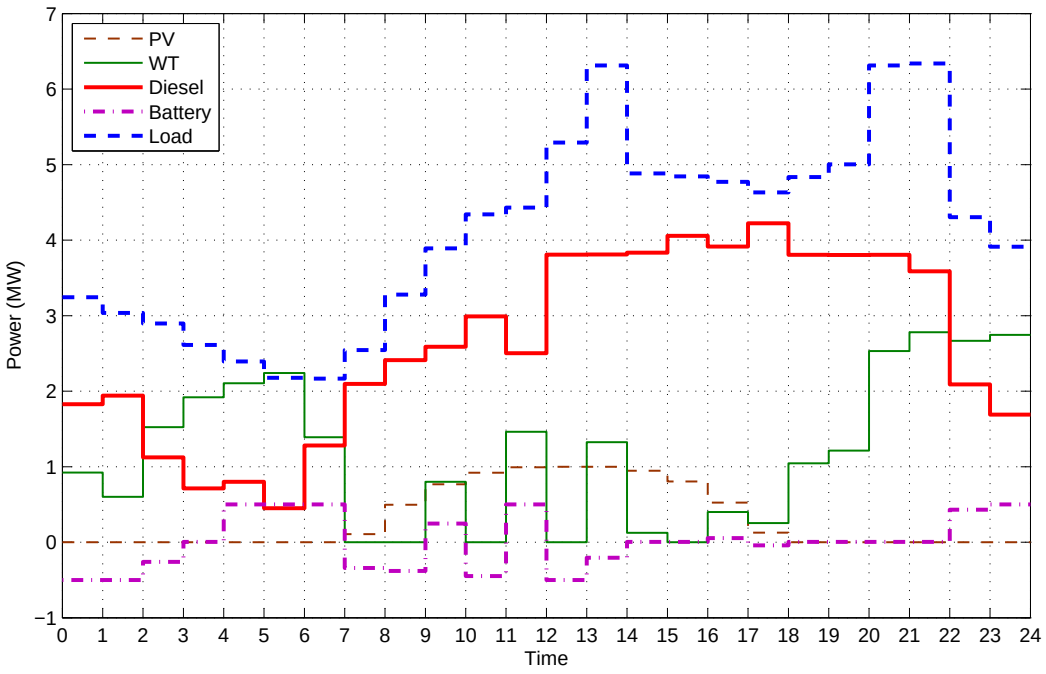

Figure 3.5: Output schedules in islanded mode.

Fig. 3.8 shows the dynamics of EMS-MGCC and EMS-LC in grid-connected mode. We can see that our proposed distributed algorithm converges fast. For the simulations, we also verify that the solution to the centralized OPF-r problem is the same as the solution to the distributed algorithm. We further verify that the equality in (3.27) is attained in the optimal solution to OPF-r, i.e., OPF-r is an exact relaxation of OPF.

3.5.3 Discussions

3.5.3.1 Location effect

In order to exemplify the effect on voltage tolerances, we increase the line lengths by 5 times. Fig. 3.9 shows the maximum and the minimum bus voltage in the microgrid over time. It can be seen from the figure that the bus voltages in the microgrid are well maintained within the allowed range. The maximum voltage reaches the upper bound when the non-dispatchable renewable generation is high and the minimum voltage reaches the lower bound when the

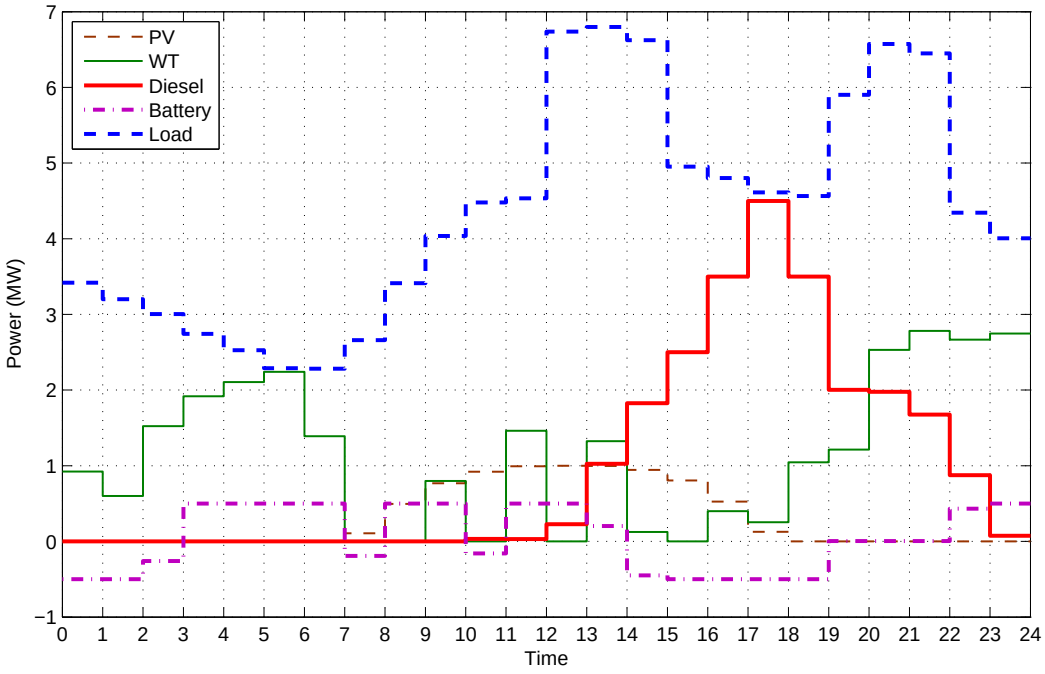

Figure 3.6: Output schedules in grid-connected mode.

load is high. This is because the generation injects power to the distribution network and hence increases the voltage, while the load consumes power and thus decreases the voltage.

In order to understand how voltage tolerances are maintained by the proposed EMS, we look into the demand reduction of each load as shown in Fig. 3.10. From the figure, it can be easily seen that the demand reduction of buses 2 and 3 is significantly larger than the other buses. This is because both buses 2 and 3 are far from the generation or the feeder and thus the voltage drop along the line is significant. Therefore, more demand reduction is required at bus 2 and 3 in order to maintain the bus voltage above the minimum allowed voltage. Similarly, those loads close to the non-dispatchable renewable generation (buses 11 and 12) need to consume more in order to reduce the high voltage due to the generation, leading to less demand reduction. The results show the location effect that a demand side management scheme may discriminate the loads based on their locations [23].

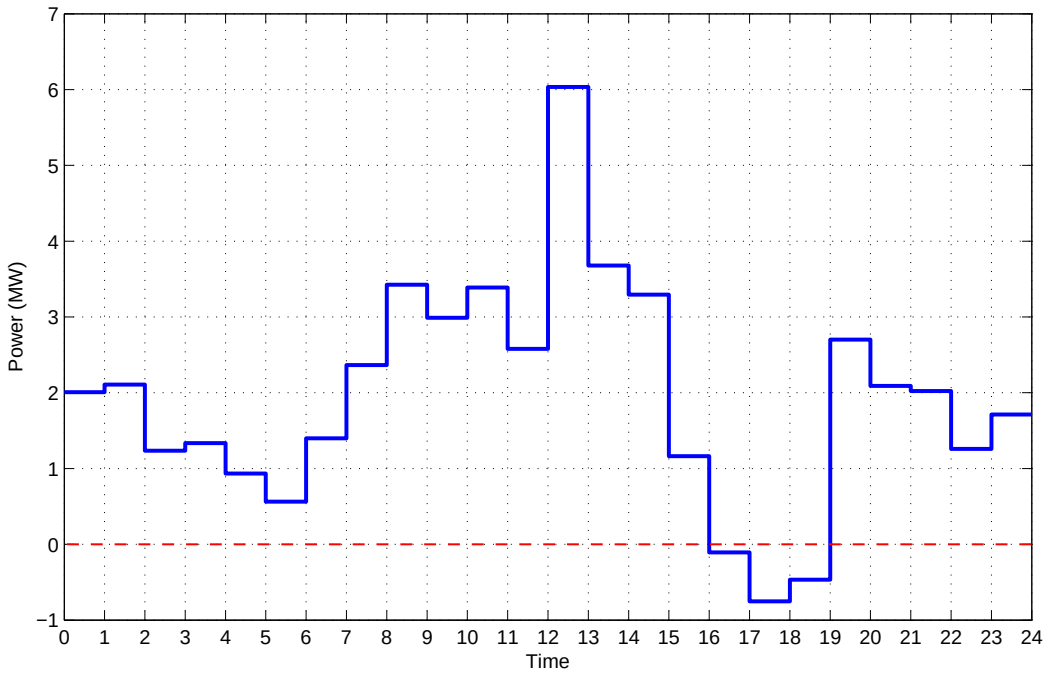

Figure 3.7: Net power injected to the microgrid.

3.5.3.2 Load shedding/shifting

Fig. 3.10 also illustrates how loads are shed in grid-connected mode. As can be expected, the loads are shed in response to the price: more loads are shed when the price is high in order to save cost. In islanded mode, load shedding is mainly used to balance the local supply. If we compare the total amount of shed loads in the two modes, we can find that islanded mode (8.91 WM) makes more load shedding than grid-connected mode (6.21 MW).

Fig. 3.11 shows the load shifting in grid-connected mode. As can be seen from the figure, the load is shifted from the time when the energy price is high ($t \in [14, 17]$) to the time when the price is low ($t \in [19, 21]$). The total consumed energy with load shifting is the same as without load shifting.

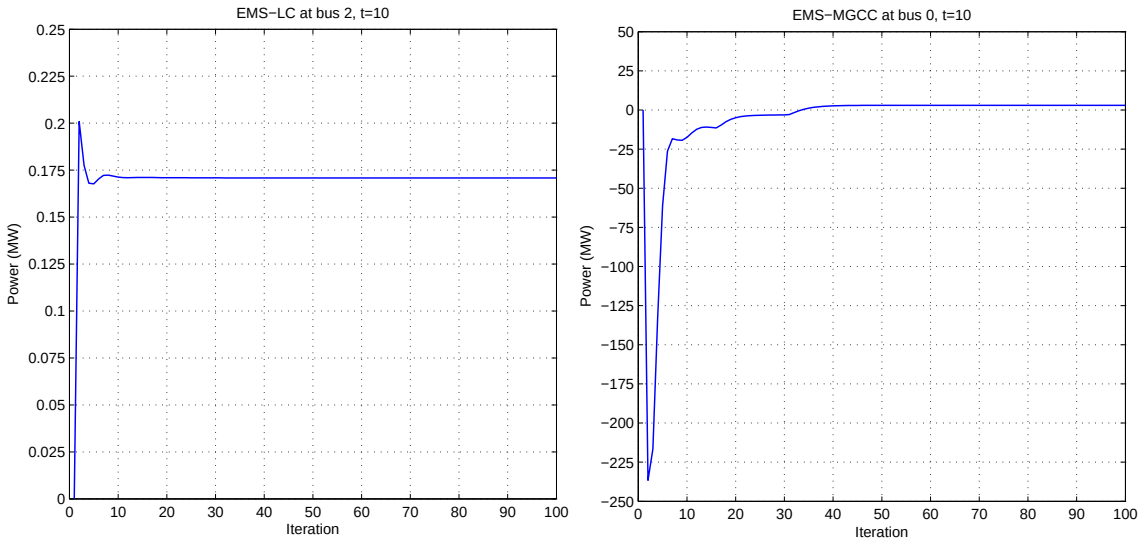

Figure 3.8: Dynamics of EMS-MGCC and EMS-LC.

3.5.3.3 Ramping constraint

Fig. 3.12 illustrates the effect of the ramping constraint on the objective. As can be seen from the figure, the total cost is non-increasing with the ramping parameter r_g in both islanded and grid-connected mode. This is because the stricter the ramping constraint is, the less available power the diesel generation can provide. It can be also seen from the figure that the marginal cost decreases in both modes as r_g increases. In particular, the cost does not decrease much when $r_g \geq 0.3$, showing that the diesel generation supply is relatively sufficient in that region of r_g. Furthermore, the marginal cost in islanded mode decreases much faster than in grid-connected mode when r_g is small. This is easy to understand as diesel is the main power supply in islanded mode and a strict ramping constraint on it would cause more load shedding/shifting that leads to a higher cost.

3.5.3.4 Trad-offs in the objective

In the objective function of the optimization, there are several parameters $(\xi_g, \xi_b, \xi_l, \xi_0, \xi_p)$. Each ξ is associated with one cost minimization in the optimization. To evaluate their effects

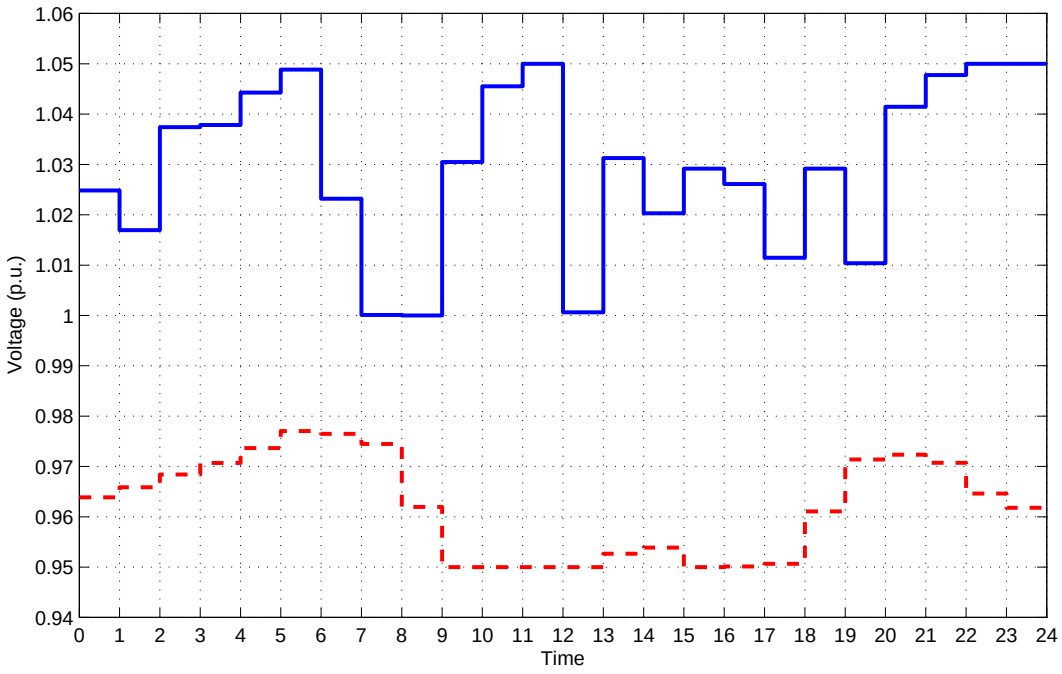

Figure 3.9: Maximum and minimum bus voltage in the microgrid.

on the proposed EMS, we conduct simulations using different ξ. We choose the baseline as the set of parameters used in our previous simulation. We then change the parameter ξ one at a time and compare the individual costs as shown in Table 3.1.

As can be seen from the table, the parameter ξ affects the trade-offs among different cost minimizations. A large ξ would decrease the corresponding cost in the optimization. The choice of ξ depends on the importance of the corresponding cost minimization in energy management. For example, if the microgrid operator is more interested in minimizing the generation cost, ξ_g can be increased and the resulting generation cost would be decreased.

3.6 Summary

In this chapter, we propose a distributed EMS for the optimal operation of microgrids. Compared with the existing distributed approaches, our proposed EMS considers the underlying

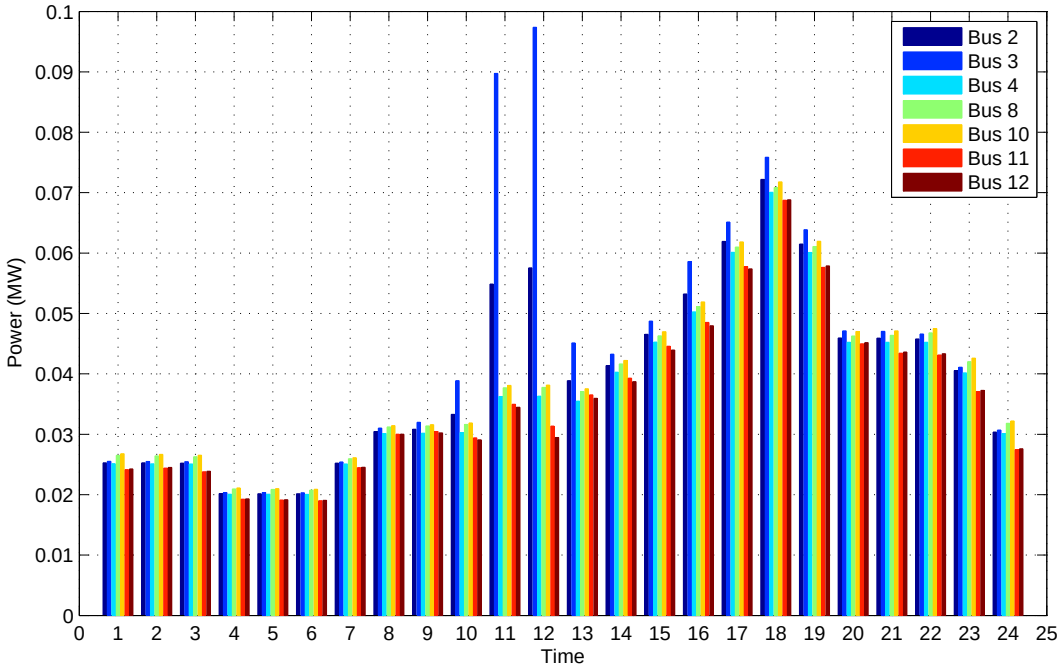

Figure 3.10: Demand reduction of the loads.

power distribution network and the associated constraints. Specifically, we formulate microgrid energy management as an OPF problem and propose a distributed EMS where the MGCC and the LCs jointly compute an optimal schedule. We also provide an implementation of the proposed EMS based on the IEC 61850 standard. As one demonstration, we apply the proposed EMS to a real microgrid in Guangdong Province, China. The simulation results demonstrate that the proposed EMS is effective in both islanded and grid-connected mode. It is shown that the proposed distributed algorithm converges fast. A comprehensive analysis of its performance is given. Future work includes implementing the proposed EMS in a real system and analyzing its performance.

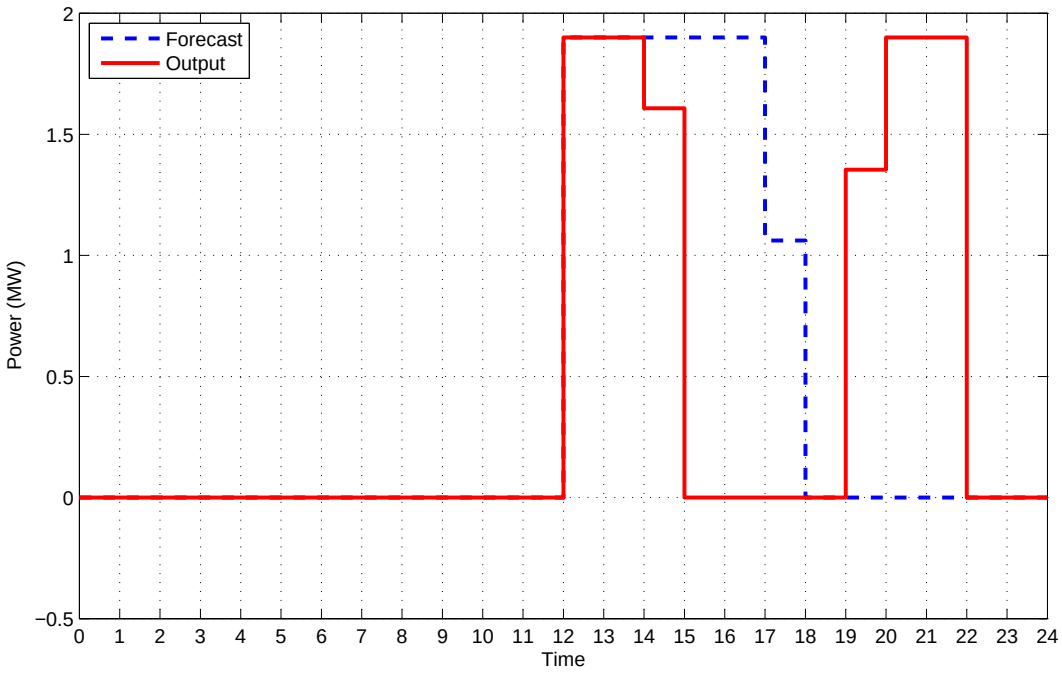

Figure 3.11: Load shifting.

Table 3.1: Cost comparison under different ξ

	Diesel	Battery	Load	Purchase	Loss
Baseline	2053.14	3.20	259.37	3167.49	0.43
$\xi_g = 10$	0.00	3.19	260.21	5743.28	0.49
$\xi_b = 10^2$	2053.23	0.27	259.45	3239.15	0.43
$\xi_l = 10$	2054.93	3.20	2.60	3632.65	0.44
$\xi_0 = 10$	19408.20	3.93	12999.53	−9245.71	0.39
$\xi_p = 10^4$	2871.53	3.45	476.58	2402.79	0.34

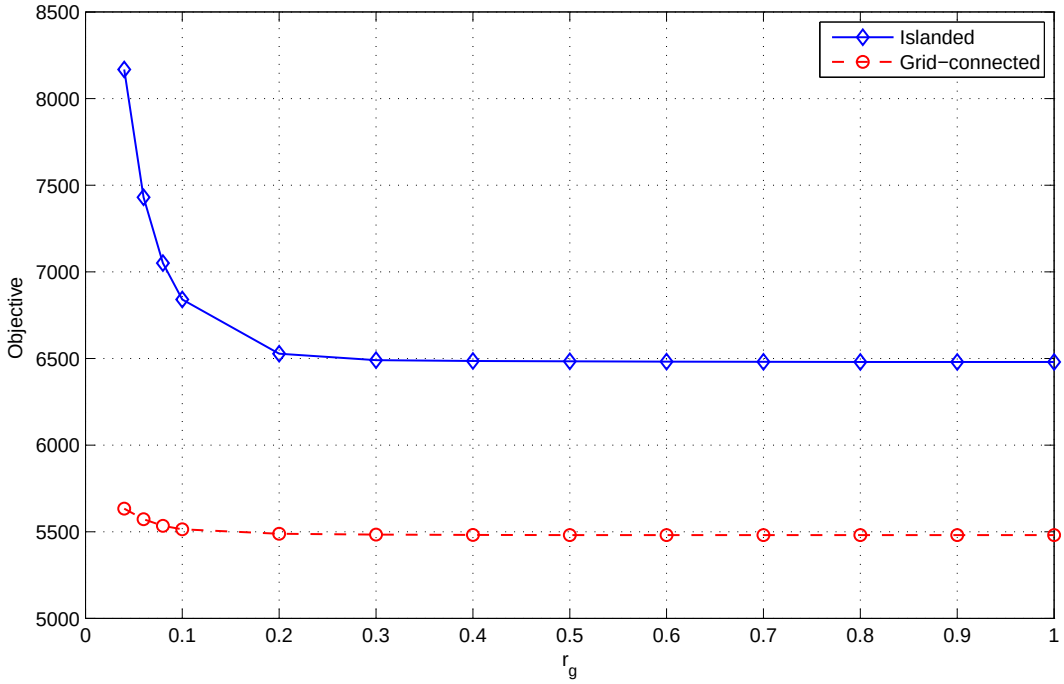

Figure 3.12: Effect of r_g on the objective.

CHAPTER 4

Real-Time Energy Management in Microgrids

Energy management in microgrids is typically formulated as an offline optimization problem for day-ahead scheduling by previous studies. Most of these offline approaches assume perfect forecasting of the renewables, the demands, and the market, which is difficult to achieve in practice. Existing online algorithms, on the other hand, oversimplify the microgrid model by only considering the aggregate supply-demand balance while omitting the underlying power distribution network and the associated power flow and system operational constraints. Consequently, such approaches may result in control decisions that violate the real-world constraints. This chapter focuses on developing an online EMS for real-time operation of microgrids that takes into account the power flow and system operational constraints on a distribution network. We model the online energy management as an SOPF problem and propose an online EMS based on Lyapunov optimization. The proposed online EMS is subsequently applied to a real microgrid system. The simulation results demonstrate that the performance of the proposed EMS exceeds a greedy algorithm and is close to an optimal offline algorithm. Lastly, the effect of the underlying network structure on the energy management is observed and analyzed.

4.1 Introduction

A microgrid is a low-voltage power distribution system integrated with DERs and controllable loads, which can operate with or without the main grid. [2]. DERs include a variety of distributed DG units such as PVs and WTs and DS units such as batteries. Controllable loads such as HVAC systems and EVs can be shed or shifted to balance supply and

demand in a microgrid. An EMS is required in a microgrid to control power flows in order to meet certain operational objectives (e.g., minimizing costs) by adjusting the power imported/exported from/to the main grid, the dispatchable DERs, and the controllable loads [2].

Energy management in microgrids is typically formulated as an offline optimization problem for day-ahead scheduling by previous studies [15,24–27]. Most of these offline approaches assume perfect forecasting of the renewables, the demands, and the market, which is difficult to achieve in practice due to the intermittency and variability of renewables, the spatial and temporal uncertainty in controllable loads (e.g., EVs), and the randomness in real-time pricing. To tackle this problem, efforts have been made to capture the uncertainties in day-ahead scheduling through modeling different scenarios [21, 28–32]. These approaches typically use stochastic programming to formulate energy management as a deterministic problem based on the scenarios that are usually generated by Monte Carlo simulations. The number of these scenarios may be large and thus it can be computationally expensive to use these methods. Although these approaches consider the uncertainties, they still require certain forecasting and usually do not adapt to real-time changes in the environment. Other studies [16, 17] consider the energy management problem at each time independently and focus on how to efficiently solve the optimization problem in real time.

Recently, there have been attempts to develop online algorithms for real-time energy management in microgrids to optimize the long-term cost, which take into account the uncertainties of the renewables, the demands, and the market [33–35]. These approaches do not require any a priori statistical knowledge of the underlying stochastic processes and can adapt to the time-varying environment. However, these existing online approaches consider the aggregate supply-demand balance while omitting the underlying power distribution network, the associated power flow (e.g., Kirchhoffs laws), and system operational constraints (e.g., voltage tolerances). Consequently, such approaches may result in control decisions that violate the real-world constraints.

Therefore, this chapter focuses on developing an online EMS for real-time operation of microgrids that takes into account the power flow and system operational constraints on a

distribution network. The objective of the EMS is to control power flows in the microgrid using only the current system state information at each time in order to (i) minimize the long-term operational cost, including the cost of generation, the cost of energy storage, the cost of load shedding, and the cost of energy purchase from the main grid, (ii) guarantee the quality-of-service for customers, and (iii) minimize the long-term power losses subject to the DER constraints, the load constraints, the power flow constraints, and the system operational constraints (e.g., voltage tolerances).

Specifically, we formulate the online energy management in microgrids as an SOPF problem. Although dynamic programming (DP) techniques could be applied to solve the stochastic optimization problem, they would result in complex solutions that are time-consuming to compute, thus preventing them to be suitable for real-time applications[1]. Moreover, because DP methods usually require assumptions of the underlying stochastic processes, it is difficult for them to adapt to any changing probabilities or any un-modelled uncertainties in the actual processes [65]. Therefore, we adopt Lyapunov optimization [66] to design an online EMS that simply uses the current system state to achieve real-time energy management without any a priori statistical knowledge of the underlying stochastic processes. Lyapunov optimization is a technique for optimizing time averages in stochastic networks. It has been recently applied to various aspects of smart grid, e.g., home energy management [65, 67], DR [68], EV charging and V2G control [69, 70], energy storage management [71–73], and microgrid energy management [33–35]. Most of the studies on Lyapunov optimization consider an infinite-time horizon, which may cause issues under certain circumstances [73]. See [73] on how to optimize over a finite-time horizon under the Lyapunov framework.

To solve the SOPF problem, we first use the concept of virtual queues from Lyapunov optimization to obtain a relaxed SOPF problem (SOPF-r) to deal with the time-coupled constraints. We then reformulate SOPF-r as an OPF to be solved at each time using the drift-plus-penalty algorithm from Lyapunov optimization. OPF is NP-hard to solve in general due to the quadratic power flow constraints [57]. We therefore relax the constraints and

[1]DP techniques generally suffer from the "curse-of-dimensionality" [65] which makes them difficult to apply to large systems due to the real-time computational requirement.

obtain a convex optimization problem for real-time computing (See [57, 58] for a tutorial on convex relaxation of OPF). Sufficient conditions for the exactness of the relaxation have been derived in recent studies [46, 59, 74], which hold for a variety of IEEE test systems and real-world distribution systems. Our proposed online EMS uses only the current system state information to solve a convex OPF problem and thus is simple and efficient to implement in real time.

As one demonstration, we apply the proposed online EMS to a real microgrid system in Guangdong Province, China. We evaluate the performance of the proposed online EMS with two benchmarks: an optimal offline algorithm that solves the optimization problem over the entire time horizon assuming that all system states over time are known a priori and a greedy algorithm that optimizes the cost at each time independently. The simulation results show that the proposed online EMS outperforms the greedy algorithm and its performance is close to the optimal offline algorithm. Regarding real-time computing, the computational time of our proposed online EMS at each time step is on average 1.13 seconds showing that it can be implemented in real time.

In order to compare with previous online approaches [33–35], we also solve the microgrid energy management problem without considering the underlying network constraints and then compute the power flows based on the obtained control decisions. Our simulation results demonstrate that those online approaches can lead to bus voltages that violate the tolerance constraints significantly. In contrast, our proposed online EMS is able to achieve the long-term objective while maintaining the voltages within the tolerance. The simulation results also show the network effect that the loads behave differently based on their locations. Therefore, by incorporating the distribution network in the modeling, this chapter presents the relationship between the physical structure of a microgrid and the online energy management on the network.

The rest of this chapter is organized as follows. We introduce the system model in Section 4.2 and propose the online EMS in Section 4.3. The simulation results are provided in Section 4.4. The summary is given in Section 4.5.

4.2 System Model

In this section, we describe the system model for developing the proposed online EMS. We first give an overview of the system followed by the DG model, the DS model, and the load model. We then model the power distribution network using a branch flow model and formulate real-time microgrid energy management as a SOPF problem.

4.2.1 System Overview

Consider a microgrid with a set of DG units denoted by $\mathcal{G} \triangleq \{g_1, g_2, \ldots, g_G\}$, DS units denoted by $\mathcal{B} \triangleq \{b_1, b_2, \ldots, b_B\}$, and controllable loads denoted by $\mathcal{L} \triangleq \{l_1, l_2, \ldots, l_L\}$. We assume the structure of the microgrid to be radial as most of the power distribution networks are radial [75]. All DER units and loads are connected by a two-way real-time communication infrastructure linking the MGCC and the LCs. The MGCC is able to gather real-time information from the LCs, perform energy management, and send control commands to the LCs. Fig. 4.1 shows the overall system architecture. In this chapter, we use a discrete-time model, assuming that the system operates in discrete time with $t \in \{0, 1, 2, \ldots\}$ and time interval Δt.

4.2.2 DG Model

We consider two types of DG units in the microgrid: non-dispatchable renewable DG units denoted by $g \in \mathcal{G}_r$ such as PVs and WTs and dispatchable conventional DG units denoted by $g \in \mathcal{G}_c$ such as diesel. For each DG $g \in \mathcal{G}$, we denote its complex output power by $s_g(t) \triangleq p_g(t) + \mathbf{i}q_g(t)$, where $p_g(t)$ is the active power and $q_g(t)$ is the reactive power.

4.2.2.1 Renewable DG

A renewable DG unit such as PV or WT is not dispatchable and its output power is dependent on the availability of the primary sources (i.e., sun irradiance or wind). Therefore, we assume $p_g(t)$ and $q_g(t)$ are both random variables due to the stochastic nature of renewable DGs

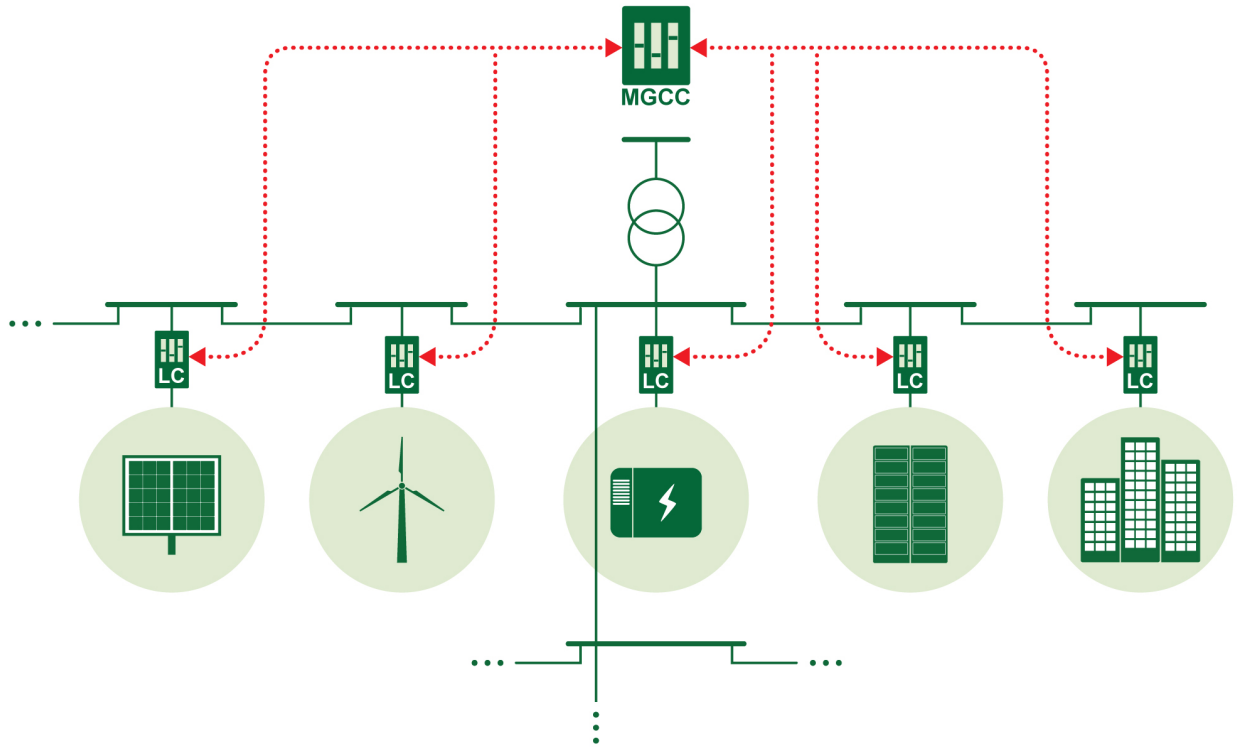

Figure 4.1: System architecture.

and there is no generation cost. Note that we consider the renewable DG unit with an on-site battery storage system as two separate units. Such a system can be modeled as a non-dispatchable DG unit and a DS unit at the same bus.

4.2.2.2 Conventional DG

A conventional DG unit such as diesel is a dispatchable source, its output power is a variable with the following constraints: $\forall g \in \mathcal{G}_c, t$,

$$0 \leq p_g(t) \leq \bar{p}_g, \tag{4.1}$$

$$|p_g(t) - p_g(t-1)| \leq r_g \bar{p}_g, \tag{4.2}$$

where $\bar{p}_g$ is the maximum output power and $r_g \in (0, 1]$ is the ramping parameter.

The reactive power generated at the inverter is bounded by:

$$p_g(t)^2 + q_g(t)^2 \leq s_g^2, \ \forall g \in \mathcal{G}_c, t, \tag{4.3}$$

where s_g is the capacity of the inverter.

We model the conventional DG generation cost at each time t using a quadratic model [21]:

$$C_g(p_g(t)) \triangleq \alpha_g \left(p_g(t)\Delta t\right)^2 + \beta_g p_g(t)\Delta t + c_g, \tag{4.4}$$

where α_g, β_g, and c_g are constants.

4.2.3 DS Model

We consider batteries as the DS units in the microgrid. For a given battery $b \in \mathcal{B}$, we denote its complex power by $s_b(t) \triangleq p_b(t) + \mathbf{i}q_b(t)$, where $p_b(t)$ is the active power (positive when charging and negative when discharging) and $q_b(t)$ is the reactive power. Let $E_b(t)$ denote the energy stored in the battery at time t. A given battery $b \in \mathcal{B}$ can be modeled by the following constraints: $\forall t$,

$$\underline{p}_b \leq p_b(t) \leq \bar{p}_b, \tag{4.5}$$

$$p_b(t)^2 + q_b(t)^2 \leq s_b^2, \tag{4.6}$$

$$E_b(t+1) = E_b(t) + p_b(t)\Delta t, \tag{4.7}$$

$$\underline{E}_b \leq E_b(t) \leq \bar{E}_b, \tag{4.8}$$

where $\bar{p}_b$ is the maximum charging rate, $-\underline{p}_b$ is the maximum discharging rate, s_b is the capacity of the inverter, and $\underline{E}_b$ and $\bar{E}_b$ are the minimum and maximum allowed energy stored in the battery, respectively.

We model the cost of operating a given battery b at each time t as [35]:

$$C_b(p_b(t)) \triangleq \alpha_b p_b(t)^2 + c_b, \tag{4.9}$$

where α_b and c_b are constants. The cost function penalizes fast (dis)charging which is harmful to battery life.

4.2.4 Load Model

We consider a demand side management in the microgrid, where flexible loads such as HVAC, EVs, and smart appliances can be shed in response to supply conditions. For each load $l \in \mathcal{L}$, we denote its complex power by $s_l(t) \triangleq p_l(t) + \mathbf{i}q_l(t)$ and it is bounded by: $\forall t$,

$$\underline{p}_l(t) \leq p_l(t) \leq \bar{p}_l(t), \tag{4.10}$$

$$\underline{q}_l(t) \leq q_l(t) \leq \bar{q}_l(t), \tag{4.11}$$

where $\underline{p}_l(t)$ is the minimum power required by the load that cannot be shed, $\bar{p}_l(t)$ is the maximum power requested by the load, and $\underline{q}_l(t)$ and $\bar{q}_l(t)$ are the minimum and maximum reactive power. $\underline{p}_l(t)$, $\bar{p}_l(t)$, $\underline{q}_l(t)$, and $\bar{q}_l(t)$ are the demand request generated by customers based on the physical constraints and their willingness to participate in the demand side management. If a customer refuses load shedding, the requested maximum and minimum power will be the same giving no flexility for the EMS. On the EMS side, the demand requests are assumed to stochastic and unknown, and they are provided by the customers at each time. Customers may use an intelligent algorithm to generate their requests. One direction for future work is to design such an algorithm on the customer side.

In order to control the quality-of-service [34] for customers in the microgrid, we impose an upper bound on the time average load shedding percentage [35]:

$$\lim_{T\to\infty} \frac{1}{T} \sum_{t=0}^{T-1} \mathbb{E}\left[\frac{\bar{p}_l(t) - p_l(t)}{\bar{p}_l(t) - \underline{p}_l(t)}\right] \leq \alpha_l, \ \forall l, \tag{4.12}$$

where $\bar{p}_l(t) - \underline{p}_l(t)$ is the total demand that can be shed, $\bar{p}_l(t) - p_l(t)$ is the shed demand, and α_l is a positive constant to control the quality-of-service. A small α_l means tighter quality-of-service control.

We use a cost function to capture the cost of load shedding:

$$C_l(t, p_l(t)) \triangleq \beta_l(\bar{p}_l(t)\Delta t - p_l(t)\Delta t)^2, \tag{4.13}$$

where β_l is a positive constant. α_l and β_l reflect the customer's tolerance and sensitivity to load shedding and they are assumed to be generated on the customer side.

Note that although both (4.12) and (4.13) can limit load shedding to some extent, they have different meanings in the model. While (4.13) captures the economic loss of load shedding in the objective of the EMS, (4.12) is a constraint to guarantee the quality-of-service in a time-average sense that can be seen as a "soft" limit on load shedding.

4.2.5 Distribution Network Model

A distribution network is composed of lines and buses. It can be modeled as a connected graph $(\mathcal{N}, \mathcal{E})$, where each node $i \in \mathcal{N}$ represents a bus and each link $(i,j) \in \mathcal{E}$ represents a branch (line or transformer). A power distribution network typically has a radial structure and the graph becomes a tree. The root of the tree is the feeder with a fixed voltage and flexible power injection, denoted by bus 0. We index the other buses in $\mathcal{N}$ by $i = 1, \ldots, n$.

For each link $(i,j) \in \mathcal{E}$, let $z_{ij} \triangleq r_{ij} + \mathbf{i}x_{i,j}$ be the complex impedance of the branch, $I_{ij}(t)$ be the complex current from buses i to j, and $S_{ij}(t) \triangleq P_{ij}(t) + \mathbf{i}Q_{ij}(t)$ be the complex power flowing from buses i to j.

For each bus $i \in \mathcal{N}$, let $V_i(t)$ be the complex voltage at bus i and $s_i(t) \triangleq p_i(t) + \mathbf{i}q_i(t)$ be the net load which is the load minus the generation at bus i. Each bus $i \in \mathcal{N} \setminus \{0\}$ is connected to a subset of DG units $\mathcal{G}_i$, DS units $\mathcal{B}_i$, and loads $\mathcal{L}_i$. The net load at each bus i satisfies:

$$s_i(t) = s_{li}(t) + s_{bi}(t) - s_{gi}(t), \ \forall i \in \mathcal{N} \setminus \{0\}, t, \tag{4.14}$$

where $s_{li}(t) \triangleq \sum_{l \in \mathcal{L}_i} s_l(t)$, $s_{bi}(t) \triangleq \sum_{b \in \mathcal{B}_i} s_b(t)$, and $s_{gi} \triangleq \sum_{g \in \mathcal{G}_i} s_g(t)$.

The steady-state power flows in a given distribution network $(\mathcal{N}, \mathcal{E})$ can be modeled using the branch flow model [57]: $\forall (i,j) \in \mathcal{E}, t$,

$$\begin{aligned}
p_j(t) &= P_{ij}(t) - r_{ij}\ell_{ij}(t) - \sum_{k:(j,k)\in\mathcal{E}} P_{jk}(t), && (4.15)\\
q_j(t) &= Q_{ij}(t) - x_{ij}\ell_{ij}(t) - \sum_{k:(j,k)\in\mathcal{E}} Q_{jk}(t), && (4.16)\\
v_j(t) &= v_i(t) - 2\left(r_{ij}P_{ij}(t) + x_{ij}Q_{ij}(t)\right) + (r_{ij}^2 + x_{ij}^2)\ell_{ij}(t), && (4.17)\\
\ell_{ij}(t) &= \frac{P_{ij}(t)^2 + Q_{ij}(t)^2}{v_i(t)}, && (4.18)
\end{aligned}$$

where $\ell_{ij}(t) \triangleq |I_{ij}(t)|^2$ and $v_i(t) \triangleq |V_i(t)|^2$.

Equations (4.15)–(4.18) define a system of equations in the variables $(\mathbf{P}(t), \mathbf{Q}(t), \mathbf{v}(t), \mathbf{l}(t), \mathbf{s}(t))$, where $\mathbf{P}(t) \triangleq (P_{ij}(t), (i,j) \in \mathcal{E})$, $\mathbf{Q}(t) \triangleq (Q_{ij}(t), (i,j) \in \mathcal{E})$, $\mathbf{v}(t) \triangleq (v_i(t), i \in \mathcal{N} \setminus \{0\})$, $\mathbf{l}(t) \triangleq (\ell_{ij}(t), (i,j) \in \mathcal{E})$, and $\mathbf{s}(t) \triangleq (s_i(t), i \in \mathcal{N} \setminus \{0\})$. The phase angles of the voltages and the currents are not included. But they can be uniquely determined for radial systems [58].

4.2.6 Real-Time Energy Management

The objective of the microgrid operator is to minimize its long-term operational cost, while delivering reliable and high-quality power to the customers. However, the introduction of DERs brings uncertainties to the energy management problem, which makes it challenging to balance supply and demand in real time. The voltages in the microgrid may also deviate significantly from the nominal values. Thus in this chapter, we study microgrid energy management aiming at achieving the long-term operational objective of the microgrid operator, while meeting the supply-demand balance and the voltage tolerance constraints in real time.

We consider the following voltage tolerance constraints in the microgrid:

$$\underline{V}_i \leq |V_i(t)| \leq \bar{V}_i, \ \forall i \in \mathcal{N} \setminus \{0\}, t, \tag{4.19}$$

where $\underline{V}_i$ and $\bar{V}_i$ correspond to the minimum and maximum allowed voltages, respectively.

The net power injected to the microgrid from the main grid is given by:

$$s_0(t) = \sum_{j:(0,j)\in\mathcal{E}} s_{0j}(t), \ \forall t. \tag{4.20}$$

If the microgrid is operated in islanded mode, then $s_0(t) = 0$. If the microgrid is operated in grid-connected mode, then $s_0(t)$ is the net complex power traded between the microgrid and the main grid. We model the cost of energy purchase from the main grid at each time t as:

$$C_0\left(t, p_0(t)\right) \triangleq \rho(t) p_0(t) \Delta t, \tag{4.21}$$

where $\rho(t)$ is the market energy price. Note that $p_0(t)$ can be negative, meaning that the microgrid can sell its surplus power to the main grid.

We define the system state vector at time t using the renewable generations, the demand requests, and the energy price:

$$\mathbf{x}(t) \triangleq (\mathbf{r}(t), \mathbf{d}(t), \rho(t)), \tag{4.22}$$

where $\mathbf{r}(t) \triangleq (s_g(t), g \in \mathcal{G}_r)$ is the vector of renewable generations and $\mathbf{d}(t) \triangleq (\underline{p}_l(t), \bar{p}_l(t), \underline{q}_l(t), \bar{q}_l(t), l \in \mathcal{L})$ is the vector of demand requests. We assume the system state to be stochastic and make no assumptions about the statistics of the underlying stochastic processes.

We define the control vector at time t as:

$$\mathbf{u}(t) \triangleq (\mathbf{P}(t), \mathbf{Q}(t), \mathbf{v}(t), \mathbf{l}(t), \mathbf{s}(t), \mathbf{g}(t), \mathbf{b}(t), \mathbf{y}(t)), \tag{4.23}$$

where $\mathbf{g}(t) \triangleq (s_g(t), g \in \mathcal{G}_c)$, $\mathbf{b}(t) \triangleq (s_b(t), b \in \mathcal{B})$, and $\mathbf{y}(t) \triangleq (s_l(t), l \in \mathcal{L})$. $\mathbf{u}(t)$ controls power flows in the microgrid.

The objective of the real-time energy management in the microgrid is to make control decision $\mathbf{u}(t)$ at each time in order to (i) minimize the long-term operational cost, including the cost of generation, the cost of energy storage, the cost of load shedding, and the cost of energy purchase from the main grid, (ii) guarantee the quality-of-service for customers, and (iii) minimize the long-term power losses subject to the DER constraints, the load constraints, the power flow constraints, and the system operational constraints (voltage tolerances).

We define the objective function of the optimization as:

$$\begin{aligned} C(t) \triangleq & \xi_g \sum_{g \in \mathcal{G}_c} C_g(p_g(t)) + \xi_b \sum_{b \in \mathcal{B}} C_b(p_b(t)) + \xi_l \sum_{l \in \mathcal{L}} C_l(t, p_l(t)) \\ & + \xi_0 C_0(t, p_0(t)) + \xi_p \sum_{(i,j) \in \mathcal{E}} r_{ij} \ell_{ij}(t), \end{aligned} \tag{4.24}$$

where ξ_g, ξ_b, ξ_l, ξ_0, and ξ_p are the parameters to trade off among different costs and power losses in the optimization.

The real-time energy management in the microgrid can be formulated as an SOPF problem:

SOPF

$$\begin{aligned} \min_{\{\mathbf{u}(t)\}} \quad & \lim_{T\to\infty} \frac{1}{T}\sum_{t=0}^{T-1} \mathbb{E}\left[C(t)\right] \\ \text{s.t.} \quad & (4.1)-(4.3), (4.5)-(4.8), (4.10)-(4.12), (4.14)-(4.20). \end{aligned}$$

where the randomness of the system state $\mathbf{x}(t)$ and the possibly random control decision $\mathbf{u}(t)$ at each time are taken into account in the expectations in the objective and constraint (4.12).

4.3 Online EMS

Solving the previous SOPF problem is challenging mainly due to the objective and constraints (4.8) and (4.12). We first use the concept of virtual queues from Lyapunov optimization (see Section 4.4 in [66]) to deal with these constraints and obtain a relaxed SOPF problem (SOPF-r). Following the Lyapunov optimization framework (see Section 4.3.1 for a brief introduction or Chapter 4 in [66] for details), we reformulate SOPF-r as a real-time problem (SOPF-l). Since we relax the constraints, the solution to SOPF-l may be infeasible to the original SOPF problem. Therefore, we restore the constraints and obtain a standard OPF problem to be solved at each time. The OPF problem is non-convex due to the quadratic equality constraints in (4.18) and thus is NP-hard to solve in general [57]. We therefore relax the constraints and obtain a convex optimization problem (OPF-r) for real-time computing. Fig. 4.2 summarizes the scheme used in the problem formulation.

4.3.1 Introduction to Lyapunov Optimization

In this chapter, we develop an online EMS using Lyapunov optimization [66] which is a technique to optimize time averages in stochastic systems. We give a very brief description of it below.

Consider a stochastic system that operates in discrete time with time slots $t \in \{0, 1, 2, \ldots\}$. In every time slot, a random system state $\omega(t)$ is observed and a control action $\alpha(t)$ is taken. The control action $\alpha(t)$ is determined within a set $\mathcal{A}_{\omega(t)}$ that may depend on

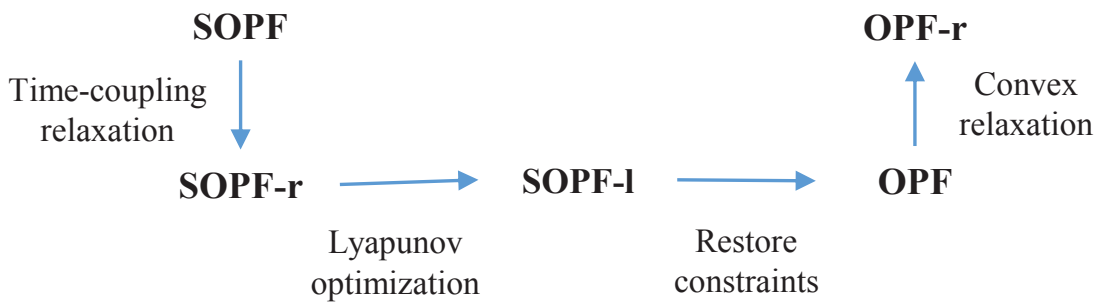

Figure 4.2: Problem formulation scheme.

$\omega(t)$. There are a collection of real-valued attributes that are depended on the system state and the control action, denoted by $\mathbf{y} := (y_0(t), y_1(t), \ldots, y_L(t)), \mathbf{e} := (e_1(t), \ldots, e_M(t))$. Let $\bar{y}_l := \lim_{T\to\infty} \frac{1}{T} \sum_{t=0}^{T-1} y_l(t)$ and $\bar{e}_m := \lim_{T\to\infty} \frac{1}{T} \sum_{t=0}^{T-1} e_m(t)$ be the time average of $y_l(t)$ and $e_m(t)$ under a particular control. The objective is to design an algorithm that solves the following problem.

$$\min_{\{\alpha(t)\in\mathcal{A}_{\omega(t)}\}} \quad \bar{y}_0 \tag{4.25}$$

$$\text{s.t.} \quad \bar{y}_l \leq 0, \quad l = 1, \ldots, L, \tag{4.26}$$

$$\bar{e}_m = 0, \quad m = 1, \ldots, M. \tag{4.27}$$

The theory of Lyapunov optimization can be used to devise a drift-plus-penalty algorithm to solve the above problem in a simple and elegant way. The steps to use it are given briefly as follows.

1. Construct virtual queues in the way described in Section 4.4 in [66] for ensuring that the time average constraints (4.26) and (4.27) are satisfied.

2. Define the Lyapunov function $L(t)$ as the sum of the squares of the backlogs of all the virtual queues. $L(t)$ is a scalar measurement of the queues' size.

3. Define the Lyapunov drift $\Delta(t) = L(t+1) - L(t)$ as the difference of the Lyapunov function in two consecutive time slots. It is shown in [66] that greedily minimizing the Lyapunov drift can stabilize the queues, which ensures the time average constraints are met.

4. In each time slot t, take actions to greedily minimize the drift-plus-penalty function defined as $\Delta(t) + V \times penalty(t)$, where V is a non-negative control parameter and $penalty(t)$ is a function mapped from the objective function.

The above drift-plus-penalty algorithm has been shown to produce a time average objective that deviates by at most $O(1/V)$ from the optimality with a $O(V)$ trade-off in time average queue backlog [66].

4.3.2 Virtual Queue Design

To deal with constraints (4.8) and (4.12), we use the concept of virtual queues (see Section 4.4 in [66]) to help satisfy the constraints.

4.3.2.1 Battery Queue

We define a virtual queue $J_b(t)$ for each $b \in \mathcal{B}$ that accumulates the charging/discharging energy. Define $J_b(0) = 0$ and it updates as follows:

$$J_b(t+1) = J_b(t) + p_b(t)\Delta t, \ \forall t, b. \tag{4.28}$$

We define $\mathbf{J}(t) \triangleq (J_b(t), b \in \mathcal{B})$.

$J_b(t)$ is in fact a shifted version of the energy stored in the battery $E_b(t)$. Instead of requiring that $E_b(t)$ is always bounded by (4.8), we relax it to keep the battery queue $J_b(t)$ mean rate stable:

$$\lim_{t\to\infty} \frac{\mathbb{E}\left[|J_b(t)|\right]}{t} = 0, \ \forall b. \tag{4.29}$$

4.3.2.2 Load Queue

We define a virtual queue $H_l(t)$ for each load $l \in \mathcal{L}$ to tackle the time average constraint in (4.12). Define $H_l(0) = 0$ and its backlog evolves as follows [66]:

$$H_l(t+1) = \max\{H_l(t) - \alpha_l, 0\} + \frac{\bar{p}_l(t) - p_l(t)}{\bar{p}_l(t) - \underline{p}_l(t)}, \ \forall t, l. \tag{4.30}$$

We define $\mathbf{H}(t) \triangleq (H_l(t), l \in \mathcal{L})$.

The arrival rate of the load queue $H_t(t)$ is the shedding percentage at time t and the departure rate is α_l. If the queue $H_l(t)$ is stable, the time average load shedding percentage must be less than or equal to α_l. Therefore, constraint (4.12) can be transformed to the following queue stability constraint [66]:

$$\lim_{t\to\infty} \frac{\mathbb{E}\left[|H_l(t)|\right]}{t} = 0, \ \forall l. \tag{4.31}$$

Now we consider a relaxed SOPF problem that fits the Lyapunov optimization framework.

SOPF-r

$$\begin{aligned} \min_{\{\mathbf{u}(t)\}} \quad & \lim_{T\to\infty} \frac{1}{T} \sum_{t=0}^{T-1} \mathbb{E}\left[C(t)\right] \\ \text{s.t.} \quad & (4.1), (4.3), (4.5)-(4.7), (4.10), (4.11), (4.14)-(4.20), (4.28)-(4.31). \end{aligned}$$

Note the time-coupled generation ramping constraint (4.2) is also relaxed here. SOPF-r provides a lower bound on SOPF. If the optimal solution to SOPF-r is feasible to SOPF, then it is also an optimal solution to SOPF.

4.3.3 Lyapunov Optimization

It is still difficult to solve SOPF-r because of the objective function and constraints (4.29) and (4.31). To address these challenges, we follow the Lyapunov optimization framework (see Section 4.3.1 for a brief introduction or Chapter 4 in [66] for details) to solve the above SOPF-r problem.

Define $\mathbf{\Theta}(t) \triangleq (\mathbf{J}(t), \mathbf{H}(t))$ and the Lyapnuov function as a scalar measure of $\mathbf{\Theta}(t)$:

$$L(\mathbf{\Theta}(t)) \triangleq \frac{1}{2}\beta \sum_{b\in\mathcal{B}} J_b(t)^2 + \frac{1}{2} \sum_{l\in\mathcal{L}} H_l(t)^2, \tag{4.32}$$

where β is a weight to treat the battery virtual queue differently from the load virtual queue.

We define the conditional 1-slot Lyapunov drift as follows:

$$\Delta(\mathbf{\Theta}(t)) \triangleq \mathbb{E}\left[L(\mathbf{\Theta}(t+1)) - L(\mathbf{\Theta}(t))|\mathbf{\Theta}(t)\right]. \tag{4.33}$$

The Lyapunov drift measures the expected queue size growth given the current state $\mathbf{\Theta}(t)$.

Minimizing the Lyapunov drift would push the queues towards a less congested state, but it may incur a high cost. Therefore, we minimize a weighted sum of the drift and cost, which is defined as a drift-plus-penalty function $\Delta(\mathbf{\Theta}(t)) + V\mathbb{E}\left[C(t)|\mathbf{\Theta}(t)\right]$, where V is a positive parameter to trade off between stabilizing queues and minimizing cost.

For any possible control policies, the defined drift-plus-penalty function is upper bounded at each time t:

$$\begin{aligned}\Delta(\mathbf{\Theta}(t)) + V\mathbb{E}\left[C(t)|\mathbf{\Theta}(t)\right] \leq B + \beta \sum_{b\in\mathcal{B}} J_b(t)\mathbb{E}\left[p_b(t)\Delta t|\mathbf{\Theta}(t)\right] \\ + \sum_{l\in\mathcal{L}} H_l(t)\mathbb{E}\left[\frac{\bar{p}_l(t) - p_l(t)}{\bar{p}_l(t) - \underline{p}_l(t)} - \alpha_l|\mathbf{\Theta}(t)\right] + V\mathbb{E}\left[C(t)|\mathbf{\Theta}(t)\right] \end{aligned} \tag{4.34}$$

where $B \triangleq \frac{1}{2}\sum_{l\in\mathcal{L}}(1+\alpha_l^2) + \frac{1}{2}\beta\sum_{b\in\mathcal{B}}\max\{\underline{p}_b^2, \bar{p}_b^2\}\Delta t^2$.

Proof: According to the definition of $L(\mathbf{\Theta}(t))$ in (4.32), we have

$$\begin{aligned}L(\mathbf{\Theta}(t+1)) - L(\mathbf{\Theta}(t)) = \frac{1}{2}\beta\sum_{b\in\mathcal{B}}\left[J_b(t+1)^2 - J_b(t)^2\right] \\ + \frac{1}{2}\sum_{l\in\mathcal{L}}\left[H_l(t+1)^2 - H_l(t)^2\right]. \end{aligned} \tag{4.35}$$

Based on the queue update of $J_b(t)$ in (4.28), the term $J_b(t+1)^2 - J_b(t)^2$ can upper bounded by

$$J_b(t+1)^2 - J_b(t)^2 \leq 2J_b(t)p_b(t)\Delta t + \max\{\underline{p}_b^2, \bar{p}_b^2\}\Delta t^2. \tag{4.36}$$

Based on the queue update of $H_l(t)$ in (4.30), the term $H_l(t+1)^2 - H_l(t)^2$ can upper bounded by

$$H_l(t+1)^2 - H_l(t)^2 \leq 2H_l(t)\left(\frac{\bar{p}_l(t) - p_l(t)}{\bar{p}_l(t) - \underline{p}_l(t)} - \alpha_l\right) + 1 + \alpha_l^2. \tag{4.37}$$

Applying (4.36) and (4.37) to (4.35), adding the term $V\mathbb{E}\left[C(t)\right]$, and taking the conditional expectation given $\mathbf{\Theta}(t)$ yields the upper bound in (4.34).

Instead of minimizing the drift-plus-penalty function directly, we minimize the upper bound in (4.34) via the framework of opportunistically minimizing an expectation (see Section 1.8 in [66]). The resulting algorithm can be described as follows. At each time t, observe

the system state $\mathbf{x}(t)$ and the virtual queue states $\mathbf{\Theta}(t)$, and determine the control decision $\mathbf{u}(t)$ by solving the following optimization problem:

SOPF-l

$$\begin{aligned} \min_{\mathbf{u}(t)} \quad & \beta \sum_{b\in\mathcal{B}} J_b(t)p_b(t)\Delta t - \sum_{l\in\mathcal{L}} \frac{H_l(t)}{\bar{p}_l(t)-\underline{p}_l(t)} p_l(t) + VC(t) \\ \text{s.t.} \quad & (4.1), (4.3), (4.5)-(4.7), (4.10), (4.11), (4.14)-(4.20), (4.28), (4.30). \end{aligned}$$

The above algorithm does not require any information of the probabilities associated with the system state $\mathbf{x}(t)$. The queue states $\mathbf{\Theta}(t)$ carry sufficient statistical information needed to determine the control decision at the next time step.

Since we relax the generation ramping constraint (4.2) and the battery energy constraint (4.8) in SOPF-l, the optimal solution to SOPF-l may violate these constraints and thus may be infeasible to the original SOPF problem. Therefore, we add constraints (4.2) and (4.8) back. The problem we consider now is indeed a standard OPF problem to be solved at each time t:

OPF

$$\begin{aligned} \min_{\mathbf{u}(t)} \quad & \beta \sum_{b\in\mathcal{B}} J_b(t)p_b(t)\Delta t - \sum_{l\in\mathcal{L}} \frac{H_l(t)}{\bar{p}_l(t)-\underline{p}_l(t)} p_l(t) + VC(t) \\ \text{s.t.} \quad & (4.1)-(4.3), (4.5)-(4.8), (4.10), (4.11), (4.14)-(4.20), (4.28), (4.30). \end{aligned}$$

The solution to OPF is always feasible to SOPF.

4.3.4 Convexification of OPF

The previous OPF problem is non-convex due to the quadratic equality constraint in (4.18) and is NP-hard to solve in general [57]. We therefore relax them to inequalities:

$$\ell_{ij}(t) \geq \frac{P_{ij}(t)^2 + Q_{ij}(t)^2}{v_i(t)}, \ \forall (i,j) \in \mathcal{E}, t. \tag{4.38}$$

We then consider the following convex relaxation of OPF:

OPF-r

$$\begin{aligned}\min_{\mathbf{u}(t)} \quad & \beta \sum_{b\in\mathcal{B}} J_b(t)p_b(t)\Delta t - \sum_{l\in\mathcal{L}} \frac{H_l(t)}{\bar{p}_l(t)-\underline{p}_l(t)} p_l(t) + VC(t) \\ \text{s.t.} \quad & (4.1)-(4.3), (4.5)-(4.8), (4.10), (4.11), (4.14)-(4.17), \\ & (4.19)-(4.20), (4.28), (4.30), (4.38).\end{aligned}$$

The above relaxation is exact if the solution to OPF-r is also an optimal solution to OPF, i.e., the equality in (4.38) is attained. In general, such a relaxation is not exact. It has been shown recently [46, 59, 74] that the convex relaxation of OPF is exact under certain mild conditions that can be checked a priori. Such conditions are verified to hold in a variety of IEEE test distribution systems and real-world distribution systems. Roughly speaking, the relaxation is exact if the power injection at each bus is not too large and the voltages are kept around their nominal values [23]. In this chapter, we assume that the sufficient conditions specified in [59] hold for the microgrid and thus we focus on solving the OPF-r problem. The exactness of the relaxation is also verified numerically in the simulation. OPF-r is a convex optimization problem and therefore can be solved efficiently for real-time computation.

4.3.5 Performance Gaps in the Optimizations

From the Lyapunov optimization theory, it can be proved that the optimal time average cost of SOPF-l is within $O(1/V)$ of the optimal time average cost of SOPF-r, i.e., SOPF-l* $\leq$ SOPF-r*+B/V, with a corresponding $O(V)$ trade-off in the average queue size with i.i.d. system state (see Theorem 4.8 in [66]), and the algorithm is robust to non-i.i.d., non-ergodic situations (see Theorem 4.13 in [66]). Since SOPF-r provides a lower bound on SOPF, i.e., SOPF-r*$\leq$ SOPF*, we obtain a deterministic performance bound on SOPF-l as SOPF-l* $\leq$ SOPF*+B/V. The choice of the control parameter V affects the performance of the optimization. A large V can decrease optimality gap but also increase the average queue size. On the other hand, a small V makes it easier to keep the queues stable but at the sacrifice of a larger optimality gap.

If the solution to OPF is the same as the solution to SOPF-l, the performance of the

proposed online EMS can be guaranteed using the above performance bound. However, as we restore the constraints in OPF, it is possible that these constraints are effective in the optimal solution and thus affect the optimality. The previous studies [33–35] deal with this issue by carefully designing the control parameters to force the time-coupled constraints to be always satisfied in the solution to the Lyapunov optimization. Unfortunately, the same method cannot be applied here due to the difficulty in characterizing the solution brought up by the introduction of the power flow and system operational constraints. We therefore validate the performance of the proposed online EMS via simulations. Our simulation results in the next section will demonstrate that the performance of the proposed EMS is desirable.

4.4 Performance Evaluation

In this section, we demonstrate the proposed online EMS by applying it to a real microgrid system. We first describe the microgrid system and the simulation setup. We then describe two benchmarks and compare the proposed online EMS with them. Finally, we discuss the battery queue and the load queue behaviors, the voltages in the microgrid, and the network effect observed in the simulations.

4.4.1 Simulation Setup

Fig. 4.3 shows the configuration of a real microgrid system [27] in Guangdong Province, China, consisting of PVs, WTs, diesel generators, and a BESS. The numbers under the DERs and the loads in the figure correspond to the maximum power. We use this microgrid to demonstrate the proposed online EMS. In the simulation, we run the proposed online EMS for 4 days denoted by $\mathcal{T} \triangleq \{0, 1, \ldots, T-1\}$. The time interval Δt in the model is 5 minutes and there are $T = 1152$ time intervals in total.

Fig. 4.4 shows the renewable generation profiles, the load profile, and the market prices used in the simulation. We use the real solar and wind data from national renewable energy laboratory (NREL) [76] to generate the renewable generation profiles. For each load, we generate the maximum power request $\bar{p}_l(t)$ based on different types of load using a Gaussian

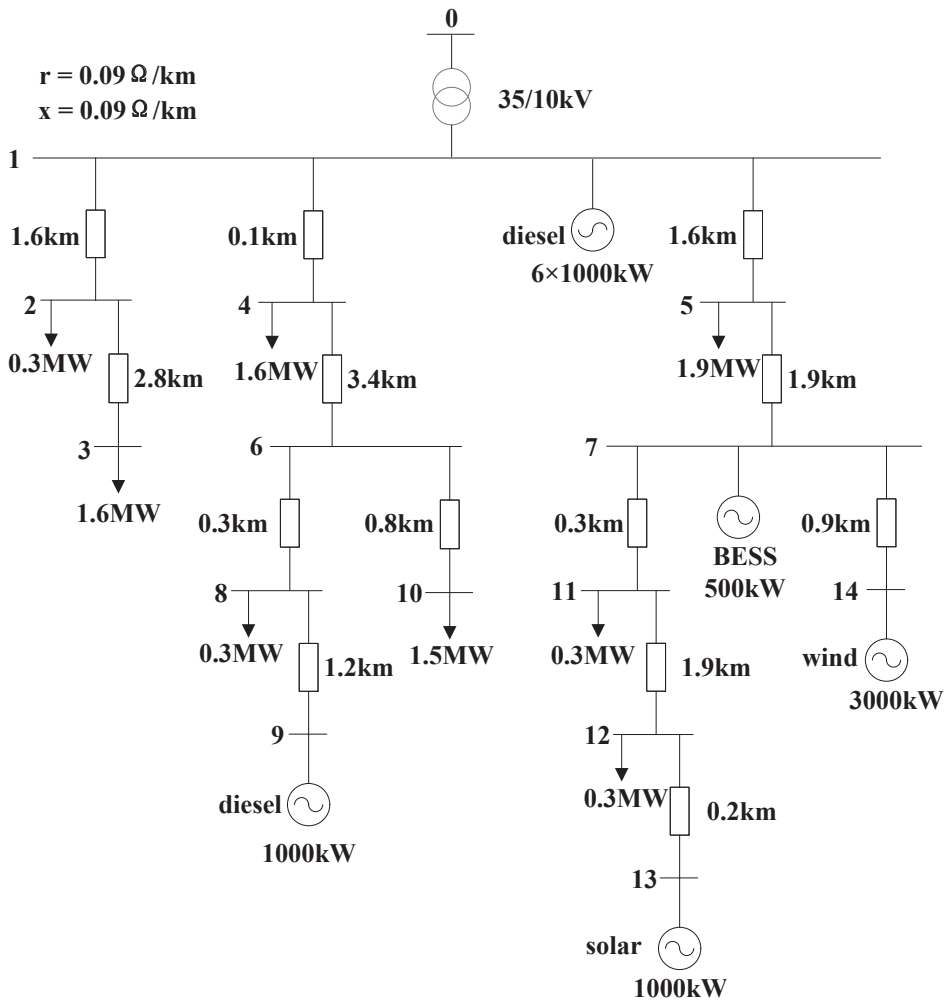

Figure 4.3: Topology of the microgrid.

random variable with hourly mean values from [27] and choose the percentage of load that can be shed $\frac{\bar{p}_l(t)-\underline{p}_l(t)}{\bar{p}_l(t)}$ randomly from $[30\%, 50\%]$. The reactive power requests $\bar{q}_l(t)$ and $\underline{q}_l(t)$ are generated based on the active power requests $\bar{p}_l(t)$ and $\underline{p}_l(t)$ using a power factor chosen randomly from $[0.8, 0.9]$. The parameters α_l and β_l are chosen to be 0.5 and 500, respectively for each load. We use the 5-minute real-time pricing data from CAISO [77] in the simulation. We set the cost function of diesel generation as $C_g(p_g(t)) \triangleq 40(p_g(t)\Delta t)^2 + 60(p_g(t)\Delta t)$ and the ramping parameter as $r_g = 0.3$. The capacity of the BESS $\bar{E}_b$ is 3 MWh and $\underline{E}_b$ is chosen to be 0.1 MWh. The initial battery energy level is set to be $E_b(0) = 1.5$ MWh. The parameters in the battery cost function are chosen as $\alpha_b = 1$ and $c_b = 0$.

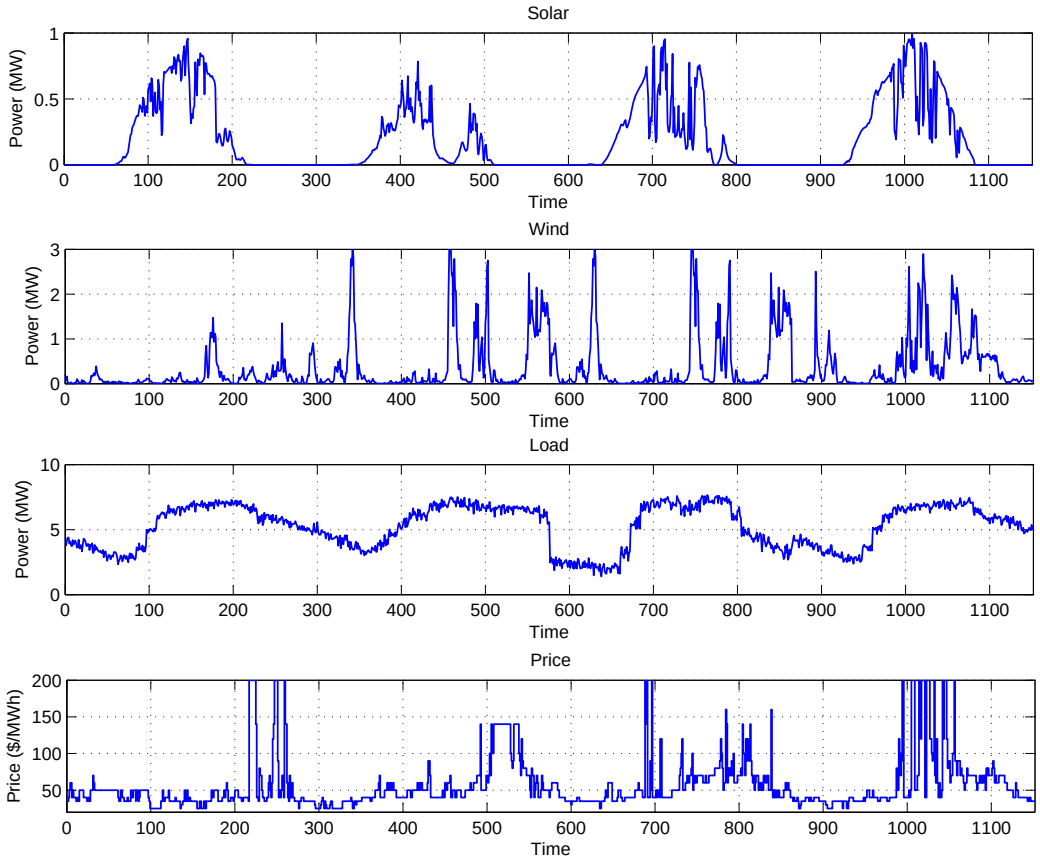

Figure 4.4: Renewable generation profiles, load profile, and real-time price.

4.4.2 Benchmarks

In order to evaluate the performance of the proposed online EMS, we use two benchmarks: one is an optimal offline algorithm that optimizes the objective over the entire time horizon $\mathcal{T}$ and the other is a greedy algorithm that optimizes the cost at each time independently.

The offline algorithm solves the following optimization problem over the entire time horizon $\mathcal{T}$:

Offline

$$\begin{aligned} \min_{\{\mathbf{u}(t)\}} \quad & \frac{1}{T}\sum_{t=0}^{T-1} C(t) \\ \text{s.t.} \quad & (4.1)-(4.3), (4.5)-(4.8), (4.10), (4.11), (4.14)-(4.20), \\ & \frac{1}{T}\sum_{t=0}^{T-1} \frac{\bar{p}_l(t)-p_l(t)}{\bar{p}_l(t)-\underline{p}_l(t)} \leq \alpha_l, \ \forall l. \end{aligned}$$

The offline algorithm provides a lower bound on any online algorithms, assuming that all system states over time (i.e., the output power of the renewables, the demand requests, and the energy prices) are known a priori, which is difficult to achieve in practice due to the stochastic nature of the problem. Although the optimal solution to the offline problem is not achievable in practice, it gives us the best performance to compare with any online algorithms.

Another benchmark we consider is a greedy algorithm that aims to minimize the cost at each time $t \in \mathcal{T}$ independently:

Greedy

$$\begin{aligned} \min_{\mathbf{u}(t)} \quad & C(t) \\ \text{s.t.} \quad & (4.1)-(4.3), (4.5)-(4.8), (4.10), (4.11), (4.14)-(4.20), \\ & \frac{\bar{p}_l(t)-p_l(t)}{\bar{p}_l(t)-\underline{p}_l(t)} \leq \alpha_l, \ \forall l. \end{aligned}$$

The greedy algorithm is shortsighted as it optimizes the cost at each time without taking the future into account.

4.4.3 Case Study

We apply the proposed online EMS to the microgrid using the setup described above. The voltage tolerances are set to be [0.95 p.u., 1.05 p.u.]. The parameters in the algorithm are chosen as $\beta = 1300$, $V = 20$, $\xi_g = 1$, $\xi_b = 1$, $\xi_l = 1$, $\xi_0 = 1$, and $\xi_p = 1$. The optimization problem is solved using the CVX package [56] in MATLAB on an Intel CORE i7 3.4 GHz machine with 12 GB RAM.

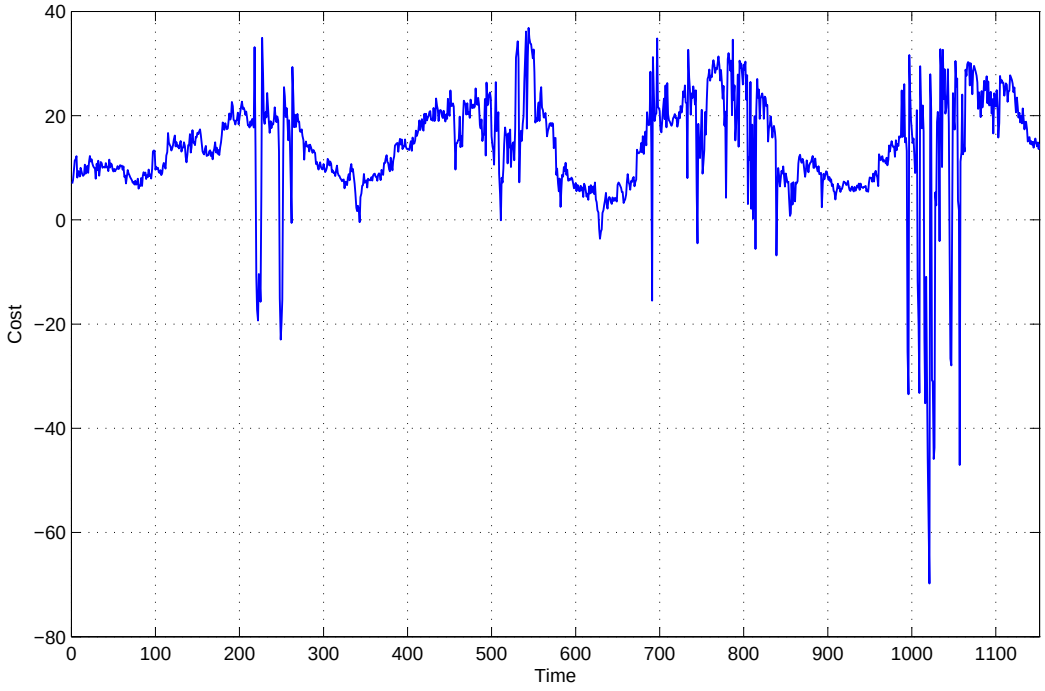

Figure 4.5: Real-time cost.

Fig. 4.5 shows the real-time cost by using the proposed EMS. It can be seen from the figure there are some significant cost drops, and negative costs exist, showing that the microgrid gains money by selling surplus power to the main grid at that time. If we compare Fig. 4.5 with Fig. 4.4, we can easily find that the cost drops coincide with the spikes of energy price. When the price is high, the cost of using DERs is relatively low. Therefore, it is beneficial for the microgrid not only to use DERs to supply its local demand but also to sell back surplus power to gain profit.

Next, we compare the performance of the proposed online EMS with the two benchmarks as shown by the time accumulated cost over time in Fig. 4.6. As shown in the figure, the shortsighted greedy algorithm performs the worst. The online EMS performs the best at first but it is surpassed by the optimal offline algorithm as time goes on. This is because the offline algorithm is optimized over the entire time horizon. It is able to make some performance sacrifices at the beginning but achieve better overall performance in the end.

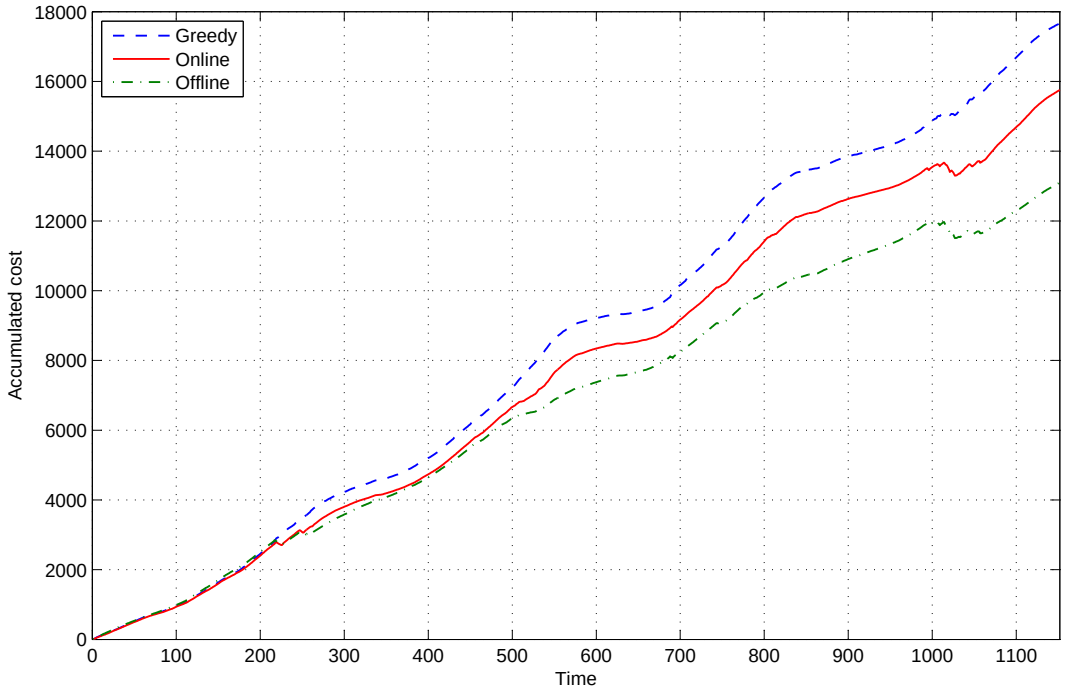

Figure 4.6: Time accumulated cost comparison. Time average cost: \$15.34 (greedy), \$13.68 (online), \$11.37 (offline).

Although the offline algorithm gives us the best performance, it requires a priori system state information, which is not applicable in practice.

Regarding real-time computing, the computational time of our proposed online EMS at each time step is on average 1.13 seconds showing that it can be implemented in real time. The total computational time of the four-day time period (1152 time steps) is 21.65 minutes, compared with 3.84 hours of the offline approach specified in Section 4.4.2. Both the online and offline problems are solved using the interior-point optimizer SDPT3 [78] from CVX. Our proposed online EMS can save the computational time significantly.

For the simulations, we also verify numerically that the equality in (4.38) is attained in the optimal solution to OPF-r, i.e., OPF-r is an exact relaxation of OPF.

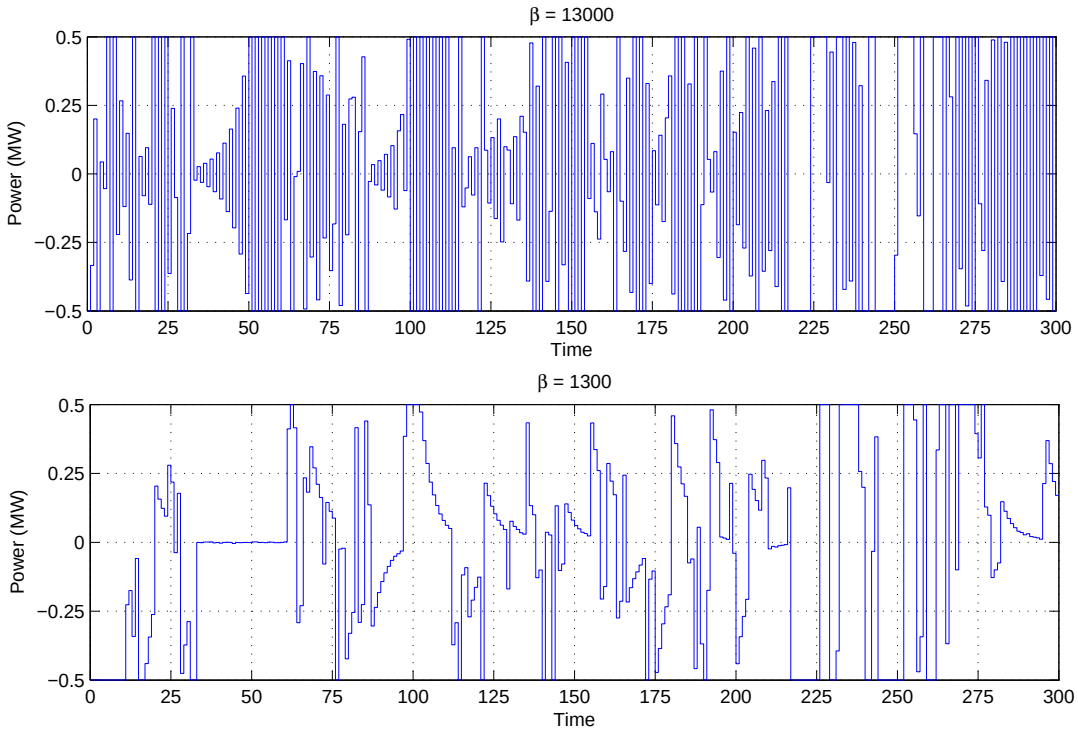

Figure 4.7: Battery charging/discharging profile with different β.

4.4.4 Discussions

4.4.4.1 Battery Queue

We first look at the effect of β on the charging/discharing profile of the BESS as shown in Fig. 4.7. As can be seen from the figure, a large β results in more charging/discharging cycles. This is because β is the weight of the battery queue stability in the optimization. A large β would push the battery queue to a less congested state and therefore cause a smaller average queue backlog. Since the battery queue backlog is the aggregate charging/discharging energy by definition, a smaller average queue backlog leads to more switches between charging (positive power) and discharging (negative power).

To investigate the effect of β on the time average cost, we run the online algorithm with different β. The result is shown in Fig. 4.8. The cost first drops significantly as β increases but later starts to increase once β is greater than a certain threshold. The reason for the

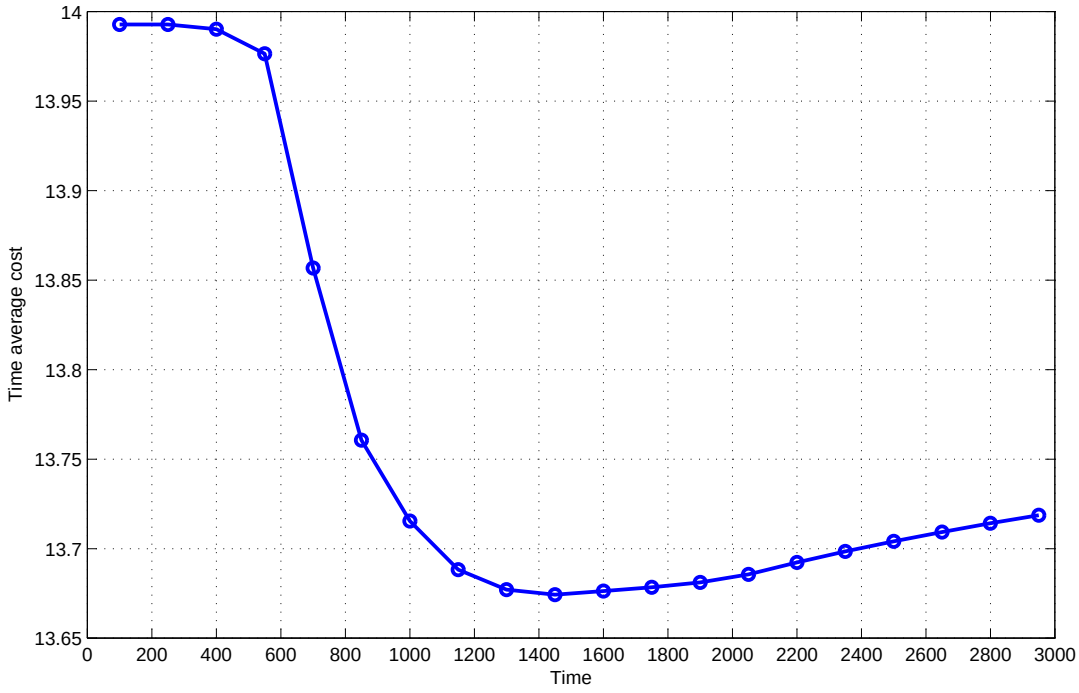

Figure 4.8: Time average cost with different β.

cost drop is that the battery energy constraint is more likely to be effective when β is small and thus affects the optimality of Lyapunov optimization. After β reaches the threshold where the battery energy level can be always bounded within the required range, the time average cost increases due to the stability-and-performance tradeoff in the drift-plus-penalty function.

4.4.4.2 Load Queue

Fig. 4.9 shows the time average load shedding percentage at bus 2 with different V. From the figure, we can see that although the time average load shedding percentage may exceed the quality-of-service requirement at the beginning, it quickly converges to a point where the time average constraint (4.12) is satisfied as the time goes on. The figure also shows the effect of V on load shedding behaviors. As V controls the trade-off between stabilizing queues and minimizing costs, a large V would cause the load queue to be more unstable as

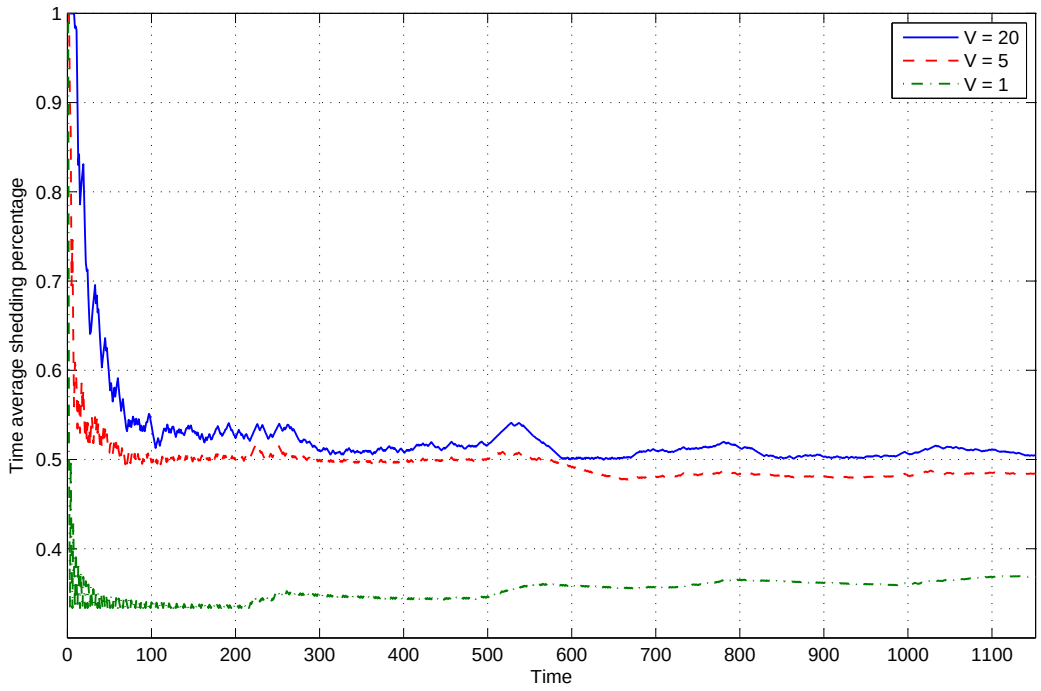

Figure 4.9: Load shedding percentage at bus 2 with different V.

can be seen from Fig. 4.9 but incur less cost as shown in Fig. 4.10.

4.4.4.3 Voltage

In order to demonstrate the effect of the online EMS on the bus voltages of the distribution network, we conduct simulations using homogeneous loads (1.0 MW) for all load buses and increasing the line lengths by 4 times.

One main advantage of our proposed online EMS is that voltages in the microgrid are kept within the allowed tolerance which guarantees the power quality in the microgrid. In order to compare our proposed online EMS with the previous online algorithms [33–35], we also solve the microgrid energy management problem without considering the underlying network constraints and then compute the power flows in the microgrid based on the obtained control decisions. The simulated bus voltages are shown in Fig. 4.11. As seen from the figure, the voltages deviate significantly away from the allowed tolerance when ignoring the network

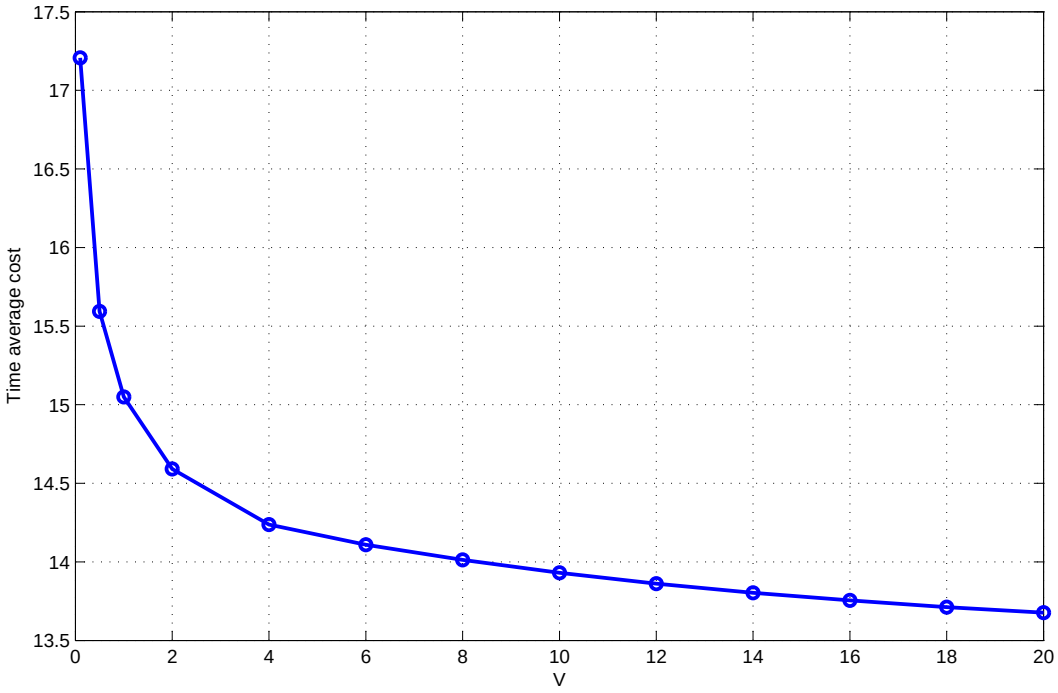

Figure 4.10: Time average cost with different V.

constraints, which may cause serious power quality issues in the microgrid. On the contrary, our proposed online EMS can achieve the long-term objective while maintaining the voltages within the tolerance.

4.4.4.4 Network Effect

Another major advantage of incorporating the distribution network in the modeling is that we can now understand how the underlying network structure interacts with the online energy management. Since the loads are homogeneous, they would behave in the same way if the network constraints are not considered in the energy management as in [33–35]. However, the underlying network constraints have an effect on the control decisions, making the location of the bus matter in the microgrid energy management.

In order to investigate this effect, we look into the load shedding behaviors at each bus

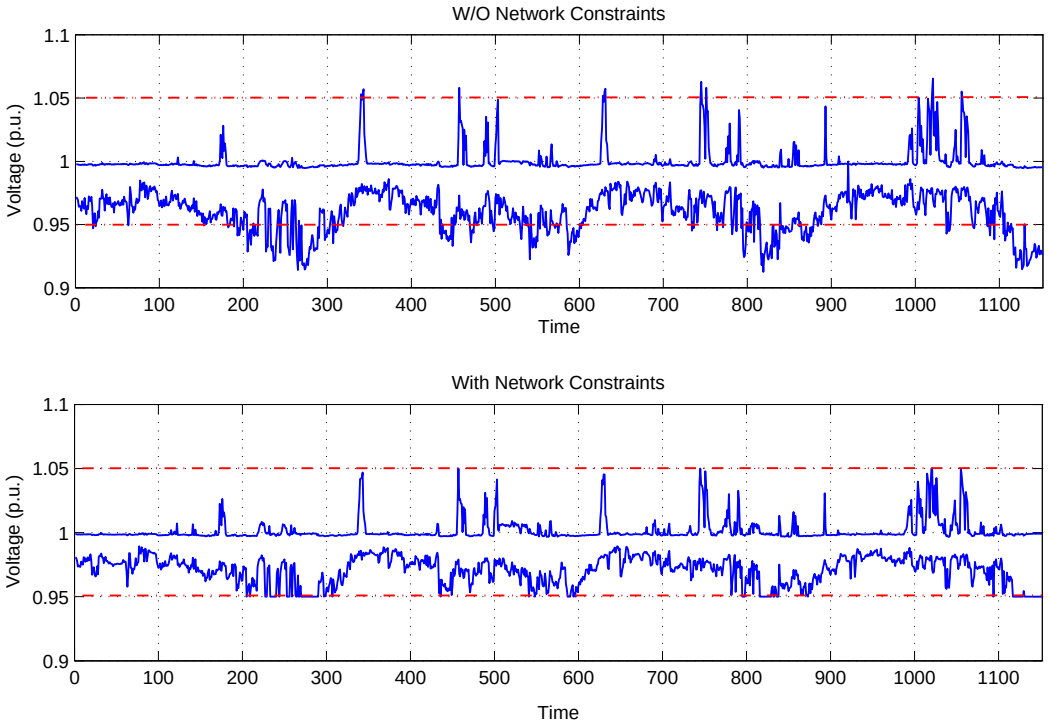

Figure 4.11: Comparison of the maximum and minimum bus voltages without and with considering the network constraints (Red lines indicate the allowed tolerance).

to see how they differ from each other in the online energy management. Fig. 4.12 shows the hourly demand reduction at each bus in day 3. It can be clearly seen from the figure that the loads at different locations behave very differently. The buses far away from the feeder and close to the DERs (e.g., buses 5, 11, and 12) are more likely to be different from the others. These buses need to shed more loads to maintain the voltage level at peak hours (e.g., hours 12-16, 18-20) because the voltage drop along the distribution line is significant. Their demand reduction is less than the others' when the renewable generation is high (e.g., hours 11, 21-24) because they are easier to be influenced by the injected power from the DERs. The farther the bus is away from the feeder and the closer it is to the DERs, the stronger the effect is. For example, bus 12 is influenced more than bus 11 that is more than bus 5.

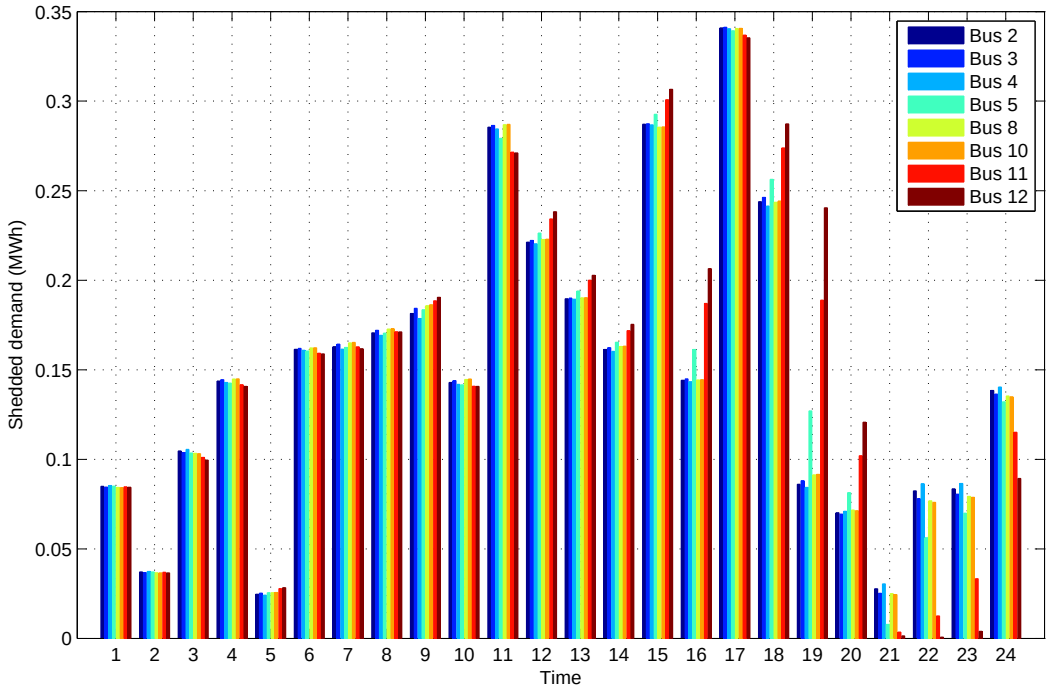

Figure 4.12: Hourly shed demands at each load bus in day 3.

4.5 Summary

An online EMS is proposed for real-time operation of microgrids in this chapter. Compared with the existing online algorithms, the proposed online EMS takes into account the underlying power distribution network and the associated constraints. Specifically, we formulate the online energy management as an SOPF problem and adopt Lyapunov optimization to devise an online algorithm to solve it in real time. As one demonstration, we apply the proposed online EMS to a real microgrid system. The simulation results show that the performance of the proposed online EMS exceeds a greedy algorithm and is close to an optimal offline algorithm. A comprehensive analysis of the proposed online EMS is given. Through this study, we observe and analyze the effect of the underlying network structure on the energy management that cannot be captured by previous online studies. One direction for future work is to develop an intelligent algorithm on the customer side to generate the demand

requests.

CHAPTER 5

Design and Implementation of a System Architecture for Microgrid Energy Management

A microgrid is a low-voltage power distribution system integrated with DERs and controllable loads that can operate with or without the main grid [2]. Such integration brings unique challenges to microgrid management and control that can be significantly different from conventional power systems [36]. In a microgrid, there are a variety of heterogeneous DERs and loads that need to be managed by an EMS. Unfortunately, most of those devices still use proprietary protocols and cannot interoperate with each other [37]. Furthermore, many devices managed by the system reside on the customer side requiring autonomy and local intelligence. In this chapter, we propose a system architecture for microgrid energy management that enables interoperability and autonomy on the customer side. We design a unified communication interface that is protocol and technology agnostic for the system to interoperate with heterogeneous devices in a microgrid. We then propose a decentralized system architecture, in which the system components are highly decoupled and independent to enable autonomy on the customer side. Moreover, we implement and deploy a prototype of the proposed system architecture and conduct experiments to evaluate microgrid management and control in real-world settings in two microgrid testbeds. Our experimental results demonstrate that the system is able to manage various DERs and loads in the testbeds using different industrial standards and protocols, interact with external systems, and perform efficient energy management using different algorithms.

5.1 Introduction

A microgrid is a low-voltage distribution network consisting of a variety of energy components including DERs and controllable loads[1] [2]. With these components, a microgrid can either be connected to the grid (i.e., grid-connected mode) or use the DERs to supply the loads without the grid (i.e., islanded mode). Integrating DERs and controllable loads within the distribution network introduces unique challenges to the microgrid management and control which are implemented by an EMS. A microgrid EMS can be significantly different from the EMS used in conventional power systems due to these challenges.

To understand the challenges, Su and Wang [36] discussed the role of EMS in microgrid operations and listed four essential functionalities that a microgrid EMS must support: forecast, optimization, data analysis, and HMI. Due to the importance of EMS in power systems, many EMS frameworks [37–40] have been investigated in the literature. While these previous studies focused on different issues in EMS, they commonly suffer from engineering challenges that must be taken into account when designing an implementable microgrid EMS.

First of all, intermittency and variability of DERs (e.g., PVs and WTs) and spatiotemporal uncertainty in controllable loads complicate the microgrid management, which the EMS must be able to cope with. Next, a microgrid triggers a number of new applications (e.g., DR, coordinated EV charging, V2G, etc.) and innovative control algorithms [1,23,41,79,80]. The EMS must be able to interface with them seamlessly. Last but not least, a microgrid instruments a number of energy components. But, most of them still use proprietary protocols and cannot interoperate with each other [37]. The EMS must handle the heterogeneity and achieve interoperation. A microgrid EMS can be implemented to perform efficient management and control only when overcoming the engineering challenges and satisfying aforementioned functional requirements. Unfortunately, few previous studies have accomplished both of them.

To address the essential functions and overcome the engineering challenges in a micro-

[1]Examples of DERs include PVs, WTs, fuel cells, combined heat and power (CHP), and energy storage systems. Examples of controllable loads include heating, ventilation, and air conditioning (HVAC) systems and EVs.

grid EMS, we propose a system architecture that enables interoperability and autonomy on the customer side in this chapter. For interoperability, we design a unified communication interface for the system to interoperate with heterogeneous devices in a microgrid. For autonomy, we propose a decentralized system structure where the system components that are highly-decoupled and independent to enable autonomy on the customer side. The decentralized architecture protects customer privacy by ensuring customer ownership of the data and control over the datas exposure. Furthermore, we implement and deploy a prototype of the proposed system architecture and conduct experiments in real-world settings at the UCLA Smart Grid Energy Research Center (UCLA SMERC) and the Korea Institute of Energy Research (KIER). Our experimental results demonstrate that the system is able to manage various devices in the testbeds, interact with external systems, and perform efficient energy management.

The rest of this chapter is organized as follows. We review the functionalities of a microgrid EMS and address the design issues in Section 5.2. The system architecture is implemented and illustrated in Section 5.3. We install the system prototype at UCLA SMERC and KIER, and conduct experiments on optimal energy scheduling and DR in Section 5.4. The summary is given in Section 5.5.

5.2 Design of a Microgrid EMS

This section discusses the design issues of an EMS for emerging microgrids - both functional requirements and engineering challenges. A microgrid EMS monitors and controls the DERs and the loads for the optimal operation. It interacts with various DERs and loads as well as external systems for utility information and weather forecast. Fig. 5.1 shows the role of a microgrid EMS. We refer to [36] for details.

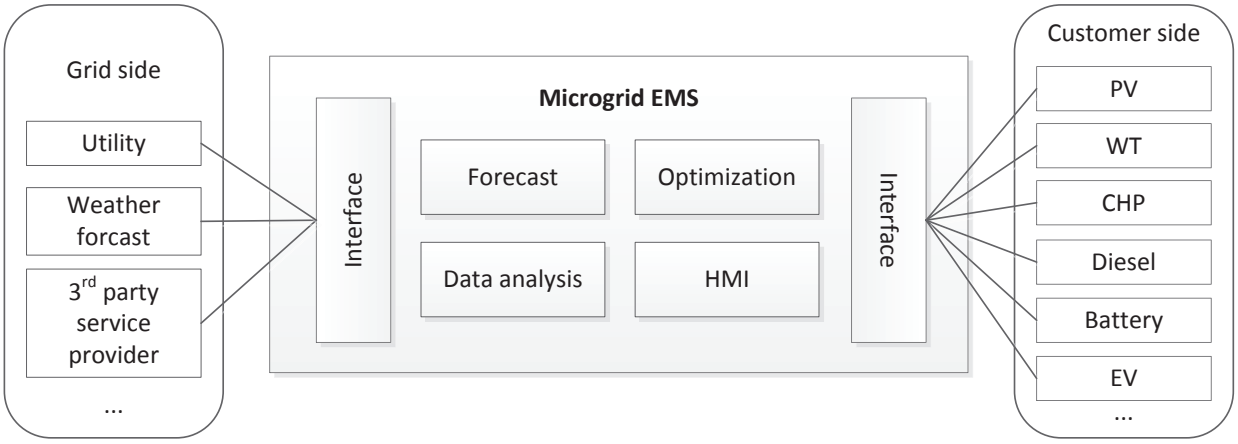

Figure 5.1: An illustration of a microgrid EMS.

5.2.1 Functional Requirements

5.2.1.1 Forecast

The EMS uses the historical data and other inputs (e.g., weather) to forecast the DERs, the loads, and the market. The forecast is preformed on different time scales (e.g., day-ahead, hour-ahead, etc.). The forecast data is used as the input for the optimization. Therefore, the accuracy of the forecast is crucial for the EMS to balance supply and demand in the microgrid. Forecast is challenging in a microgrid setting due to the inherent intermittency and variability of DERs (e.g., PVs and WTs) and the spatial and temporal uncertainty in controllable loads (e.g., EVs). Various forecast methods [61, 81, 82] have been proposed in the literature.

5.2.1.2 Optimization

The EMS must be able to make control decisions to optimize the power flows in the microgrid by adjusting the dispatchable DERs, the controllable loads, and the power imported/exported from/to the grid. Different optimizations are performed for different applications (e.g. energy/power management, DR, coordinated EV charging, V2G, etc.). Those applications are typically formulated as non-linear optimization problems with different ob-

jectives. Extensive algorithms have been proposed for energy/power management, DR, coordinated EV charging, and V2G in microgrids [1, 23, 41, 79, 80].

5.2.1.3 Data Analysis

The EMS collects a huge amount of data from the DERs, the loads, and the market. The data collection is analyzed, providing insights to better understand the characteristics of energy resources. This can be further used to improve the performance of the forecast and the optimization models [83, 84].

5.2.1.4 HMI

The EMS must provide a HMI for real-time monitor and control of the microgrid. The HMI is also the interface for the microgrid operator to interact with other modules in the EMS. Useful information rather than raw data should be provided [85] by means of data visualization, archiving, etc. It should also allow more customer interactions [36].

5.2.2 Unified Communication Interface

A microgrid is a distributed system consisting of heterogeneous types of energy resources [37], in which the EMS is responsible for interacting with the resources in an interoperable manner. The microgrid EMS is also responsible for communicating with external systems outside the microgrid - the EMS translates the information delivered from the external systems to internal semantics and protocols. The communication interfaces in the microgrid EMS must be extensible, indicating that it can be easily extended to support emerging functionalities. New applications such as coordinated EV charging and innovative algorithms such as various forecasts and optimizations have been introduced to cope with the challenges brought by the introduction of DERs and controllable loads. Thus, it is critical that the EMS is able to adopt such new applications and algorithms without affecting the existing functionalities. Therefore, a unified communication interface for managing the devices that is protocol and technology agnostic is required to achieve the aforementioned needs.

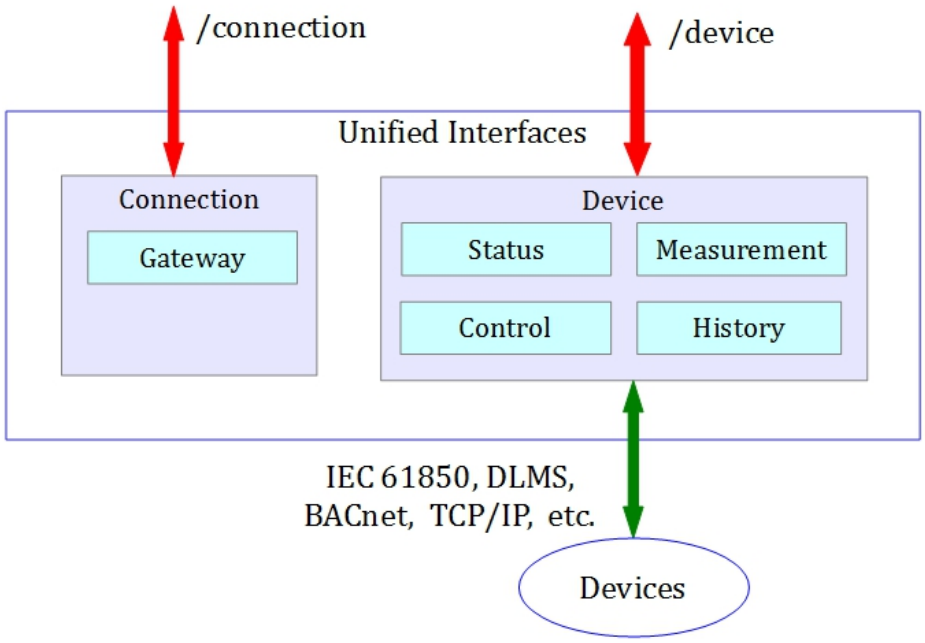

Figure 5.2: A unified communication interface for devices.

To design such a unified communication interface, we abstract the common functionalities for managing devices based on the characteristics of a variety of common devices in a microgrid and provide a compact unified interface that is not dependent on the specific protocol or the communications technology used by the device. Fig. 5.2 shows the design of the communication interface. There are mainly two types of interfaces - connection management and device management. The connection interface manages the connection with a device or a gateway. It is typically used when a long connection is required to be established before any device specific communications. The device interface manages the communications with a device. There are four types of device interfaces that must be implemented - status, measurement, control, and history. The status interface provides the current status information associated with the device such as system status, mode, state-of-charge, inverter status, etc. The measurement interface provides the current values measured by the device such as active/reactive power, frequency, voltage, power factor, etc. The control interface accepted control commands to issue control signals to the device such as turning on/off, setting values, etc. The history interface provides the historical data of the device that may be needed for

analysis. Underneath the interface is the communication with the real devices using the protocol and technology supported by the devices. Some commonly-used industrial protocols and standards include IEC 61850 for DER devices [42], device language message specification (DLMS) [86] for smart meters, digital addressable lighting interface (DALI) [87] for lighting, building automation and control network (BACnet) [88] for HVAC control, oBix [89] for building automation, and other proprietary protocols by different vendors. By using the unified communication interface that is protocol and technology agnostic, the system can manage the devices without knowing the underlying protocols and technologies used by the devices and thus achieve interoperability and extensibility.

5.3 Implementation

In this section, we introduce the implementation of a microgrid EMS architecture with consideration of the design issues discussed in the previous section. We describe the decentralized system architecture, the microgrid testbeds, and the microgrid controls.

5.3.1 Decentralized System Architecture

In this chapter, we propose a microgrid EMS architecture, taking into account the requirements discussed in the previous section. We implement it in a resource-oriented architecture (ROA) style [90] that abstracts energy components in a microgrid in the form of resources. Resources have well-defined interfaces, which enables the system to support plug-and-play of DERs, loads, and functionalities. The ROA provides advantages over a service-oriented architecture (SOA) in previous studies [37–40]: (i) best fit for "linking and referring" to energy resources, thus maximizing the interactivity efficiency in the system and (ii) more lightweight without complicated interface description.

More technically, the system fulfills the interoperability via energy service interfaces (ESIs) [50] to interact with DERs, loads, and external systems. In the ESI, energy data is represented in open building information exchange (oBIX) [89] or IEC 61850 [42]. It is then exchanged using the web service model in the representational state transfer (REST)

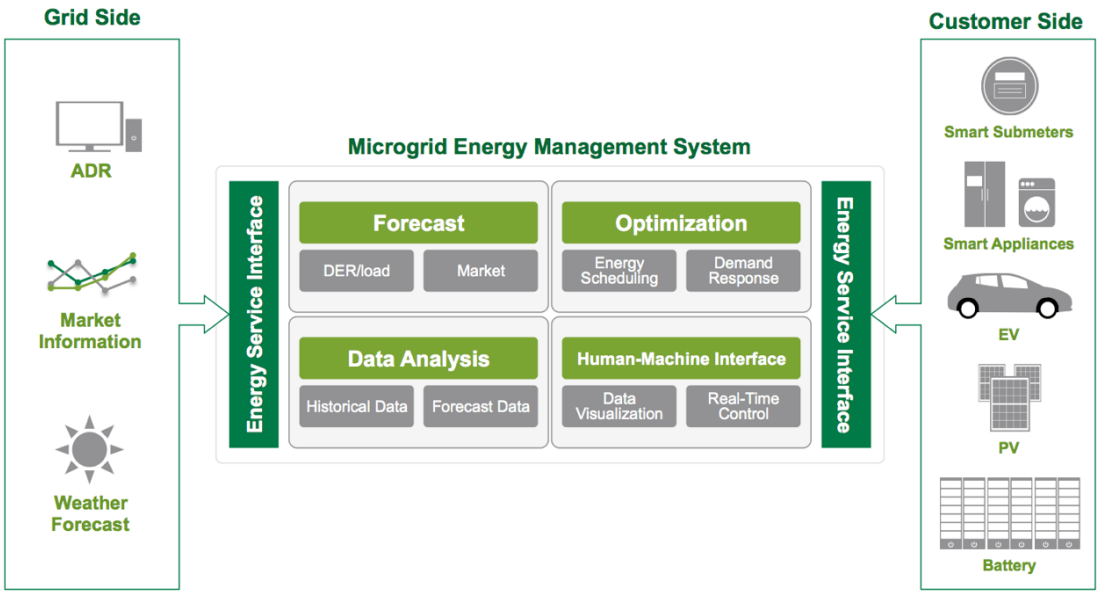

Figure 5.3: An illustration of the overall EMS architecture.

style [90]. The resource centric security (RCSec) [91] is carried out on action levels (i.e., read, write, and invoke). An illustration of the overall system architecture is shown in Fig.5.3.

Fig. 5.4 shows the proposed decentralized system architecture. Each box in the figure represents an independent system component that is implemented as a server-hosted web application. Communication among the components is implemented as REST web services. Due to this web-based communication scheme, the system components are highly decoupled, allowing deployment at different locations. For example, the ESIs can reside on the customers premises to give customers full autonomy to manage their own devices, the coordinator and control director can be deployed in the cloud, and the control center can be in the control room of the microgrid operator.

As can be seen from Fig. 5.4, the proposed system architecture is composed of the following components: ESIs which reside on the customer side, coordinator, control director, and control center, all of which are on the operator side. The system can also interact with external systems such as a demand response automated server (DRAS) from the utility for demand response functionality. In the following, we describe each of the system components

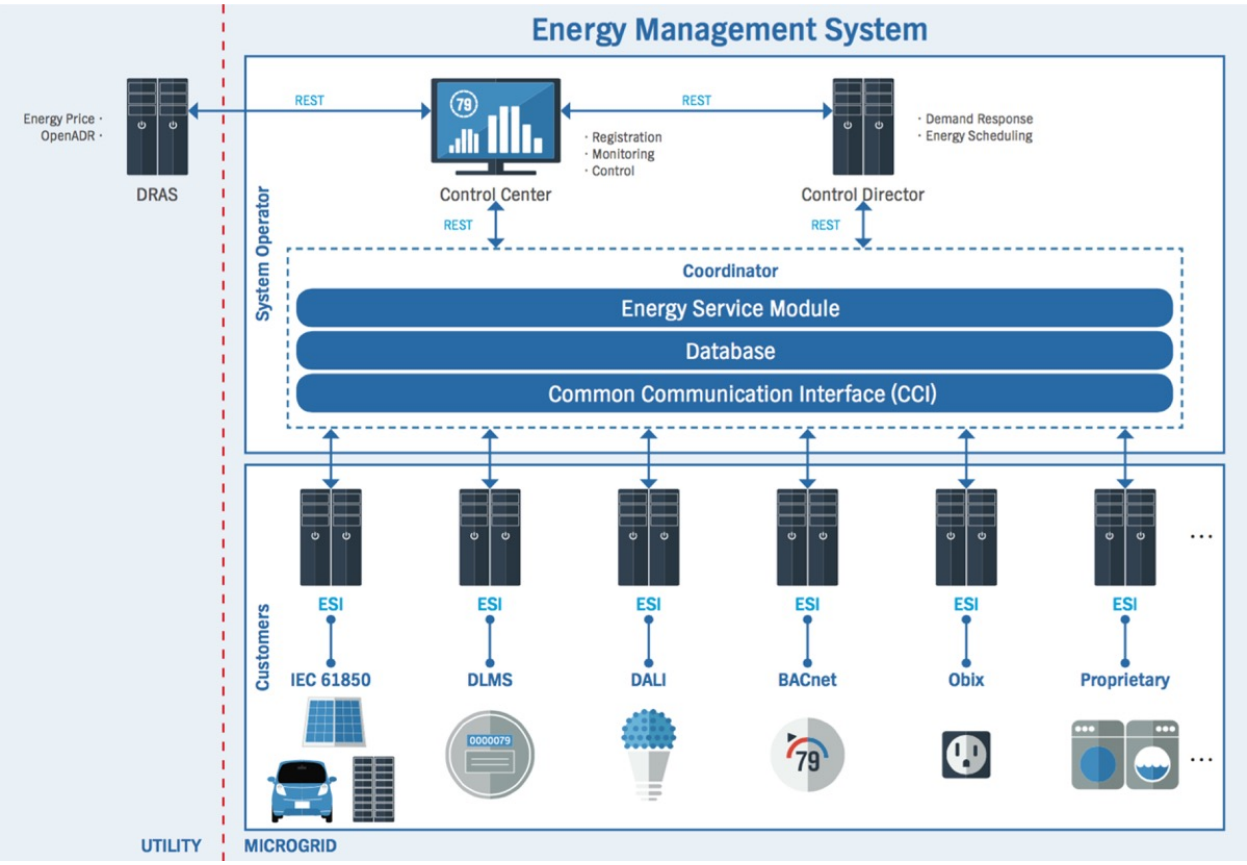

Figure 5.4: An illustration of the decentralized system architecture.

in detail.

The ESI sits between the system and the end devices. It acts as the gateway that translates various protocols used by different devices into standardized interfaces to enable interoperation of the system using our proposed unified communication interface. The ESI implements one or multiple protocol specifications that the end devices use. Each ESI supports at least one protocol and it is able to connect multiple devices using their protocols. Common protocols in microgrids include IEC 61850 [42], DLMS [86], DALI [87], BACnet [88] for HVAC control, oBix [89], and other proprietary protocols by different vendors. The ESI can be organized based on the protocol it supports or its location. For example, each ESI in the system can support one protocol to connect with the devices that use the protocol as shown in Fig. Or an ESI can be placed in a specific location to connect only the devices at that location (e.g., one ESI in each room). In reality, the ESI is owned by the customer,

giving full autonomy to the customer who can use the ESI to manage their own devices. The customer can also choose what data and how the data is exposed through the ESI. In this way, customer privacy can be fully protected.

The coordinator in the system connects with multiple ESIs in order to provide the interfaces for the system operator to manage the various devices in the microgrid. The coordinator maintains a list of devices that are managed by the system in the database and allows registration of new devices and deletion of existing ones. The coordinator exploits Web Service over HTTP binding in REST style in order to provide energy services to the control director and the control center.

The control director optimizes the operations in the microgrid using algorithms to control subsets of the registered devices in the coordinator. Each device can be controlled by only one algorithm and if a device is not associated with any algorithm, it is assumed to be manually controlled. The control algorithm manages the operations of the associated devices by obtaining information from the devices and sending control commands using the defined algorithm via the coordinator. Multiple algorithms can be registered at the control director, which supports plug-and-play of new control algorithms, for different applications (e.g., DR, EV charging, V2G, etc.). Each algorithm in the system defines a set of rules for how to control the associated devices based on inputs (e.g., energy prices, customer preferences, etc.). Once the algorithm starts, it will automatically control the associated devices in order to achieve the desired objectives.

The control center in the system is a web interface for real-time monitoring and control of the microgrid, as well as for the user to interact with the system; Fig. displays a sample web interface showing overall system information. Real-time monitoring and control are realized via the real-time data and control services provided by the coordinator that reads real-time measurements and sends control commands to the DERs and loads. The web interface provides different forms of data visualization (i.e., tables and interactive graphs) that show data from the real-time/forecast/historical data of the DERs, the loads, and the market; for instance, Fig. 5.5 displays the user interface showing market pricing information. The control center also provides an interface for the control director to register/unregister

Figure 5.5: A screenshot of the control center showing the market pricing information.

devices and algorithms, manage the device-algorithm mapping, and manage the algorithms.

5.3.2 Microgrid Testbeds

We have two microgrid testbeds-UCLA SMERC and KIER. There are a number of DERs and loads in each testbed and several grid services are also implemented for experiments.

5.3.2.1 UCLA SMERC Testbed

The DERs and loads in the testbed at UCLA SMERC include smart submeters, smart appliances, EVs, PVs, and batteries as shown in Fig. 5.6.

Smart submeters provide fine-grained measurement and control of energy usage. We use two types of smart submeters: smart plugs and smart power strips in the testbed to monitor and control (i.e., on/off) the plug loads in the lab including computers, laptops, desk lamps, and network switches. The submeters communicate with the system using ZigBee.

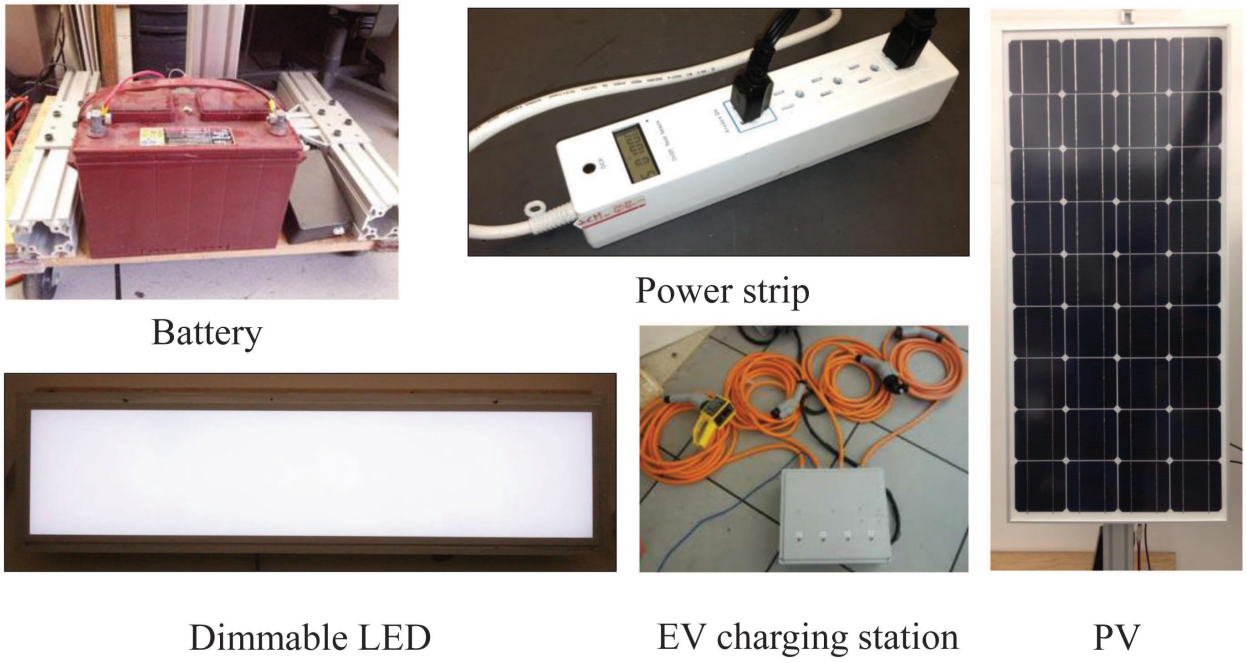

Figure 5.6: Some of the devices in the UCLA SMERC testbed.

We also deploy smart appliances which provide interfaces to control the operations including LED lights, a cloth dryer and a refrigerator. We have dimmable LED lights which can change brightness and color. The LEDs use ZigBee to communicate with the system. For the scalability test, we additionally simulate 200 LEDs which operate exactly the same as the real device (brightness, temperature, and power consumption). The system connects with the dryer and the refrigerator using Ethernet. The dryer provides interfaces to change the operation mode (high heat, low heat, or no heat) and turn on/off. The refrigerator can adjust the operating cycles of the compressor, the defrost, and the fan. Both the dryer and the refrigerator have submeters to measure the power consumption.

The UCLA SMERC is developing a smart EV charging infrastructure[2] on campus which supports charging rate control and serving multiple EVs by power multiplexing using J1772 connectors. The charging stations are connected with a control center which monitors and controls the EV charging using 3G technologies. The system communicates with the EVs via the control center. Due to the low penetration of EVs, we simulate two EV charging

[2]http://smartgrid.ucla.edu/projects_evgrid.html

Figure 5.7: Some of the devices in the KIER testbed.

stations (level 1 and level 2) based on the real data in the system for experiments.

The system is also connected to a PV panel and a BESS in our lab. We are currently installing a 50kW PV system on the roof and a 25kWh BESS in the lab. This version of the testbed implements the PV and the BESS using the simulated data that follows the specifications of the real devices. The simulated PV and BESS communicate with the system using the IEC 61850 standard [42]. The details of the simulators can be found in [64].

The system provides two data interfaces for the DERs and the loads in the microgrid. They are (i) historical energy data (e.g., active/reactive power, voltage, current, frequency, etc.) for a given period of time; and (ii) forecast data which are the outputs of the corresponding forecast methods. The historical data and the forecast data can be further analyzed using data visualization in the web interface.

5.3.2.2 KIER Testbed

The DERs and loads in the testbed at KIER include PVs, WTs, a diesel generator, EVs, energy storage systems (ESSes), smart meters, LEDs, smart submeters, and a HVAC unit as shown in Fig. 5.7

The KIER testbed uses real-time power hardware-in-the-loop simulation systems for PVs, WTs, ESSes, and diesel, and real-hardware slow/quick EV charging systems. The hardware-in-the-loop simulators in the testbed provide real-time power system simulation, which can be used to verify the operation of the microgrid. The testbed adopts IEC 61850 [42] as the communication and control interface. The PVs, WTs, diesel generator, EVs, and ESSes are connected to two IEC 61850 gateways. The system communicates with the IEC 61850 gateways using the manufacturing message specification (MMS).

The smart meters at the the KIER testbed are Itron ACE SL7000. The system communicates with the smart meters using DLMS [86]. The smart submeters and some of the LEDs are the same as the ones used in the UCLA SMERC testbed. There are 8 LEDs that use the DALI protocol [87]. The DALI LED system used at KIER is the Helvar system which consists of multiple DALI LEDs and a DALI router that provides Ethernet connection to the system. The HVAC unit used in the testbed is a LG HVAC system that includes a LG BACnet gateway to provide the BACnet interface [88] to communicate with the system.

5.3.2.3 Grid Services

Several services on the grid side are implemented and utilized in our testbed including ADR, market information (i.e., day-ahead pricing, hour-ahead pricing, and real-time pricing).

We implement and deploy an DRAS that provides the ADR service to the system using the OpenADR standard [92]. The market information is provided by a server which fetches the data from the California Independent System Operator (CAISO) [77]. The server obtains three types of retail market prices from CAISO: day-ahead pricing which gives the day-ahead price of every hour, hour-ahead pricing which gives the hour-ahead price of every 15 minutes, and real-time pricing which gives the 10-minute-ahead price of every 5 minutes.

5.3.3 Microgrid Controls

The system implements two algorithms for the optimal operation of the microgrid: an energy scheduling algorithm and a DR algorithm. The system provides forecast services of the DERs and loads for optimization. Specifically, it uses a persistence model for load forecasting, an auto regressive moving average (ARMA) model for PV forecasting [93], and a machine learning model for EV forecasting [81]. The market forecast services are implemented using the forecast data from the CAISO.

Now we present the system model of the microgrid and formulate the energy scheduling and DR as optimization problems.

Consider a microgrid consisting of a set of DG units denoted by $\mathcal{G} := \{g_1, g_2, \ldots, g_G\}$, DS units denoted by $\mathcal{B} := \{b_1, b_2, \ldots, b_B\}$ and loads denoted by $\mathcal{L} := \{l_1, l_2, \ldots, l_L\}$. We use a discrete time model with a finite horizon in this chapter. We consider a time period or namely a scheduling horizon which is divided into T equal intervals Δt, denoted by $\mathcal{T} := \{0, 1, \ldots, T-1\}$, where t_0 is the start time.

DG Model: For each DG unit $g \in \mathcal{G}$, we assume that there is an upper bound and a lower bound on its power:

$$p_g^{\min}(t) \leq p_g(t) \leq p_g^{\max}(t), \forall t \in \mathcal{T}, \tag{5.1}$$

where $p_g^{\min}(t)$ and $p_g^{\max}(t)$ are the minimum and maximum output power, respectively. If the DG unit is dispatchable (e.g., diesel), the output power $p_g(t)$ is a variable. If the DG unit is non-dispatchable (e.g., PVs and WTs), the output power $p_g(t)$ cannot vary and its value is equal to the forecasted value (i.e., $p_g^{\min}(t) = p_g^{\max}(t) = p_g^f(t)$ where $p_g^f(t)$ is the forecasted power at time t).

We denote the generation cost of a DG unit $g \in \mathcal{G}$ by $C_g(p_g(t))$. We assume that the cost function is strictly convex. For renewable DG units such as PVs and WTs, the generation cost is zero.

DS Model: We consider batteries as the DS units in the microgrid. Given a battery $b \in \mathcal{B}$, we assume its output power $p_b(t)$ is positive when charging and negative when discharging.

Let $E_b(t)$ denote the energy stored in the battery at time t. The battery can be modeled by the following constraints:

$$p_b^{\min} \leq p_b(t) \leq p_b^{\max}, \forall t \in \mathcal{T}, \tag{5.2}$$

$$E_b(t+1) = E_b(t) + p_b(t)\Delta t, \forall t \in \mathcal{T}, \tag{5.3}$$

$$E_b^{\min} \leq E_b(t) \leq E_b^{\max}, \forall t \in \mathcal{T}, \tag{5.4}$$

$$E_b(T) \geq E_b^e, \tag{5.5}$$

where $p_b^{\max}$ is the maximum charging rate, $-p_b^{\min}$ is the maximum discharging rate, $E_b^{\min}$ and $E_b^{\max}$ are the minimum and maximum allowed energy stored in the battery, respectively, and E_b^e is the minimum energy that the battery should maintain at the end of the scheduling horizon.

We model the cost of operating a given battery b as:

$$C_b(\mathbf{p}_b) \triangleq \alpha_b \sum_{t\in\mathcal{T}} p_b(t)^2 - \beta_b \sum_{t=0}^{T-2} p_b(t+1)p_b(t) + \gamma_b \sum_{t\in\mathcal{T}} \left(\min(E_b(t) - \delta_b E_b^{\max}, 0)\right)^2, \tag{5.6}$$

where $\mathbf{p}_b$ is the charging/discharging vector $\mathbf{p}_b \triangleq (p_b(t), t \in \mathcal{T})$, α_b, β_b, γ_b, and δ_b are positive constants.

The above function is convex when $\alpha_b > \beta_b$. This cost function captures the damages to the battery by the charging and discharging operations. The three terms in the function penalize the fast charging, the charging/discharging cycles, and the deep discharging, respectively. We choose $\delta_b = 0.2$.

Load Model: For each load, the demand is constrained by a minimum and a maximum power denoted by $p_l^{\min}(t)$ and $p_l^{\max}(t)$, respectively:

$$p_l^{\min}(t) \leq p_l(t) \leq p_l^{\max}(t), \forall t \in \mathcal{T}. \tag{5.7}$$

For deferrable loads such as EVs, the cumulative energy consumption of the loads must exceed a certain threshold in order to finish their tasks before deadlines. Let $E_l^{\min}$ and $E_l^{\max}$ denote the minimum and maximum total energy that the load is required to consume, respectively. The constraint on the total energy consumed by a deferrable load is given by:

$$E_l^{\min} \leq \sum_{t\in\mathcal{T}} p_l(t)\Delta t \leq E_l^{\max}. \tag{5.8}$$

We use a cost function to capture customer loss of comfort in the scheduling. The cost function $C_l(\mathbf{p}_l)$ quantifies a customer's loss or discomfort obtained by the load $l \in \mathcal{L}$ using the demand vector $\mathbf{p}_l \triangleq (p_l(t), t \in \mathcal{T})$. We assume the cost function is a convex function.

Supply-demand Matching: The net demand of the microgrid is equal to the total demand minus the total generation:

$$P(t) = \sum_{l \in \mathcal{L}} p_l(t) + \sum_{b \in \mathcal{B}} p_b(t) - \sum_{g \in \mathcal{G}} p_g(t), \forall t \in \mathcal{T}. \tag{5.9}$$

If the microgrid is operated in islanded mode, then $P(t) = 0$. If the microgrid is operated in grid-connected mode, then $P(t)$ is the power traded between the microgrid and the main grid. We model the cost of energy purchase from the main grid as $C_0(t, P(t)) \triangleq \rho(t)P(t)\Delta t$, where $\rho(t)$ is the market energy price. Note that $P(t)$ can be negative meaning that the microgrid can sell its surplus power to the main grid.

5.3.3.1 Energy Scheduling

The objective of the energy scheduling is to schedule the day-ahead operation of the DERs and the loads such that (i) the total costs of generation, energy storage, load, and energy purchase are minimized, and (ii) the DER constraints, the load constraints, and the supply-demand matching constraint are satisfied. The scheduling horizon $\mathcal{T}$ in this problem is one day.

We define $\mathbf{p}_g \triangleq (p_g(t), t \in \mathcal{T})$, $\mathbf{p}_b \triangleq (p_b(t), t \in \mathcal{T})$, $\mathbf{p}_l \triangleq (p_l(t), t \in \mathcal{T})$, and $C_g(\mathbf{p}_g) \triangleq \sum_{t \in \mathcal{T}} C_g(p_g(t))$. The energy scheduling in the microgrid can be formulated as a convex optimization problem [94]:

$$\begin{aligned} \min_{\mathbf{p}_g, \mathbf{p}_b, \mathbf{p}_l} \quad & \xi_g \sum_{g \in \mathcal{G}} C_g(\mathbf{p}_g) + \xi_b \sum_{b \in \mathcal{B}} C_b(\mathbf{p}_b) + \xi_l \sum_{l \in \mathcal{L}} C_l(\mathbf{p}_l) + \xi_0 \sum_{t \in \mathcal{T}} C_0(t, P(t)) \\ \text{s.t.} \quad & (5.1) - (5.9), \end{aligned}$$

where ξ_l, ξ_g, ξ_b, and ξ_0 are the parameters to trade off among the utility maximization and the cost minimizations.

Solving the above optimization problem gives the optimal schedules including the generation schedules $\mathbf{p}_g$, the battery schedules $\mathbf{p}_b$, and the load schedules $\mathbf{p}_l$.

5.3.3.2 DR

The system can receive DR events issued by the utility and it must be able to coordinate the operation of the devices in the microgrid in order to respond properly.

A DR event can be characterized by a time schedule $\mathcal{T}$ which specifies the start time and the end time and a demand limit $P_{\max}(t)$ which can be determined from the event information. The DR constraint on the net demand of the microgrid is given by:

$$P(t) \leq P_{\max}(t), \forall t \in \mathcal{T}. \tag{5.10}$$

Similar to the day-ahead scheduling problem, the DR problem can be formulated as a convex optimization problem:

$$\begin{aligned} \min_{\mathbf{p}_g, \mathbf{p}_b, \mathbf{p}_l} \quad & \xi_g \sum_{g \in \mathcal{G}} C_g(\mathbf{p}_g) + \xi_b \sum_{b \in \mathcal{B}} C_b(\mathbf{p}_b) + \xi_l \sum_{l \in \mathcal{L}} U_l(\mathbf{p}_l) \\ \text{s.t.} \quad & (5.1) - (5.10). \end{aligned}$$

In the above problems, the control variables are assumed to be all continuous. However, some of them may be discrete in reality (e.g., on/off). A two-stage approach [15] can be used to solve this issue. In the first stage, a solution is obtained assuming that all the control variables are continuous. Then, the discrete variables are rounded to the nearest discrete levels and treated as constants in the second-stage solution.

5.4 Experiments

To test the effectiveness of the system, we conduct various experiments to evaluate the microgrid management and control in the testbeds. We present the results of the optimal energy scheduling and DR in this section. Refer to [50] for our previous results.

5.4.1 Energy Scheduling

We run the energy scheduling algorithms in both testbeds to schedule the day-ahead operation of the devices.

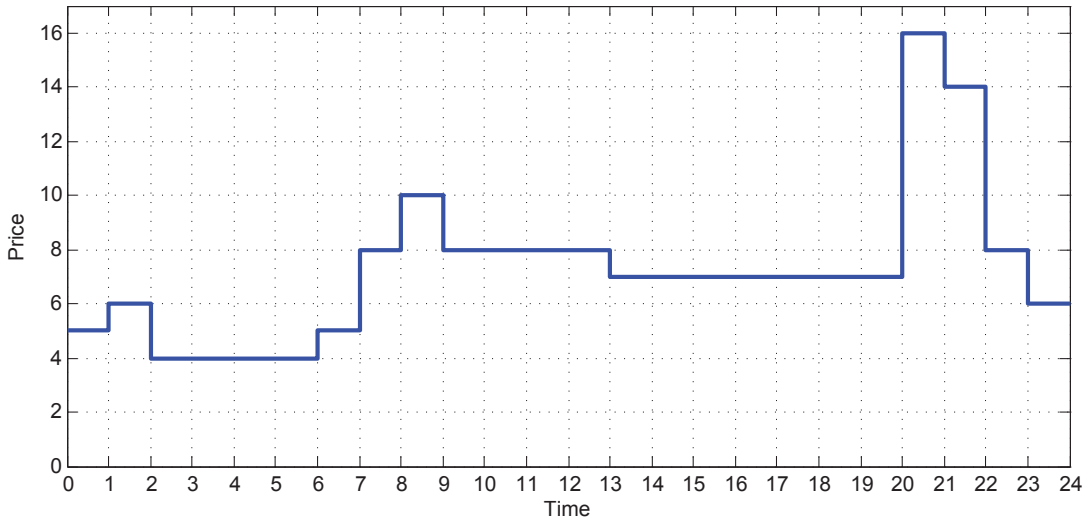

Figure 5.8: Day-ahead energy price for the UCLA SMERC testbed.

5.4.1.1 UCLA SMERC Testbed

We consider the day-ahead scheduling of the PV panel, the battery, the plugloads (including the refrigerator), the dimmable LEDs, and the EVs in the UCLA SMERC testbed. The PV is a 5kW simulator using the model in [64] and data from the solar resources and meteorological assessment project (SOLARMAP)[3]. The maximum energy allowed to be stored in the battery $E_b^{\max}$ is 20kWh and we set $E_b^{\min} = 5$kWh. The maximum battery charging/discharging rate is 3kW. We set $E_b(t_0) = E_b^e = 5$kWh. The parameters in the battery cost function are chosen to be $\alpha_b = 1$, $\beta_b = 0.75$, and $\gamma_b = 0.5$. We choose $U_l(p_l(t)) \triangleq \sum_{t\in\mathcal{T}} -\eta_l(p_l(t) - p_l^f(t))^2$ for the plugloads and the LEDs and $U_l(p_l(t)) \triangleq \eta_l(\sum_{t\in\mathcal{T}} p_l(t)\Delta t)$ for the EVs, where $p_l^f(t)$ is the forecasted load and η_l is the priority of the load given by the customer. The higher the priority is, the more important the load is to the customer. The maximum charging rate is 1.4kW for level 1 EV charging and 2.9kW for level 2 EV charging. In our experiment, we assume that the plugloads cannot be shed, the LEDs can be shed, and the EVs can be shifted. Perfect forecasting of the DERs and loads is assumed. We use the day-ahead market price from the CAISO in the experiment. The parameters are chosen as $\xi_l = 1$, $\xi_g = 1$, $\xi_b = 0.01$, and $\xi_0 = 1$.

[3]http://www.nrel.gov/midc

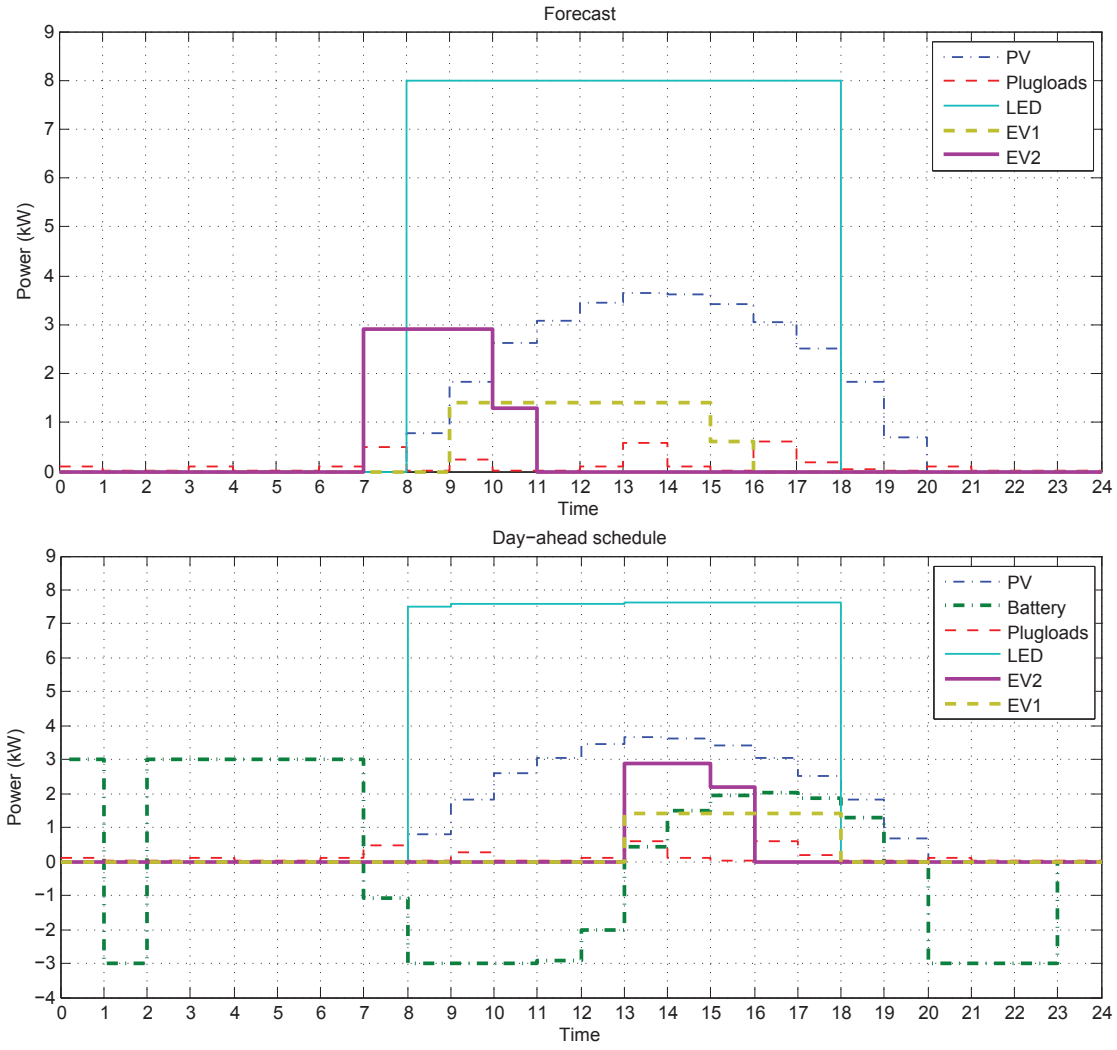

Figure 5.9: Forecast and day-ahead schedule for the UCLA SMERC testbed.

We conduct the energy scheduling experiment for March 27th, 2014. Fig. 5.8 shows the day-ahead price. Fig. 5.9 shows the comparison of the forecasts and the day-ahead schedules. From the figures, we can see the battery charging/discharging cycles: the battery is charged when the energy price is low and discharged when the price is high. We can also observe load shedding and load shifting from the results: the LEDs are shed and the EVs are shifted to the time periods when the price is low. The total operational costs of the testbed using the schedules are ¢ 367.62 compared with ¢ 564.07 without scheduling, saving the costs by $\frac{564.07-367.62}{564.07} = 34.83\%$.

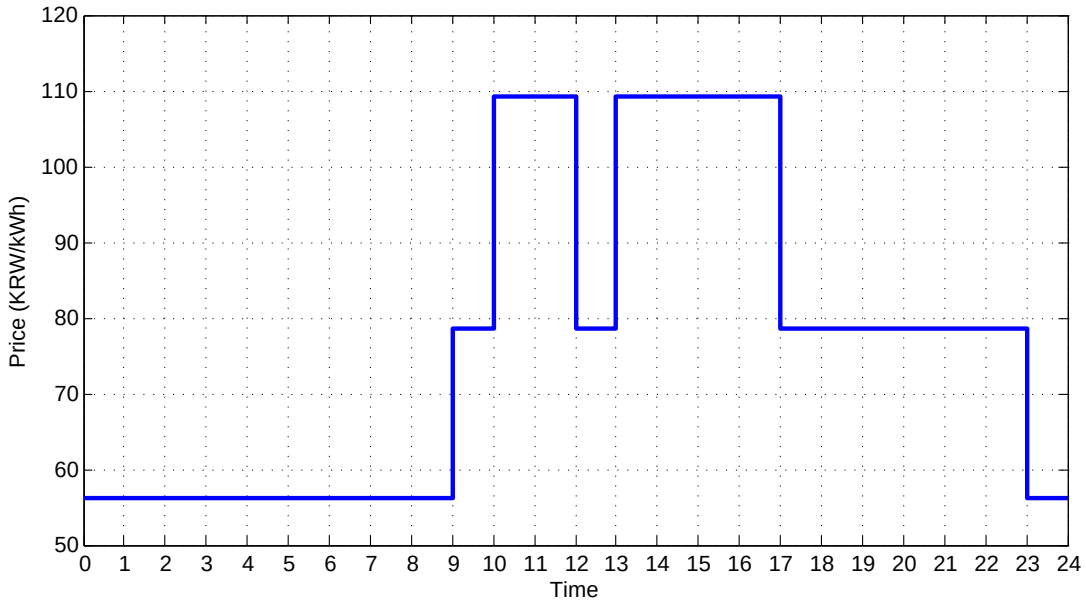

Figure 5.10: Time-of-use price for the KIER testbed.

5.4.1.2 KIER Testbed

The devices in the KIER testbed considered in the energy scheduling include a 16kW PV, a 5kW ESS, a 16kW quick charging EV system, two 2.5kW slow charging EV systems, and two hundred 63W dimmable LEDs. The maximum energy allowed to be stored in the battery $E_b^{\max}$ is 50kWh and we set $E_b^{\min} = 5$kWh. We set $E_b(0) = E_b^e = 12.5$kWh. The parameters in the battery cost function are chosen to be $\alpha_b = 1$, $\beta_b = 0.75$, and $\gamma_b = 0.5$. We choose $C_l(p_l(t)) := \sum_{t\in\mathcal{T}} \eta_l (p_l(t) - p_l^f(t))^2$ for the LEDs and $C_l(p_l(t)) := \eta_l(\sum_{t\in\mathcal{T}} p_l(t)\Delta t - \sum_{t\in\mathcal{T}} p_l^f(t)\Delta t)$ for the EVs, where $p_l^f(t)$ is the forecasted load and η_l is the priority of the load given by the customer. The higher the priority is, the more important the load is to the customer. In our experiment, we assume that the LEDs can be shed and the EVs can be shifted. The maximum shedding percentage of the LEDs $\frac{E_l^{\max} - E_l^{\min}}{E_l^{\max}}$ is assumed to be 30%. The energy upper bound of the EVs $E_l^{\max}$ is chosen randomly from $[18\text{kWh}, 23\text{kWh}]$ and the energy lower bound of the EVs $E_l^{\min}$ is chosen randomly from $[13\text{kWh}, 18\text{kWh}]$. Perfect forecasting of the DERs and loads is assumed. We use the Korean time-of-use (TOU) price in the experiment as shown in Fig. 5.10. The parameters in the algorithm are chosen as $\xi_l = 1$, $\xi_g = 1$, $\xi_b = 0.01$, and $\xi_0 = 1$.

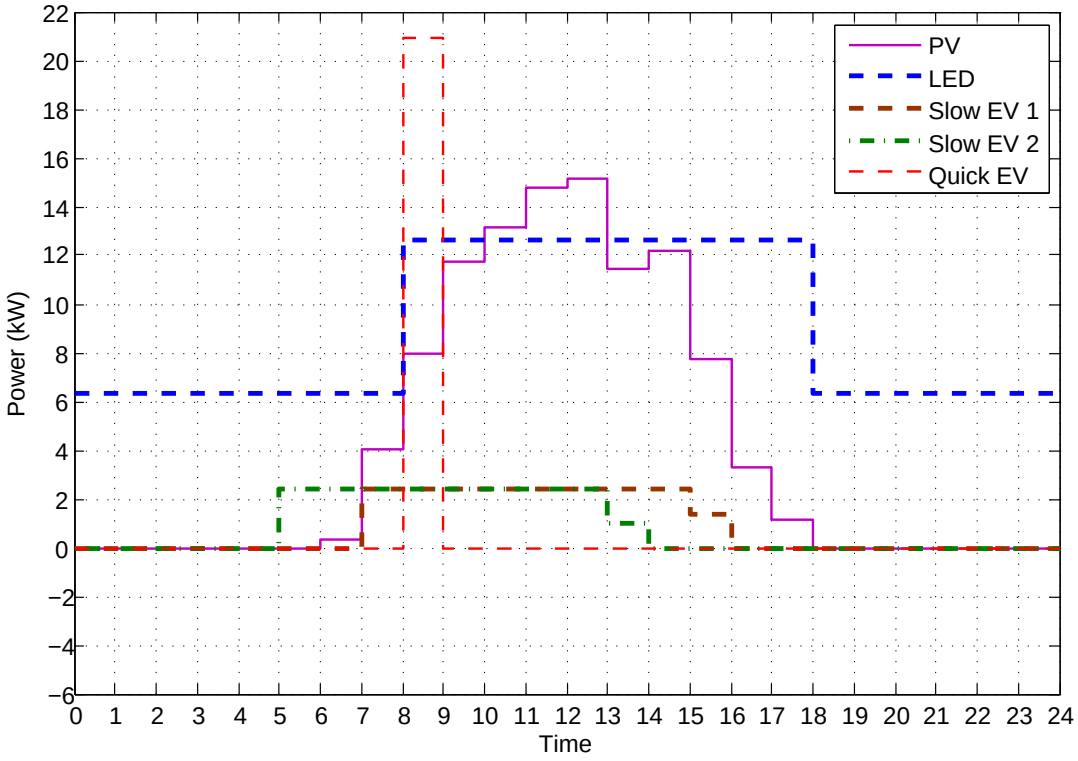

Figure 5.11: Forecast for the KIER testbed.

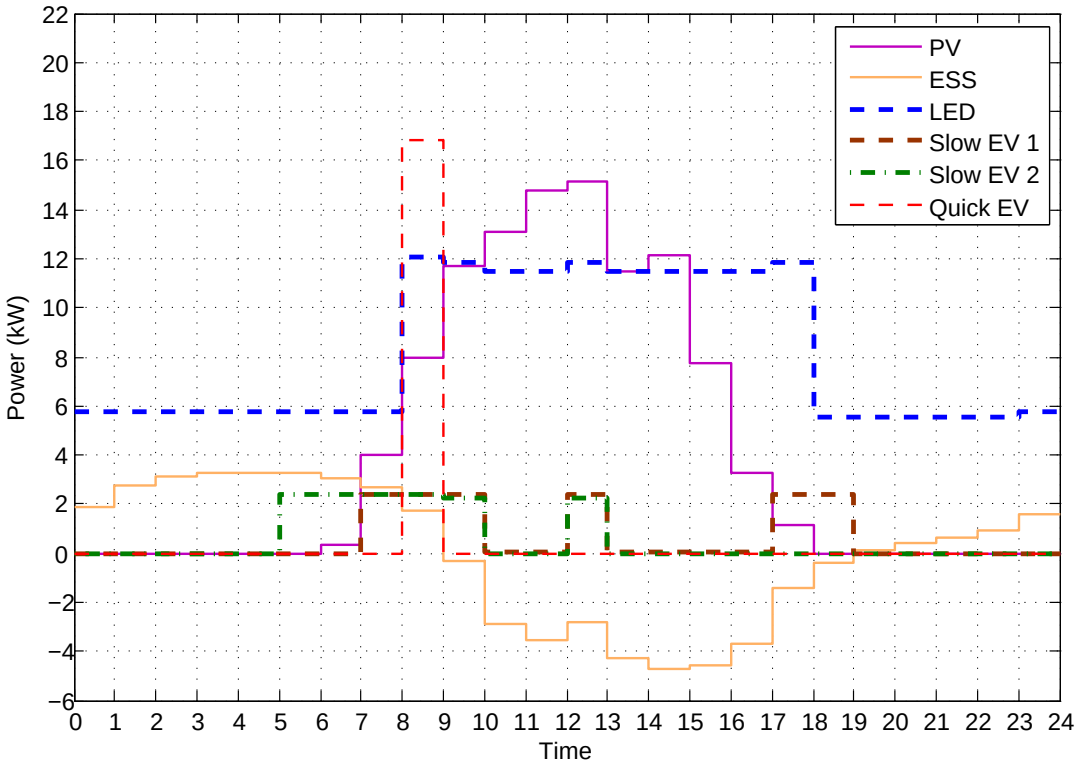

Figure 5.12: Simulated day-ahead schedule for the KIER testbed.

Fig. 5.11 shows the forecast of the devices, serving as the baseline consumption. We then run the algorithm in Matlab to produce the optimized day-ahead schedules as shown in Fig. 5.12. Comparing Fig. 5.12 with Fig. 5.11, we can observe the battery charging/discharging cycles: the battery is charged when the energy price is low and discharged when the price is high. We can also observe load shedding and load shifting from the results: the LEDs are shed, the EVs are shifted to the time when the price is low, and the total charging energy of the EVs is also reduced. The total operational cost of the testbed using the optimized schedule is $12,424$ KRW, compared with $7,899$ KRW without scheduling, saving the cost by $\frac{12,424-7,899}{12,424} = 36.43\%$.

Next, we use the schedule produced by the algorithm to control the hardware-in-the-loop simulators in the testbed in order to validate the simulation in real-hardware settings. The experimental result is presented in Fig. 5.13. Compared with the simulation result in Fig. 5.12, the result of using the real-time hardware simulators roughly follows the optimized schedule obtained from the simulation. The main cause of the differences between them lies in the resolution of the inputs for the hardware simulators. The hardware simulators are not able to accept inputs of any precision. The effect of communication delay can be also observed in the LEDs control: the total power of the LEDs changes linearly in time. This is because we have 200 LEDs and it takes time to control all of them and wait for them to respond to the control signals. Both the input resolution and the communication delay need to be considered for optimal energy scheduling in a real microgrid system.

5.4.2 DR

We consider a DR where the system changes the demand in the microgrid in response to the real-time energy prices. We conduct DR experiments in both testbeds. In the UCLA SMERC testbed, we use only LEDs in DR. In the KIER testbed, we use four different types of devices to respond to the real-time prices.

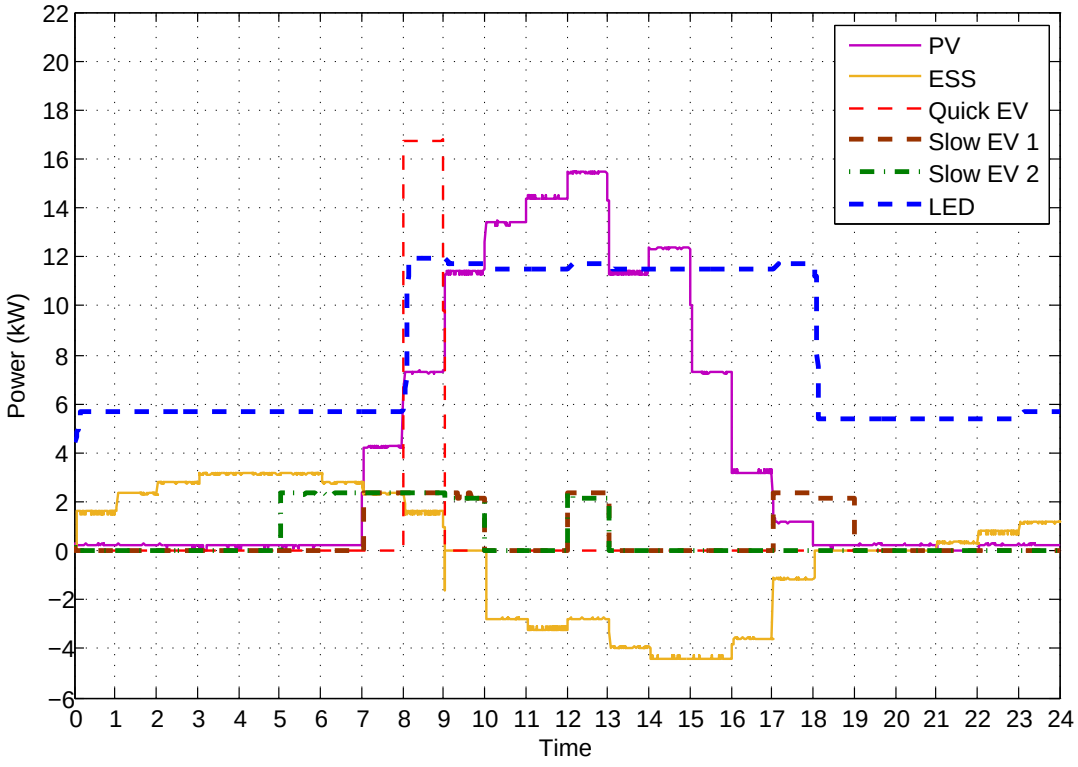

Figure 5.13: Real-time hardware-in-the-loop result in the KIER testbed.

5.4.2.1 UCLA SMERC Testbed

In order to focus on the DR effect, we pick only the dimmable LEDs to participate in the DR in the UCLA SMERC testbed. The DR optimization can then be simplified as a problem to be solved at each time t:

$$\begin{aligned} \min_{p_l(t)} \quad & \sum_{l\in\mathcal{L}} \eta_l (p_l(t) - p_l^f(t))^2 \\ \text{s.t.} \quad & p_l^{\min}(t) \le p_l(t) \le p_l^{\max}(t), \forall l \in \mathcal{L} \\ & \sum_{l\in\mathcal{L}} p_l(t) \le P_{\max}(t), \end{aligned}$$

where $\mathcal{L}$ includes only the LEDs and $p_l^f(t)$ corresponds to the brightness preferred by the customer. In our DR experiment, $P_{\max}(t)$ is defined as a linear piecewise function which translates the real-time price $\rho(t)$ from the CAISO to the maximum allowed total power:

$$P_{\max}(t) = \begin{cases} \sum_{l\in\mathcal{L}} p_l^f(t), & \rho(t) < 6 \text{ ¢/kWh} \\ 0.8 \sum_{l\in\mathcal{L}} p_l^f(t), & 6 \text{ ¢/kWh} \le \rho(t) \le 10 \text{ ¢/kWh} \\ 0.7 \sum_{l\in\mathcal{L}} p_l^f(t), & 10 \text{ ¢/kWh} < \rho(t) \le 14 \text{ ¢/kWh} \\ 0.6 \sum_{l\in\mathcal{L}} p_l^f(t), & \text{otherwise} \end{cases} \tag{5.11}$$

The LEDs are assumed to be equally deployed in four offices with different priorities ($\eta_l = 5, 10, 15, 20$). The brightness of the LED can be dimmed within the range $[0, 100]$. The minimum, maximum, and preferred brightness are set to 20, 100, and 80, respectively. The DR algorithm is implemented as a web service using JOptimizer [4]. It is able to accept DR signals from the DRAS and sends out control signals to the LEDs via the system.

We conduct the DR experiment on March 27th, 2014. The real-time price, the total power consumption, and the power consumption by each priority group are shown in Fig. 5.14. From the figure, we can see that the system is able to reduce the total power consumption in response to the price changes. The demand reduction is based on priorities where the devices with lower priorities reduce more than those with higher priorities.

[4] http://www.joptimizer.com/

Figure 5.14: Result of the DR experiment in the UCLA SMERC testbed.

5.4.2.2 KIER Testbed

We use four different types of devices in the DR experiment in the KIER testbed. The devices selected to participate in the DR include eight DALI LEDs, one BACnet HVAC unit, one smart plug (SP) that is connected with a lamp, and one smart submeter (SM) that is connected with a set of LEDs. Among these devices, only the DALI LEDs can be controlled continuously (brightness 0-100) and all the others are on/off devices.

We define the DR control strategy based on the energy price. Four price ranges are used for DR controls:

- Range 1: $\rho(t) < 6$ ¢/kWh (low price)
- Range 2: 5.5 ¢/kWh $\leq \rho(t) \leq 8$ ¢/kWh (medium price)
- Range 3: 8 ¢/kWh $< \rho(t) \leq 10.5$ ¢/kWh (high price)
- Range 4: 10.5 ¢/kWh $< \rho(t)$(ultra-high price)

The corresponding control strategy is defined as follows:

- Range 1: The DALI LEDs are set to be the maximum brightness and the HVAC unit, SP, and SM are turned on.
- Range 2: The total energy consumption of the DALI LEDs is cut by 20% based on the priorities using the algorithm defined in Section 5.4.2.1, SP is turned off, HVAC and SM are turned on.
- Range 3: The total energy consumption of the DALI LEDs is cut by 50% based on the priorities using the algorithm defined in Section 5.4.2.1, SP and SM are turned off, HVAC is turned on.
- Range 4: The total energy consumption of the DALI LEDs is cut by 80% based on the priorities using the algorithm defined in Section 5.4.2.1, SP, HVAC, and SM are turned off.

We conduct the DR experiment in the KIER testbed using the following sequence of prices generated by a OpenADR 2.0 DRAS: 4.0 ¢/kWh–6.5 ¢/kWh–9.0 ¢/kWh–11.5 ¢/kWh–9.0 ¢/kWh–6.5 ¢/kWh–4.0 ¢/kWh. Once the new price is received by a DRAS client in the system, the system will send out the corresponding control signals to the devices using the above DR strategy. At the same time, the system also reads the power consumption of all the devices every one second and plots the real-time consumption data in the control center. We present the results when the price changes from 6.5 ¢/kWh to 9.0 ¢/kWh in Fig. 5.15 and when the price changes from 9.0 ¢/kWh to 6.5 ¢/kWh in Fig. 5.16. As can be seen from the figures, the devices behave as defined in the DR strategy. From the figures, we can also see the delays of the DR controls. It may take a few seconds for the actual control of the device to take effect after the price change. Such delay is due to multiple reasons including the computational time of the DR algorithm, the communication time between the system and the device, the response time of the hardware once it receives a control command, and the response time that the power change can be correctly measured. In our experiment, we found that the delay of the HVAC unit is mostly due to the hardware response time. The

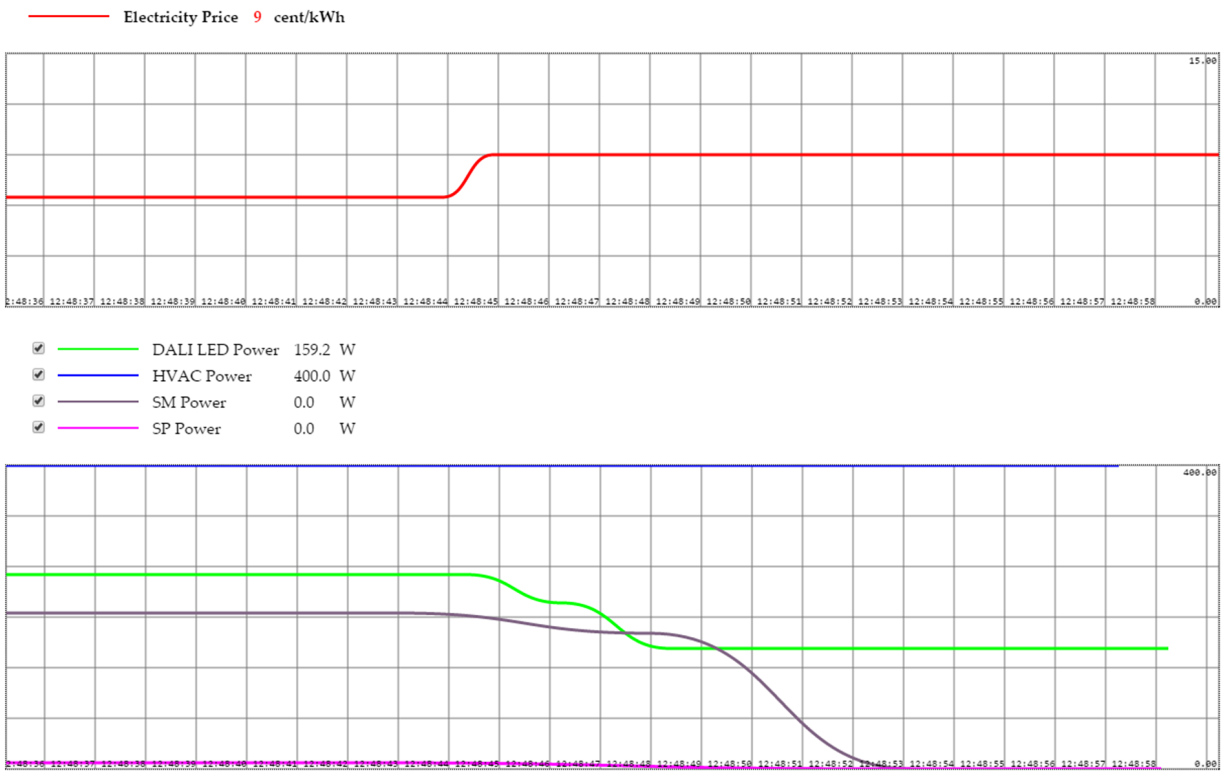

Figure 5.15: Result of the DR experiment in the KIER testbed when the price changes from range 2 to range 3.

delay of the DALI LEDs is mostly due to the communications as there are eight LEDs to control. The delays of the SM and SP are due to the hardware response time and the response time that the power can be correctly measured. It happened sometimes that although the hardware status changed, the power consumption cannot be correctly read, which is believed to be a stability issue of the commercial gateway that connects the SM and SP.

5.5 Summary

In this chapter, we design and implement a system architecture for microgrid energy management, taking into account both the functional requirements and the engineering challenges. We design a unified communication interface that is protocol and technology agnostic for the system to interoperate with heterogeneous devices in a microgrid and propose a novel

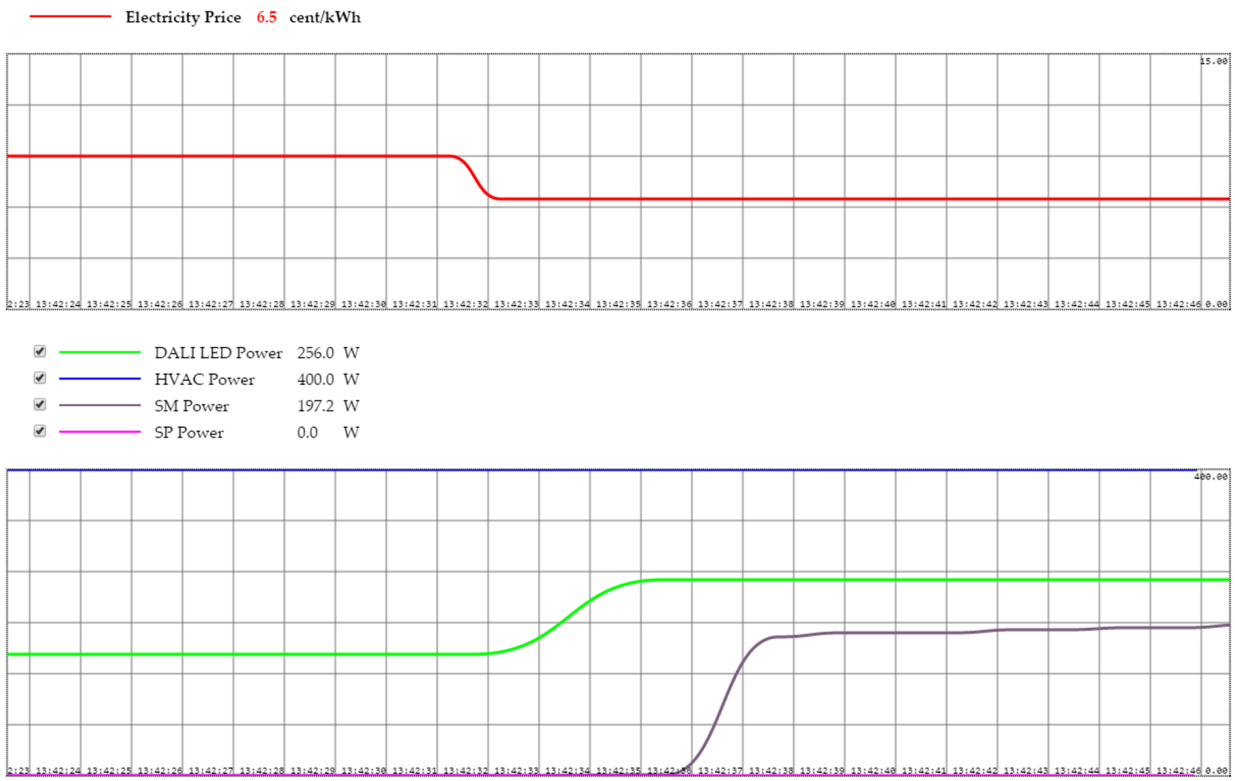

Figure 5.16: Result of the DR experiment in the KIER testbed when the price changes from range 3 to range 2.

decentralized system architecture to enable autonomy on the customer side. We develop and deploy the prototype system in two microgrid testbeds in UCLA SMERC and KIER, and conduct experiments to evaluate the microgrid management and control in real-world settings. Our experimental results demonstrate that the system is able to manage various DERs and loads in the testbeds, interact with external systems, and perform optimal energy scheduling and DR.

CHAPTER 6

Conclusions

A microgrid is a low-voltage power distribution system integrated with DERs and controllable loads that can operate with or without the main grid. The integration of DERs and controllable loads brings significant challenges in managing the DERs and loads to maintain the fundamental supply-demand balance in a microgrid due to the intermittency and variability of DERs and limited supply especially when the microgrid is operating in islanded mode. In this dissertation, we solve the supply-demand balancing problem in microgrids by proposing novel optimization-based algorithms under more realistic conditions and a system architecture for microgrid energy management that enables interoperability and autonomy on the customer side. We give the conclusions of this dissertation and discuss the directions for future work in the following.

In Chapter 2, we study the residential DR problem with consideration of the underlying power distribution network and the associated power flow and system operational constraints. The residential DR is formulated as an OPF problem that is typically non-convex and thus is difficult to solve. We then relax the non-convex OPF problem to be a convex problem and propose a distributed DR scheme where the LSE and the households jointly compute an optimal demand schedule. Using an IEEE test distribution system as an illustrative example, we demonstrate two interesting effects of DR. One is the location effect, meaning that the households far away from the feeder tend to reduce more demands in DR. The other is the rebound effect, meaning that DR may create a new peak after the DR event ends if the DR parameters are not chosen carefully. The two effects suggest certain rules we should follow when designing a DR program. Future work includes designing compensation mechanisms for the location discrimination and heuristic methods to deal with the rebound effect.

In Chapter 3, we study the distributed energy management problem in microgrids where both supply side and demand side management are considered. Most existing distributed energy management algorithms typically assume that all generations and loads are connected to one bus and ignore the underlying power distribution network and the associated power flow and system operational constraints. Consequently, the schedules produced by these algorithms may violate those constraints and thus are not feasible in practice. Therefore, we propose a distributed EMS for the optimal operation of microgrids with consideration of the distribution network and the associated constraints. Specifically, we formulate microgrid energy management as an OPF problem and propose a distributed EMS where the MGCC and the LCs jointly compute an optimal schedule. We also provide an implementation of the proposed EMS based on the IEC 61850 standard. As one demonstration, we apply the proposed EMS to a real microgrid in Guangdong Province, China. The simulation results demonstrate that the proposed EMS is effective in both islanded and grid-connected mode. It is shown that the proposed distributed algorithm converges fast. We also provide a comprehensive analysis of the proposed algorithm. Future work includes implementing the proposed EMS in a real system and analyzing its performance.

In Chapter 4, we study the real-time energy management problem that uses only real-time information to make control decisions without any a priori statistical knowledge. Compared with the existing online algorithms, the proposed online EMS takes into account the underlying power distribution network and the associated constraints. More specifically, we model the online energy management as an SOPF problem and adopt Lyapunov optimization to devise an online algorithm to solve it in real time. The proposed online EMS is subsequently applied to a real microgrid system. The simulation results demonstrate that the performance of the proposed EMS exceeds a greedy algorithm and is close to an optimal offline algorithm. Through this study, we observe and analyze the effect of the underlying network structure on the energy management that cannot be captured by previous online studies. One direction for future work is to develop an intelligent algorithm on the customer side to generate the demand requests.

In Chapter 5, we focus on the design and implementation of a system architecture that

enables interoperability and autonomy on the customer side for microgrid energy management. We design a unified communication interface that is protocol and technology agnostic for the system to interoperate with heterogeneous devices in a microgrid and propose a novel decentralized system architecture to enable autonomy on the customer side. We further implement a prototype of the proposed system architecture and deploy the system in two microgrid testbeds in UCLA SMERC and KIER. We conduct various experiments in the testbeds to test the system in real-world settings. Our experimental results demonstrate that the system is able to manage various DERs and loads using different standards and protocols, interact with external systems such as a DRAS from the utility, and perform efficient energy management using different algorithms. In our experiments, we observe some delays in controlling some of the hardware which may have an impact on microgrid management. More detailed investigations into the delay issue in order to minimize or compensate the delays can be one direction for future work. Another direction is to further optimize system reliability and stability.

References

[1] X. Fang, S. Misra, G. Xue, and D. Yang, "Smart grid - the new and improved power grid: A survey," *IEEE Commun. Surveys Tuts.*, vol. 14, no. 4, pp. 944–980, 2012.

[2] F. Katiraei, R. Iravani, N. Hatziargyriou, and A. Dimeas, "Microgrids management," *IEEE Power Energy Mag.*, vol. 6, no. 3, pp. 54–65, May 2008.

[3] J. Stamp, "The SPIDERS project - smart power infrastructure demonstration for energy reliability and security at US military facilities," in *Proc. IEEE PES ISGT*, Washington, DC, Jan. 2012.

[4] B. Washom, J. Dilliot, D. Weil, J. Kleissl, N. Balac, W. Torre, and C. Richter, "Ivory tower of power: Microgrid implementation at the University of California, San Diego," *IEEE Power Energy Mag.*, vol. 11, no. 4, pp. 28–32, Jul. 2013.

[5] L. T. Berger and K. Iniewski, *Smart Grid: Applications, Communications, and Security.* Wiley, Apr. 2012.

[6] *Assessment of Demand Response and Advanced Metering.* Federal Energy Regulatory Commission, Dec. 2012.

[7] Y. Li, B. L. Ng, M. Trayer, and L. Liu, "Automated residential demand response: Algorithmic implications of pricing models," *IEEE Trans. Smart Grid*, vol. 3, no. 4, pp. 1712–1721, Dec. 2012.

[8] P. Samadi, A. H. Mohsenian-Rad, R. Schober, V. W. S. Wong, and J. Jatskevich, "Optimal real-time pricing algorithm based on utility maximization for smart grid," in *Proc. IEEE SmartGridComm*, Gaithersburg, MD, Oct. 2010.

[9] L. Chen, N. Li, S. H. Low, and J. C. Doyle, "Two market models for demand response in power networks," in *Proc. IEEE SmartGridComm*, Gaithersburg, MD, Oct. 2010.

[10] R. Yu, W. Yang, and S. Rahardja, "A statistical demand-price model with its application in optimal real-time price," *IEEE Trans. Smart Grid*, vol. 3, no. 4, pp. 1734–1742, Dec. 2012.

[11] N. Li, L. Chen, and S. H. Low, "Optimal demand response based on utility maximization in power networks," in *Proc. IEEE PES Gen. Meet.*, Detroit, MI, Jul. 2011.

[12] L. P. Qian, Y. Zhang, J. Huang, and Y. Wu, "Demand response management via real-time electricity price control in smart grids," *IEEE J. Sel. Areas Commun.*, vol. 31, no. 7, pp. 1268–1280, Jul. 2013.

[13] H. Mohsenian-Rad and A. Davoudi, "Optimal demand response in DC distribution networks," in *Proc. IEEE SmartGridComm*, Vancouver, Canada, Oct. 2013.

[14] S. Choi, S. Park, D.-J. Kang, S.-J. Han, and H.-M. Kim, "A microgrid energy management system for inducing optimal demand response," in *Proc. IEEE SmartGridComm*, Brussels, Belgium, Oct. 2011.

[15] C. Cecati, C. Citro, and P. Siano, "Combined operations of renewable energy systems and responsive demand in a smart grid," *IEEE Trans. Sustain. Energy*, vol. 2, no. 4, pp. 468–476, Oct. 2011.

[16] S. Pourmousavi, M. Nehrir, C. Colson, and C. Wang, "Real-time energy management of a stand-alone hybrid wind-microturbine energy system using particle swarm optimization," *IEEE Trans. Sustain. Energy*, vol. 1, no. 3, pp. 193–201, Oct. 2010.

[17] P. Siano, C. Cecati, H. Yu, and J. Kolbusz, "Real time operation of smart grids via FCN networks and optimal power flow," *IEEE Trans. Ind. Informat.*, vol. 8, no. 4, pp. 944–952, Nov. 2012.

[18] A. Dimeas and N. Hatziargyriou, "Operation of a multiagent system for microgrid control," *IEEE Trans. Power Syst.*, vol. 20, no. 3, pp. 1447–1455, Aug. 2005.

[19] Z. Wang, K. Yang, and X. Wang, "Privacy-preserving energy scheduling in microgrid systems," *IEEE Trans. Smart Grid*, vol. 4, no. 4, pp. 1810–1820, Dec. 2013.

[20] A. Dominguez-Garcia and C. Hadjicostis, "Distributed algorithms for control of demand response and distributed energy resources," in *Proc. IEEE CDC*, Orlando, FL, Dec. 2011.

[21] Y. Zhang, N. Gatsis, and G. Giannakis, "Robust energy management for microgrids with high-penetration renewables," *IEEE Trans. Sustain. Energy*, vol. 4, no. 4, pp. 944–953, Oct. 2013.

[22] E. Crisostomi, M. Liu, M. Raugi, and R. Shorten, "Plug-and-play distributed algorithms for optimized power generation in a microgrid," *IEEE Trans. Smart Grid*, vol. 5, no. 4, pp. 2145–2154, Jul. 2014.

[23] W. Shi, N. Li, X. Xie, C.-C. Chu, and R. Gadh, "Optimal residential demand response in distribution networks," *IEEE J. Sel. Areas Commun.*, vol. 32, no. 7, pp. 1441–1450, Jul. 2014.

[24] A. Chaouachi, R. Kamel, R. Andoulsi, and K. Nagasaka, "Multiobjective intelligent energy management for a microgrid," *IEEE Trans. Ind. Electron.*, vol. 60, no. 4, pp. 1688–1699, Apr. 2013.

[25] R. Palma-Behnke, C. Benavides, F. Lanas, B. Severino, L. Reyes, J. Llanos, and D. Saez, "A microgrid energy management system based on the rolling horizon strategy," *IEEE Trans. Smart Grid*, vol. 4, no. 2, pp. 996–1006, Jun. 2013.

[26] A. Khodaei, "Microgrid optimal scheduling with multi-period islanding constraints," *IEEE Trans. Power Syst.*, vol. 29, no. 3, pp. 1383–1392, May 2014.

[27] W. Shi, X. Xie, C.-C. Chu, and R. Gadh, "Distributed optimal energy management in microgrids," *IEEE Trans. Smart Grid*, vol. 6, no. 3, pp. 1137–1146, May 2015.

[28] W. Su, J. Wang, and J. Roh, "Stochastic energy scheduling in microgrids with intermittent renewable energy resources," *IEEE Trans. Smart Grid*, vol. 5, no. 4, pp. 1876–1883, Jul. 2014.

[29] Z. Wang, B. Chen, J. Wang, M. Begovic, and C. Chen, "Coordinated energy management of networked microgrids in distribution systems," *IEEE Trans. Smart Grid*, vol. 6, no. 1, pp. 45–53, Jan. 2015.

[30] A. Khodaei, "Resiliency-oriented microgrid optimal scheduling," *IEEE Trans. Smart Grid*, vol. 5, no. 4, pp. 1584–1591, Jul. 2014.

[31] F. Farzan, M. Jafari, R. Masiello, and Y. Lu, "Toward optimal day-ahead scheduling and operation control of microgrids under uncertainty," *IEEE Trans. Smart Grid*, vol. 6, no. 2, pp. 499–507, Mar. 2015.

[32] Y. Xiang, J. Liu, and Y. Liu, "Robust energy management of microgrid with uncertain renewable generation and load," *IEEE Trans. Smart Grid*, to be published.

[33] S. Salinas, M. Li, P. Li, and Y. Fu, "Dynamic energy management for the smart grid with distributed energy resources," *IEEE Trans. Smart Grid*, vol. 4, no. 4, pp. 2139–2151, Dec. 2013.

[34] Y. Huang, S. Mao, and R. Nelms, "Adaptive electricity scheduling in microgrids," *IEEE Trans. Smart Grid*, vol. 5, no. 1, pp. 270–281, Jan. 2014.

[35] S. Sun, M. Dong, and B. Liang, "Joint supply, demand, and energy storage management towards microgrid cost minimization," in *Proc. IEEE SmartGridComm*, Venice, Italy, Nov. 2014.

[36] W. Su and J. Wang, "Energy management systems in microgrid operations," *The Electricity J.*, vol. 25, no. 8, pp. 45 – 60, Oct. 2012.

[37] A. Vaccaro, M. Popov, D. Villacci, and V. V. Terzija, "An integrated framework for smart microgrids modeling, monitoring, control, communication, and verification," *Proc. IEEE*, vol. 99, no. 1, pp. 119–132, 2011.

[38] Q. Chen, H. Ghenniwa, and W. Shen, "Web-services infrastructure for information integration in power systems," in *Proc. IEEE PES Gen. Meet.*, Montreal, Canada, Jun. 2006.

[39] G.-H. Yang and V. O. Li, "Energy management system and pervasive service-oriented networks," in *Proc. IEEE SmartGridComm*, Gaithersburg, MD, Oct. 2010.

[40] A. Mercurio, A. Di Giorgio, and P. Cioci, "Open-source implementation of monitoring and controlling services for EMS/SCADA systems by means of web services," *IEEE Trans. Power Del.*, vol. 24, no. 3, pp. 1148–1153, Jul. 2009.

[41] W. Shi and V. W. S. Wong, "Real-time vehicle-to-grid control algorithm under price uncertainty," in *Proc. IEEE SmartGridComm*, Brussels, Belgium, Oct. 2011.

[42] *Communication networks and systems for power utility automation - Part 7-420: Basic communication structure - Distributed energy resources logical nodes.* IEC Standard 61850-7-420, 2009.

[43] W. Shi, N. Li, C.-C. Chu, and R. Gadh, "Real-time energy management in microgrids," *IEEE Trans. Smart Grid*, to be published.

[44] W. Shi, E.-K. Lee, D. Yao, R. Huang, C.-C. Chu, and R. Gadh, "Evaluating microgrid management and control with an implementable energy management system," in *Proc. IEEE SmartGridComm*, Venice, Italy, Nov. 2014.

[45] M. Farivar and S. H. Low, "Branch flow model: Relaxations and convexification-part I," *IEEE Trans. Power Syst.*, vol. 28, no. 3, pp. 2554–2564, Aug. 2013.

[46] N. Li, L. Chen, and S. H. Low, "Exact convex relaxation of OPF for radial networks using branch flow model," in *Proc. IEEE SmartGridComm*, Tainan, Taiwan, Nov. 2012.

[47] L. Gan, N. Li, U. Topcu, and S. H. Low, "On the exactness of convex relaxation for optimal power flow in tree networks," in *Proc. IEEE CDC*, Maui, HI, Dec. 2012.

[48] ——, "Optimal power flow in tree networks," in *Proc. IEEE CDC*, Florence, Italy, Dec. 2013.

[49] W. H. Kersting, "Radial distribution test feeders," in *Proc. IEEE PES Winter Meet.*, Columbus, OH, Jan. 2001.

[50] E.-K. Lee, R. Gadh, and M. Gerla, "Energy service interface: Accessing to customer energy resources for smart grid interoperation," *IEEE J. Sel. Areas Commun.*, vol. 31, no. 7, pp. 1195–1204, Jul. 2013.

[51] M. Pipattanasomporn, M. Kuzlu, and S. Rahman, "An algorithm for intelligent home energy management and demand response analysis," *IEEE Trans. Smart Grid*, vol. 3, no. 4, pp. 2166–2173, Dec. 2012.

[52] M. E. Baran and F. F. Wu, "Network reconfiguration in distribution systems for loss reduction and load balancing," *IEEE Trans. Power Del.*, vol. 4, no. 2, pp. 1401–1407, Apr. 1989.

[53] *American National Standard for Electric Power Systems and Equipment-Voltage Ratings (60 Hertz).* ANSI C84.1-2006, 2006.

[54] G. Chen and M. Teboulle, "A proximal-based decomposition method for convex minimization problems," *Math. Program.*, vol. 64, no. 1, pp. 81–101, Mar. 1994.

[55] D. P. Bertsekas and J. N. Tsitsiklis, *Parallel and Distributed Computation: Numerical Methods.* Prentice-Hall, 1989.

[56] M. Grant and S. Boyd. CVX: Matlab software for disciplined convex programming, version 2.1. [Online]. Available: http://cvxr.com/cvx

[57] S. H. Low, "Convex relaxation of optimal power flow-part I: Formulations and equivalence," *IEEE Trans. Control Netw. Syst.*, vol. 1, no. 1, pp. 15–27, Mar. 2014.

[58] ——, "Convex relaxation of optimal power flow-part II: Exactness," *IEEE Trans. Control Netw. Syst.*, vol. 1, no. 2, pp. 177–189, Jun. 2014.

[59] L. Gan, N. Li, U. Topcu, and S. H. Low, "Exact convex relaxation of optimal power flow in radial networks," *IEEE Trans. Autom. Control*, vol. 60, no. 1, pp. 72–87, Jan 2015.

[60] L. Gan and S. H. Low, "Convex relaxations and linear approximation for optimal power flow in multiphase radial networks," *arXiv:1406.3054*, 2014.

[61] R. Huang, T. Huang, R. Gadh, and N. Li, "Solar generation prediction using the ARMA model in a laboratory-level micro-grid," in *Proc. IEEE SmartGridComm*, Tainan, Taiwan, Nov. 2012.

[62] G. Sideratos and N. Hatziargyriou, "An advanced statistical method for wind power forecasting," *IEEE Trans. Power Syst.*, vol. 22, no. 1, pp. 258–265, Feb. 2007.

[63] Q. Peng and S. H. Low, "Distributed algorithm for optimal power flow on a radial network," *arXiv:1404.0700*, 2014.

[64] R. Huang, E.-K. Lee, C.-C. Chu, and R. Gadh, "Integration of IEC 61850 into a distributed energy resources system in a smart green building," in *Proc. IEEE PES Gen. Meet.*, National Harbor, MD, Jul. 2014.

[65] M. J. Neely, A. S. Tehrani, and A. G. Dimakis, "Efficient algorithms for renewable energy allocation to delay tolerant consumers," in *Proc. IEEE SmartGridComm*, Gaithersburg, MD, Oct. 2010.

[66] M. J. Neely, *Stochastic Network Optimization with Application to Communication and Queueing Systems*. Morgan & Claypool, 2010.

[67] Y. Guo, M. Pan, Y. Fang, and P. P. Khargonekar, "Decentralized coordination of energy utilization for residential households in the smart grid," *IEEE Trans. Smart Grid*, vol. 4, no. 3, pp. 1341–1350, Sept. 2013.

[68] L. Zheng and L. Cai, "A distributed demand response control strategy using Lyapunov optimization," *IEEE Trans. Smart Grid*, vol. 5, no. 4, pp. 2075–2083, Jul. 2014.

[69] S. Sun, M. Dong, and B. Liang, "Real-time welfare-maximizing regulation allocation in dynamic aggregator-EVs system," *IEEE Trans. Smart Grid*, vol. 5, no. 3, pp. 1397–1409, May 2014.

[70] C. Jin, X. Sheng, and P. Ghosh, "Optimized electric vehicle charging with intermittent renewable energy sources," *IEEE J. Sel. Topics Signal Process.*, vol. 8, no. 6, pp. 1063–1072, Dec. 2014.

[71] S. Sun, M. Dong, and B. Liang, "Real-time power balancing in electric grids with distributed storage," *IEEE J. Sel. Topics Signal Process.*, vol. 8, no. 6, pp. 1167–1181, Dec. 2014.

[72] S. Lakshminarayana, T. Q. S. Quek, and H. V. Poor, "Cooperation and storage tradeoffs in power grids with renewable energy resources," *IEEE J. Sel. Areas Commun.*, vol. 32, no. 7, pp. 1386–1397, Jul. 2014.

[73] T. Li and M. Dong, "Real-time energy storage management: Finite-time horizon approach," in *Proc. IEEE SmartGridComm*, Venice, Italy, Nov. 2014.

[74] S. Sojoudi and J. Lavaei, "Physics of power networks makes hard optimization problems easy to solve," in *Proc. IEEE PES Gen. Meet.*, San Diego, CA, Jul. 2012.

[75] W. Shi, X. Xie, C.-C. Chu, and R. Gadh, "A distributed optimal energy management strategy for microgrids," in *Proc. IEEE SmartGridComm*, Venice, Italy, Nov. 2014.

[76] National Renewable Energy Laboratory (NREL) Measurement and Instrumentation Data Center (MIDC). [Online]. Available: http://www.nrel.gov/midc

[77] California ISO Open Access Same-time Information System (OASIS). [Online]. Available: http://oasis.caiso.com

[78] R. H. Tutuncu, K. C. Toh, and M. J. Todd, "Solving semidefinite-quadratic-linear programs using SDPT3," *Math. Program.*, vol. 95, pp. 189–217, 2003.

[79] Y. Wang, O. Sheikh, B. Hu, C.-C. Chu, and R. Gadh, "Integration of V2H/V2G hybrid system for demand response in distribution network," in *Proc. IEEE SmartGridComm*, Venice, Italy, Nov. 2014.

[80] R. Huang, Y. Wang, W. Shi, D. Yao, B. Hu, C.-C. Chu, and R. Gadh, "Integration of iec 61850 into a vehicle-to-grid system with networked electric vehicles," in *Proc. IEEE PES ISGT*, Washington, DC, Feb. 2015.

[81] M. Majidpour, C. Qiu, P. Chu, R. Gadh, and H. R. Pota, "Fast demand forecast of electric vehicle charging stations for cell phone application," in *Proc. IEEE PES Gen. Meet.*, National Harbor, MD, Jul. 2014.

[82] Y. Wang, B. Wang, R. Huang, C.-C. Chu, H. R. Pota, and R. Gadh, "Two-tier prediction of solar power generation with limited sensing resource," *arXiv:1508.02669*, 2015.

[83] G. Bellala, M. Marwah, M. Arlitt, G. Lyon, and C. Bash, "Towards an understanding of campus-scale power consumption," in *ACM BuildSys*, 2011.

[84] E. Mills and P. Mathew, "Monitoring-Based Commissioning: Benchmarking Analysis of 24 UC/CSU/IOU Projects," Lawrence Berkeley National Laboratory, Tech. Rep. LBNL-1972E, June 2009.

[85] P. Zhang, F. Li, and N. Bhatt, "Next-generation monitoring, analysis, and control for the future smart control center," *IEEE Trans. Smart Grid*, vol. 1, no. 2, pp. 186–192, Sept. 2010.

[86] *Electricity metering Data exchange for meter reading, tariff and load control Part 53: COSEM application layer.* IEC Standard 62056-53, 2006.

[87] *Digital addressable lighting interface - Part 101: General requirements - System components.* IEC Standard 62386-101:2014, 2014.

[88] *BACnet A Data Communication Protocol for Building Automation and Control Networks.* ANSI/ASHRAE Standard 135-2012, 2012.

[89] *OASIS Open Building Information Exchange (oBIX).* oBix Specification 1.1, 2014.

[90] R. T. Fielding, D. Software, and R. N. Taylor, "Principled design of the modern web architecture," *ACM Trans. Internet Technology*, vol. 2, pp. 115–150, 2002.

[91] E.-K. Lee, R. Gadh, and M. Gerla, "Resource centric security to protect customer energy information in the smart grid," in *Proc. IEEE SmartGridComm*, Tainan, Taiwan, Nov. 2012.

[92] M. A. Piette, G. Ghatikar, S. Kiliccote, E. Koch, D. Hennage, P. Palensky, and C. McParland, "Open Automated Demand Response Communications Specification v1.0," *California Energy Commission - PIER Program*, vol. CEC-500-2009-063, 2009.

[93] R. Huang, T. Huang, R. Gadh, and N. Li, "Solar Generation Prediction using the ARMA Model in a Laboratory-level Micro-grid," in *Proc. IEEE SmartGridComm*, Taiwan, Nov. 2012.

[94] S. Boyd and L. Vandenberghe, *Convex Optimization.* Cambridge University Press, 2004.